Benthic ecology in two British Columbian fjords: compositional and functional patterns

by

Ryan Gasbarro
B.A. Arizona State University, 2015

A Thesis Submitted in Partial Fulfillment
of the Requirements for the Degree of

MASTER OF SCIENCE

in the Department of Earth & Ocean Sciences

Supervisory Committee

Benthic ecology in two British Columbian fjords: compositional and functional patterns

by

Ryan Gasbarro
B.A. Arizona State University, 2015

Supervisory Committee

Dr. Verena Tunnicliffe, Supervisor
Department of Earth & Ocean Sciences

Dr. S. Kim Juniper, Departmental Member
Department of Earth & Ocean Sciences

Dr. Julia Baum, Outside Member
Department of Biology

Abstract

As global change alters the chemical and physical dynamics of the ocean, it is increasingly necessary to determine ecological responses across environmental gradients. The benthic ecosystems of fjords often contain a multitude of environmental gradients conducive to multivariate field studies. In this thesis, I describe the benthic community structure of two British Columbian fjords in relation to markedly different environmental variables. In Chapter 2, I show a strong correlation between suspension-feeder abundance and flow structure on the steep fjord walls of Douglas Channel, BC. I also describe distinct assemblages with depth and with location along the fjord head-mouth axis. Using a suite of biological traits, I show that the deep portion (> 400 m depth) of the most seaward site is the most taxonomically and functionally diverse in the fjord. My results suggest fjord walls form an expansive ecosystem containing diverse and dense assemblages of suspension feeders relevant to the flow of energy through fjord basins and as biodiversity reservoirs. In Chapter 3, I extend a long-term hypoxia time-series (2006 - 2016) to document the response of soft-bottom epibenthic megafauna of Saanich Inlet, BC to a prolonged hypoxic event in 2016 that caused abundance declines, community aggregation and shifts in species composition more extreme than those seen in the 2013 hypoxia cycle. I also assess community threshold responses along the oxygen gradient; I found community transitions consistent across years and with Northeast Pacific oxygen thresholds based in ecophysiological studies. Taken together, these studies show a strong coupling between oceanographic conditions and the community structure of fjord benthos. I suggest that climate-driven alterations in North Pacific oceanographic regimes may portend major changes in fjord ecosystems.

Table of Contents

List of Tables

List of Figures

Acknowledgements

First, I would like to thank Dr. Verena Tunnicliffe for being my supervisor. Verena propelled me forward at every step of this endeavor with patience and generosity, and has given me a highly memorable learning experience. I am grateful for the opportunity to work under such a kind and inspirational scientist, and I will carry what she has taught me through the rest of my career.

This research would not have been possible without the contributions of many others. Thank you to my committee members, Dr. S. Kim Juniper and Dr. Julia Baum, for guiding my work with thoughtful comments along the way. A big thank you is also due to the staff and graduate students in both the Earth & Ocean Sciences and Biology departments for their support and inspiration. Thank you to the ONC staff, CCGS Tully captains and crew, and ROV ROPOS team, who were all instrumental in completing the fieldwork. Thanks to Di Wan, whose collaboration greatly enhanced my work in Douglas Channel. I am also indebted to the many members of the Tunnicliffe lab that facilitated my research. Thanks to Jonathan Rose for his invaluable technical expertise and support throughout. Thanks to Cherisse du Preez for starting me with video annotation and to Nick Brown for his timesaving efforts annotating video later on. I am grateful for Rachel Boschen's assistance with statistical software and for helpful feedback. A special thank you goes out to Jackson Chu for lending his expertise towards extending the Saanich Inlet hypoxia time-series, and for all of the comments and encouragement he provided along the way.

Finally, I would like to extend my most heartfelt gratitude towards my family. Thanks to Nathan and Sam for bringing levity into my life whenever it was needed (and often when it was not). To my brother and sister-in-law, Michael and Lindsay, thank you for the contagious joy and enthusiasm you bring into my life, and for inspiring me to work hard like you. To my mother and father, Scott and Patricia, I am forever grateful for your care and encouragement – I needed both during this time. A person is lucky to have one great supporter and I am so fortunate to have two in you.

Dedication

To Dad

For leading an exemplary life, and lending unconditional support to mine.

Chapter 1: General Introduction

The importance of biodiversity patterns

The diversity of living organisms on Earth is a result of three-plus billion years of evolution, and remains the diagnostic feature of our planet in the cosmos. Biological diversity – or biodiversity – can be defined as the diversity of living organisms; I will focus this overview of biodiversity primarily on species, but biodiversity, *sensu stricto,* includes ecosystem diversity, species diversity and the genetic variability within species (Giller & O'Donovan 2002).

Human-induced changes in biodiversity, principally driven by habitat alterations, climate change, invasive species, exploitation and pollution, all look to impact, continually or increasingly, every major ecosystem on the planet (Millennium Ecosystem Assessment 2005). As species extinctions, both local and global, proceed at alarming rates (Barnosky et al. 2011), it is important to understand and predict the large-scale consequences. Hence, there has been a great interest (Fig. 1a) in discerning the relationships between biodiversity and ecosystem functioning (BEF; Hooper et al. 2005; Hooper et al. 2012). A meta-analyses by Cardinale et al. (2012) provides the major 'consensus' outcomes of the early 21st century emphasis on BEF studies, including the wide support for the hypothesis that greater species diversity leads to temporal community stability. There may be a number of mechanisms for this stabilizing effect, as biodiversity lessens the impacts of plant herbivory by providing heterogeneous resources to consumers; species richness also provides resistance to pathogens and invasive species (Giller & O'Donovan 2002). Species richness may aid in recovery from fisheries collapse and is also positively correlated with average catch (Worm et al. 2012). In contrast, some

functions, namely organic matter decomposition, appear location-dependent and idiosyncratically related to species richness (Giller & O'Donovan 2002).

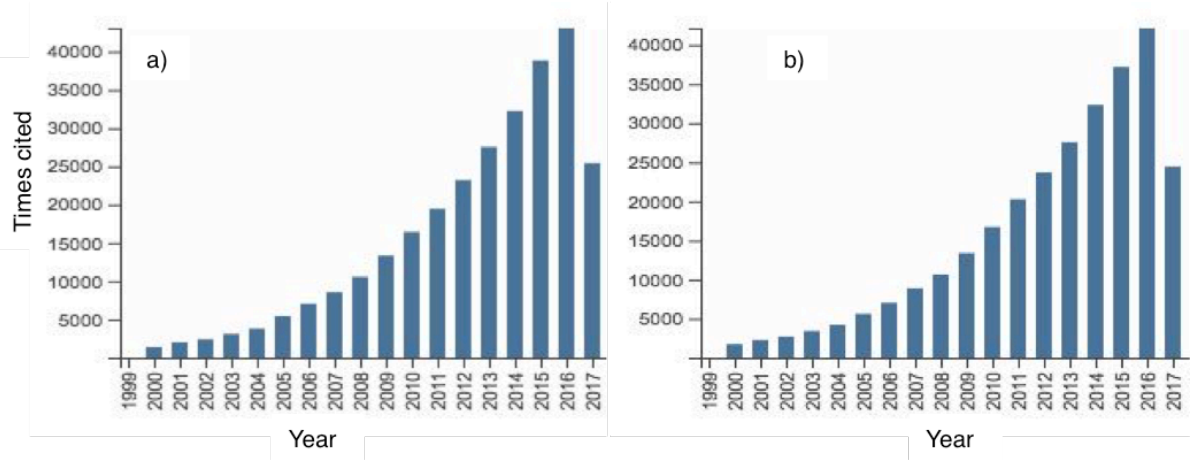

Figure 1.1. The yearly increase in citations for papers under the search terms a) 'biodiversity ecosystem functioning' and b) 'functional diversity'. The functional diversity search was limited to journals in the fields of ecology and plant sciences in order to keep the total number of studies below 10,000 to allow for data extraction from the Web of Science database. Note that data for 2017 only includes papers from January-July.

The other consensus outcomes of Cardinale et al. (2012) relate to the newfound importance of functional diversity (Figure 1.1b); that is, it is not the presence of species that affect ecosystem functioning but the biological traits expressed by those species. Thus, not all species equally contribute to ecosystem functioning, and some may be functionally redundant or possess traits that vary widely among species (Messier et al. 2010; Violle et al. 2012). However, the ability of many species to execute multiple functions in time and/or space may lead to overestimates of functional redundancy, and thus species diversity may have greater impacts on overall ecosystem functioning than some studies report (Gamfeldt et al. 2008). Greater functional trait diversity leads to greater ecosystem service provision rates, and buffers against the nonlinear decreases in ecosystem functioning created by species removal; the ecosystem functionality losses

caused by extinctions may be comparable to those related to major climate stressors (Hooper et al. 2012). As these general BEF relationships are established, the delineation of traits that affect ecosystem function versus those that respond to ecosystem changes is important for predicting ecosystem responses to stressors (Naeem & Wright 2003).

Estimates of Earth's biodiversity still require notable extrapolation despite major cataloguing efforts (e.g. www.catalogueoflife.org). Therefore, we cannot fully conserve or manage global biodiversity. However, advances in molecular methods continue to uncover new and cryptic diversity, and coarse biodiversity monitoring has become more feasible with the advent of eDNA (Thomsen et al. 2015). Estimates of distinct fungi on Earth, for example, have increased from 1.5 to 5.1 million since 1991 alone (Blackwell 2010). Barcoding of microbes in various deep-sea environments reveals large reserves of genetic diversity (Sogin et al. 2006), and the vast expanses of unexplored seafloor continue to provide many species new to science (Brandt et al. 2007; Ramirez-Llodra 2010). In contrast, the first entomological surveys of tropical rainforest canopies revealed seemingly unending reserves of new insect species that bolstered estimates of global biodiversity (Rosenzweig 1995), but a finding of low spatial turnover of rainforest insects in some tropical areas may lower those estimates (Novotny et al. 2005). So, locating patterns in biodiversity and the processes that influence it are of great importance as we continue to catalogue biodiversity and prioritize areas of perceived importance. Here, I begin with an overview of the widely reported biodiversity patterns and their potential causes with an emphasis on marine macroecological patterns. Finally, I will discuss fjordic environments and their utility as natural marine laboratories rich in ecological gradients.

Patterns and drivers of diversity

There are many patterns of species richness that exist, and while understanding the role that spatial scale plays in altering these patterns is one of the principal challenges in ecology (Rahbek 2005), they are useful for understanding why species richness varies from place to place. Species richness decreases with distance from the equator; this pattern holds for nearly all taxa (but see Gaines & Lubchenco 1982) and through evolutionary time (i.e. 10^5-10^7 years; Rosenzweig 1995). The causes of these large-scale species patterns have been studied, but never entirely resolved, since Macarthur and Wilson (1963) showed that diversity increases with both area and proximity to source populations in their work on island biogeography. While no single mechanism has been found to drive the latitudinal gradient in species richness, both habitable area (Rosenzweig & Sandlin 1997) and temperature-productivity (as a proxy for usable energy) contribute (Gaston 2000) to the pattern. On local to regional scales, species richness displays a hump-shaped response to both usable energy and disturbance (Rosenzweig 1992). Species diversity also tends to increase with habitat heterogeneity (Girard et al. 2016; Patru-Stupariu 2017).

The effects of biotic interactions on diversity have caused some controversy, particularly in community ecology (Connor et al. 2013). Diamond (1975) noted that some species never occurred on islands together, and suggested their segregation was caused by interspecific competition due to overlapping niches; null models in which species distributions are compared to those generated at random from the data have since been used to test whether Diamond's assertion was correct (Connor and Simberloff 1979; Gotelli 2010). Despite continued debate on both sides, competition has been shown to

shape species diversity in a variety of settings, and increases species diversity in densely populated ecosystems such as tropical coral reefs (Chadwick & Morrow 2011) and subtidal rock walls (Miller & Etter 2011). Facilitative interactions may be overlooked drivers of evolution as well (Brooker et al. 2008). However, as the spatiotemporal scale is increased, species interactions and the structure of species niches explain less of the observed changes in species diversity (Hubbell 1997; Witman & Roy 2009).

While there are many biodiversity patterns, global biodiversity can only change with the addition or subtraction of species. Global species diversity change is the speciation rate minus the extinction rate. Speciation is the only mechanism that creates species diversity, and is one of two major processes, along with immigration, augmenting current sub-global biodiversity stocks (Rosenzweig 1995). The current extinction rate is so high that some paleontologists worry we are approaching a sixth mass extinction within the next handful of centuries if large swaths of the Earth are not reserved to protect biodiversity (Barnosky et al. 2011; Dirzo et al. 2011). Additionally, the current speciation rate shows a latitudinal gradient opposite to species richness (Schluter & Pennell 2017), suggesting instability in the species richness gradient in the long-term future. Further, we do not know how many species are living at or near ecophysiological thresholds that will be reached in the near future, or how many species may harbor a rapid evolutionary or plastic capacity to withstand changes in environmental parameters (Hoffman & Sgro 2011).

Immigration changes diversity, either by shifting geographic patterns in species distributions or by influencing speciation/extinction rates through interactions. So, while the global biodiversity stock is not directly altered by immigration, the species in some

areas (e.g. fjords, abyssal plains) all immigrated following major climatic events. In shallow marine systems, physical oceanographic features dictate larval delivery and thus immigration (Smith & Witman 1999), and the latitudinal diversity pattern largely holds. Marine exotic species continue to increase and alter biodiversity patterns along coastlines, and the supply of invaders – modified by shipping and oceanic circulation patterns – and local resistance to invasion are the principal variables affecting their distribution (Ruiz et al. 2000). The deep sea (depths > 200 m) diverges from the latitudinal diversity pattern, as the equatorial temperature-productivity gradient is flipped in some expanses (e.g. the North Atlantic) and biogeographic patterns vary by taxon (Lambshead et al. 2000) with historical immigration events playing a large role in determining extant distributions (Brown & Thatje 2014).

The deep sea – an environment covering much of the area on Earth – displays a more consistent bathymetric diversity pattern, with a unimodal peak in the bathyal zone from 1000-3000 m (Rex 1993; Carney 2005). Landscape-regional features such as oxygen minimum zones (Levin et al. 2001), seamounts (Rowden et al. 2010), whale falls (Smith & Baco 2003), cold seeps (Cordes et al. 2010), hydrothermal vents (Tunnicliffe 1991) and submarine canyons (Quattrini et al. 2015) interrupt this pattern, however. The mid-bathyal peak in deep-sea diversity may be a result of increased speciation at these depths; as global dysoxic events and subsequent re-colonization of the deep sea by shallow-water species proceeded, the combination of hydrostatic pressure and low-temperature stress may have caused a bottleneck that produced rapid evolution in the mid-bathyal zone (Young et al. 1997; Brown & Thatje 2014). In addition, the exponential decline in detrital food with depth may contribute to the lower depth boundary for species

(Carney 2005; but see Watts et al. 1992). While an excess of food would not create an upper depth boundary, antagonistic interactions in these areas may do so (Carney 2005). The composition of detritus may play a part in depth-related zonation of deep-sea species as well. Geochemical analyses show that 'high-quality' detritus converts to biomass more readily and that the quality of detritus decreases with depth (Danovaro et al. 2001).

Resolving the causes of the major global biodiversity patterns remains an intriguing and important area of study, but logistical constraints often limit the study of these patterns to meta-analyses that can contain biases caused by the conglomeration of sampling methods. Mapping methods continue to unveil rugosity in areas of the seafloor assumed to be relatively featureless; therefore, estimates of the total area of the ocean floor continue to increase (Sandwell et al. 2014). Quantifying the drivers of benthic diversity in the global ocean becomes increasingly important in light of these findings. Smaller-scale studies may be better suited for rigorous measurement of diversity pattern drivers, and may continue to reveal the importance of regional diversity (Levin et al. 2001).

Fjord benthic environments as natural laboratories for gradient ecology

Fjords are glacially carved estuaries in temperate-to-high latitudes that provide natural laboratories for the study of marine organism abundances and distributions. The deep basins of fjords lie in close proximity to land, making fjords attractive environments to study deep benthic communities without the logistical constraints of open-ocean sampling. The seaward ends of fjords interact with the open ocean, creating dynamic land-estuary-ocean interfaces over relatively short distances (~ 100 km, generally). Thus,

fjords also allow for studies on the effects of both anthropogenic and natural terrestrial materials on benthic organisms.

In his summary of the major factors affecting fjord macrobenthos, Pearson (1980) suggests that the major biogeographic differences in fjord fauna are due to hydrodynamic (i.e. high versus low energy input fjords) and latitudinal differences (i.e. glacier-fed versus non-glaciated fjords), and that these physical distinctions are the determining factors of whether the fjords are carbon/nutrient sinks. An example of two nearby fjords with varied hydrodynamic energy and distinct fauna are Jervis Inlet and Howe Sound, British Columbia (Levings et al. 1983). There are many examples of polar versus boreal faunal distinctions in fjords, with some notable intermediates (Hop et al. 2002).

Pearson's 2x2 classification scheme may be an oversimplification, however, as many environmental parameters in various fjords have since been associated with distinct assemblages and abundances. Particle inputs at both fjord ends and distinct hydrodynamic features often create sharp vertical and along-fjord gradients in important ocean parameters. Figure 1.2 shows the typical hydrodynamic features and environmental gradients seen both vertically and horizontally in fjordic environments. While this schematic is of use to generalize for simplicity's sake, note that some fjords may not possess these gradients or mass flux structure, and that the magnitudes of their strength vary. In addition, some phenomena are dependent (e.g. the development of seasonal anoxia in deep basins depends partly on low hydrodynamic energy fluxes) or augmented by the presence of other factors (e.g. high sedimentation rates in the presence of tidewater glaciers, anthropogenic inputs). Thus, quantifying the interaction between various

processes and environmental responses on a more local basis is of interest to the fjord benthic ecologist.

Sedimentation rate is an important driver of community structure, especially in fjords receiving large influxes of terrestrial materials at their heads (Farrow et al. 1983; Syvitsky et al. 1989; Wlodarska-Kowalczuk 2004). Sediment organic matter content (Rosenberg et al. 2002) and grain size (Pearson 1971) also tend to vary as depositional energy decreases from fjord head to mouth, with concomitant shifts in macrobenthos. Steep gradients in important oceanic parameters such as salinity (Pickard 1961), dissolved oxygen (Anderson & Devol 1973), sediment loading (Carney et al. 1999), pH (Jantzen et al. 2013), larval supply (Quijon & Snelgrove, 2005) and disturbance from glacial scouring (Moon et al. 2015) have been documented, *inter alia*, in fjords as well. Human-created gradients from mining waste (Josefson et al. 2008), hydrocarbon spills (Payne et al. 2008) and artificial organic matter enrichment (Pearson & Rosenberg 1978) also impact fjord benthos, but are limited by the degree to which the fjord-adjacent areas are industrialized.

Fjords afford insights into the temporal dynamics of many processes too. Diurnal, tidal, and seasonal cycles in precipitation and terrigenous inputs contribute to their short-term temporal dynamism (Hoskin & Burrell 1972); some high-productivity fjords experience seasonal anoxia as organic matter is processed over summer in stagnant deep waters (Anderson & Devol 1973; Pearson & Rosenberg 1978). Climate change effects can be seen on longer time-scales through changes in glacial inputs to high altitude fjords (Grange & Smith 2013), long-term oxygen loss (Chu & Tunnicliffe 2015) and alterations

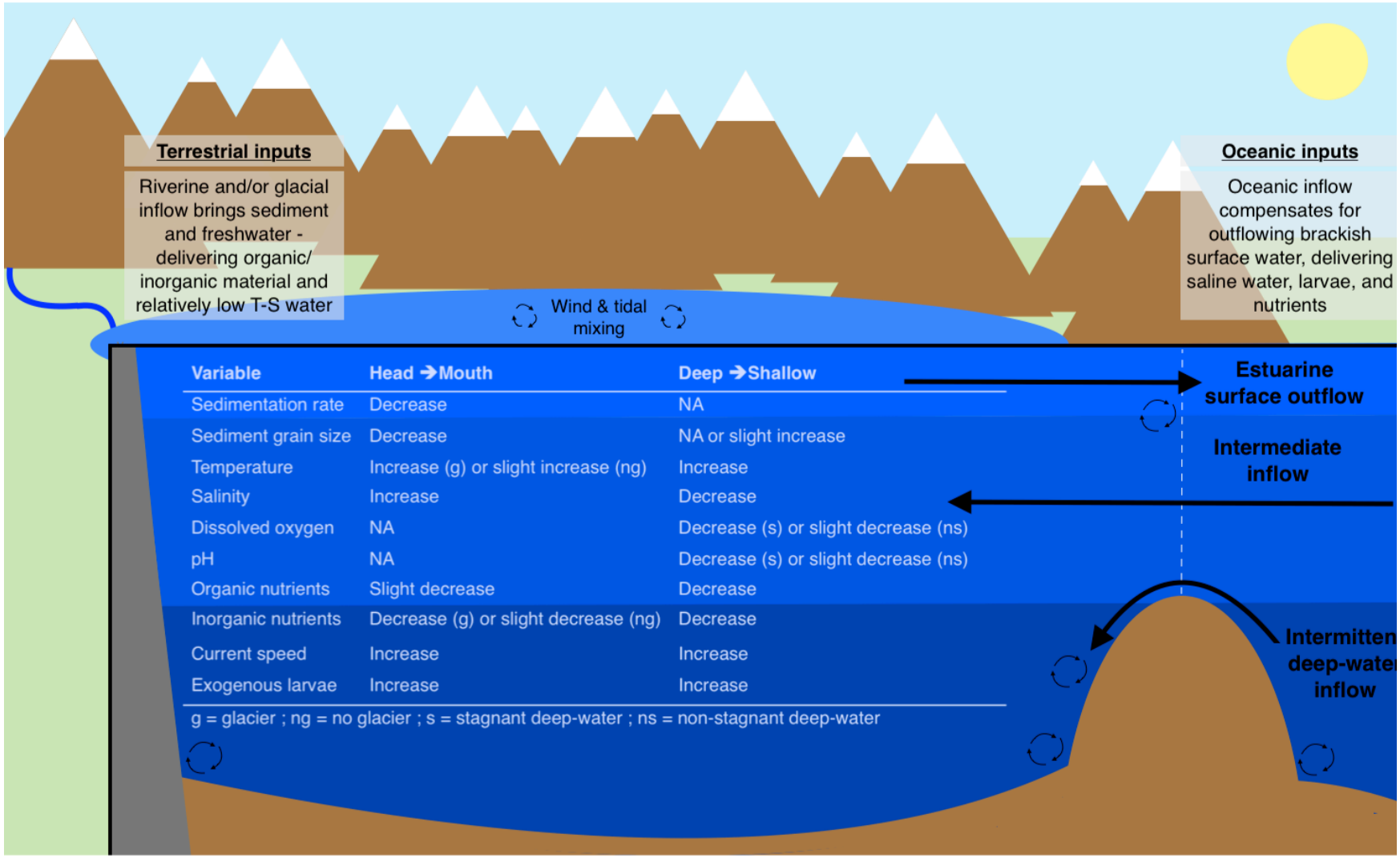

Figure 1.2. Cross-section of the three-layer structure (e.g. surface outflow, intermediate inflow, & deep-water) typical of fjordic environments. Terrestrial inputs at the fjord head and oceanic inputs at the fjord mouth create sharp gradients (table) in environmental variables relative to those seen in the open ocean. Wind and tidal mixing, entrainment of the water of adjacent layers, and flows over heterogeneous topography (e.g. sills, vertical-horizontal steps) create localized turbulence (circular arrows).

in benthic community structure related to oscillating climate indices (Beuchel et al. 2006). Fjord benthos in the Arctic, where ecosystems are under stress from rapid climate change (Post et al. 2009), can abruptly change as continued warming causes a switch to more temperate communities dominated by macroalgae (Kortsch et al. 2012). Taken together, the presence of spatial gradients and temporal dynamism creates widely varied environmental milieux that allow for the diverse fauna often noted within and among fjords (Pearson 1980; Levings et al. 1983). At the extreme ends of these gradients we may also gain insight into *in situ* benthic organismal responses to stressor levels predicted in future climate scenarios that may improve the fidelity of predicted responses based off laboratory studies. Jantzen et al. (2013), for example, describe cold-water corals living below the aragonite saturation threshold in a Chilean fjord. High-diversity assemblages exist in severe hypoxia in some fjords (Tunnicliffe 1981). Other fjordic populations may be acclimatized to extreme environments, and it is not known how frequent a phenomenon such local acclimatization is, or whether adaptation can occur on timescales relevant to predicated rates of ocean change (Munday et al. 2013). A more thorough understanding of the way community structure changes along myriad and mixed environmental gradients may allow for better predictions of the ecological consequences of a changing ocean.

Research Objectives

In this thesis, I present the two studies from benthic environments that display the ecological variability associated with natural environmental gradients in two British Columbian fjords. While the two studies occurred in disparate ecosystems, they display

both the ecological importance of fjordic environments, and their utility as natural laboratories for measuring the consequences of a changing ocean.

In Chapter 2, I present the results from vertical hard substrata imaging surveys in Douglas Channel, BC in order to:

i) Document the macrofaunal functional and taxonomic diversity, abundance and assemblage zonation present on the fjord walls

ii) Resolve the environmental variables that likely control the animal distributions, with particular emphasis on relating animal abundance to the vertical mass flux structure of the fjord.

In Chapter 3 I relay the results from three soft-bottom benthic transects in Saanich Inlet, BC with the goals of:

i) Determining the extent to which the seasonal community reorganization seen in 2013 (Chu & Tunnicliffe 2015) is repeated in 2016 after consecutive weak deep-water renewals and continued long-term deoxygenation, and to quantify changes in bottom oxygen and community structure.

ii) Determining the locations of critical transitions in Saanich Inlet megafaunal assemblage structure along an oxygen gradient using a novel spatial adaptation of Fisher's Information index, and to compare the results to common hypoxia thresholds and results obtained with previously established statistical methods.

Literature Cited

Anderson JJ, Devol AH (1973) Deep water renewal in Saanich Inlet, an intermittently anoxic basin. Estuarine and Coastal Marine Science 1:1–10

Barnosky AD, Matzke N, Tomiya S, Wogan GOU, Swartz B, Quental TB, Marshall C, McGuire JL, Lindsey EL, Maguire KC, Mersey B, Ferrer EA (2011) Has the Earth's sixth mass extinction already arrived? Nature 471:51–57

Beuchel F, Gulliksen B, Carroll ML (2006) Long-term patterns of rocky bottom macrobenthic community structure in an Arctic fjord (Kongsfjorden, Svalbard) in relation to climate variability (1980–2003). J Mar Syst 63:35–48

Blackwell M (2011) The fungi: 1, 2, 3 ... 5.1 million species? Am J Bot 98:426–438

Brandt A, Gooday AJ, Brandao SN, Brix S, Broekeland W, Cedhagen T, Choudhury M, Cornelius N, Danis B, De Mesel I, Diaz RJ, Gillan DC, Ebbe B, Howe JA, Janussen D, Kaiser S, Linse K, Malyutina M, Pawlowski J, Raupach M, Vanreusel A (2007) First insights into the biodiversity and biogeography of the Southern Ocean deep sea. Nature 447:307–311

Brooker RW, Maestre FT, Callaway RM, Lortie CL, Cavieres LA, Kunstler G, Liancourt P, Tielboerger K, Travis JMJ, Anthelme F, Armas C, Coll L, Corcket E, Delzon S, Forey E, Kikvidze Z, Olofsson J, Pugnaire FI, Quiroz CL, Saccone P, Schiffers K, Seifan M, Touzard B, Michalet R (2008) Facilitation in plant communities: the past, the present, and the future. J Ecol 96:18–34

Brown A, Thatje S (2014) Explaining bathymetric diversity patterns in marine benthic invertebrates and demersal fishes: physiological contributions to adaptation of life at depth. Biol Rev 89:406–426

Carney D, Oliver JS, Armstrong C (1999) Sedimentation and composition of wall communities in Alaskan fjords. Polar Biology 22:38–49

Carney RS (2005) Zonation of deep biota on continental margins. In: Gibson RN, Atkinson RJA, Gordon JDM (eds) Oceanography and Marine Biology - an Annual Review, Vol. 43. Crc Press-Taylor & Francis Group, Boca Raton, p 211–

Chadwick NE, Morrow KM (2011) Competition Among Sessile Organisms on Coral Reefs. In: Dubinsky Z, Stambler N (eds) Coral Reefs: An Ecosystem in Transition. Springer Netherlands, Dordrecht, p 347–371

Chu JWF, Tunnicliffe V (2015) Oxygen limitations on marine animal distributions and the collapse of epibenthic community structure during shoaling hypoxia. Global Change Biology 21:2989–3004

Connor EF, Collins MD, Simberloff D (2013) The checkered history of checkerboard distributions. Ecology 94:2403–2414

Connor EF, Simberloff DS (1979) The assembly of species communities: chance or competition? Ecology 60:1132–1140

Cordes EE, Cunha MR, Galeron J, Mora C, Olu-Le Roy K, Sibuet M, Van Gaever S, Vanreusel A, Levin LA (2010) The influence of geological, geochemical, and biogenic habitat heterogeneity on seep biodiversity. Mar Ecol-Evol Persp 31:51–65

Danovaro R, Dell'Anno A, Fabiano M (2001) Bioavailability of organic matter in the sediments of the Porcupine Abyssal Plain, northeastern Atlantic. Mar Ecol-Prog Ser 220:25–32

Dirzo R, Young HS, Galetti M, Ceballos G, Isaac NJB, Collen B (2014) Defaunation in the Anthropocene. Science 345:401–406

Diamond JM (1975) Assembly of species communities. In: Cody ML, Diamond JM (eds) Ecology and evolution of communities. Cambridge, Mass: Harvard Univ Press

Farrow G, Syvitski J, Tunnicliffe V (1983) Suspended Particulate Loading on the Macrobenthos in a Highly Turbid Fjord - Knight Inlet, British-Columbia. Can J Fish Aquat Sci 40:273–288

Gaines SD, Lubchenco J (1982) A Unified Approach to Marine Plant-Herbivore Interactions. II. Biogeography. Annual Review of Ecology and Systematics 13:111–138

Gaston KJ (2000) Global patterns in biodiversity. Nature 405:220–227

Giller PS, O'Donovan G (2002) Biodiversity and Ecosystem Function: Do Species Matter? Biology and Environment: Proceedings of the Royal Irish Academy 102B:129–139

Girard F, Lacharite M, Metaxas A (2016) Colonization of benthic invertebrates in a submarine canyon in the NW Atlantic. Mar Ecol-Prog Ser 544:53–64

Gotelli NJ, Ulrich W (2010) The empirical Bayes approach as a tool to identify non-random species associations. Oecologia 162:463–477

Grange LJ, Smith CR (2013) Megafaunal Communities in Rapidly Warming Fjords along the West Antarctic Peninsula: Hotspots of Abundance and Beta Diversity. PLOS ONE 8:e77917

Hoffmann AA, Sgro CM (2011) Climate change and evolutionary adaptation. Nature 470:479–485

Hooper DU, Adair EC, Cardinale BJ, Byrnes JEK, Hungate BA, Matulich KL, Gonzalez A, Duffy JE, Gamfeldt L, O'Connor MI (2012) A global synthesis reveals biodiversity loss as a major driver of ecosystem change. Nature 486:105–108

Hooper DU, Chapin FS, Ewel JJ, Hector A, Inchausti P, Lavorel S, Lawton JH, Lodge DM, Loreau M, Naeem S, Schmid B, Setälä H, Symstad AJ, Vandermeer J, Wardle DA (2005) Effects of Biodiversity on Ecosystem Functioning: A Consensus of Current Knowledge. Ecological Monographs 75:3–35

Hop H, Pearson T, Hegseth EN, Kovacs KM, Wiencke C, Kwasniewski S, Eiane K, Mehlum F, Gulliksen B, Wlodarska-Kowalczuk M, Lydersen C, Weslawski JM, Cochrane S, Gabrielsen GW, Leakey RJG, Lonne OJ, Zajaczkowski M, Falk-Petersen S, Kendall M, Wangberg SA, Bischof K, Voronkov AY, Kovaltchouk NA, Wiktor J, Poltermann M, Prisco G di, Papucci C, Gerland S (2002) The marine ecosystem of Kongsfjorden, Svalbard. Polar Res 21:167–208

Hoskin CM & Burrell DC (1972) Sediment transport and accumulation in a fjord basin, Glacier Bay, Alaska, J. Geol., 80, 539-551

Hubbell SP (1997) A unified theory of biogeography and relative species abundance and its application to tropical rain forests and coral reefs. Coral Reefs 16:S9–S21

Jantzen C, Haeussermann V, Foersterra G, Laudien J, Ardelan M, Maier S, Richter C (2013) Occurrence of a cold-water coral along natural pH gradients (Patagonia, Chile). Mar Biol 160:2597–2607

Josefson AB, Hansen JLS, Asmund G, Johansen P (2008) Threshold response of benthic macrofauna integrity to metal contamination in West Greenland. Mar Pollut Bull 56:1265–1274

Kortsch S, Primicerio R, Beuchel F, Renaud PE, Rodrigues J, Lønne OJ, Gulliksen B (2012) Climate-driven regime shifts in Arctic marine benthos. PNAS 109:14052–14057

Lambshead PJD, Tietjen J, Ferrero T, Jensen P (2000) Latitudinal diversity gradients in the deep sea with special reference to North Atlantic nematodes. Mar Ecol-Prog Ser 194:159–167

Levin LA, Etter RJ, Rex MA, Gooday AJ, Smith CR, Pineda J, Stuart CT, Hessler RR, Pawson D (2001) Environmental influences on regional deep-sea species diversity. Annual Review of Ecology and Systematics 32:51–93

Levings C, Foreman R, Tunnicliffe V (1983) Review of the Benthos of the Strait of Georgia and Contiguous Fjords. Can J Fish Aquat Sci 40:1120–1141

MacArthur RH, Wilson EO (1963) An Equilibrium Theory of Insular Zoogeography. Evolution 17:373–387

Millennium Ecosystem Assessment 2005. Ecosystems and human well-being: Biodiversity synthesis. World Resources Institute, Washington, D.C., USA.

Miller RJ, Etter RJ (2011) Rock walls: small-scale diversity hotspots in the subtidal Gulf of Maine. Mar Ecol-Prog Ser 425:153–165

Moon H-W, Hussin WMRW, Kim H-C, Ahn I-Y (2015) The impacts of climate change on Antarctic nearshore mega-epifaunal benthic assemblages in a glacial fjord on King George Island: Responses and implications. Ecol Indic 57:280–292

Munday PL, Warner RR, Monro K, Pandolfi JM, Marshall DJ (2013) Predicting evolutionary responses to climate change in the sea. Ecol Lett 16:1488–1500

Naeem S, Wright JP (2003) Disentangling biodiversity effects on ecosystem functioning: deriving solutions to a seemingly insurmountable problem. Ecology Letters 6:567–579

Novotny V, Basset Y (2005) Host specificity of insect herbivores in tropical forests. Proc Biol Sci 272:1083–1090

Patru-Stupariu I, Stupariu M-S, Stoicescu I, Peringer A, Buttler A, Fuerst C (2017) Integrating geo-biodiversity features in the analysis of landscape patterns. Ecol Indic 80:363–375

Payne JR, Driskell WB, Short JW, Larsen ML (2008) Long term monitoring for oil in the Exxon Valdez spill region. Mar Pollut Bull 56:2067–2081

Pearson TH (1971) The benthic ecology of Loch Linnhe and Loch Eil, a sea-loch system on the west coast of Scotland. III. The effect on the benthic fauna of the introduction of pulp mill effluent. Journal of Experimental Marine Biology and Ecology 6:211–233

Pearson TH, Rosenberg R (1978) Macrobenthic succession in relation to organic enrichment and pollution of the marine environment. Oceanogr Mar Biol Ann Rev 16:229–311

Pearson TH (1980) Macrobenthos of Fjords. In: Fjord Oceanography. Springer, Boston, MA, p 569–602

Pickard G (1961) Oceanographic Features of Inlets in the British-Columbia Mainland Coast. Journal of the Fisheries Research Board of Canada 18:907–999

Post E, Forchhammer MC, Bret-Harte MS, Callaghan TV, Christensen TR, Elberling B, Fox AD, Gilg O, Hik DS, Hoye TT, Ims RA, Jeppesen E, Klein DR, Madsen J,

McGuire AD, Rysgaard S, Schindler DE, Stirling I, Tamstorf MP, Tyler NJC, Wal R van der, Welker J, Wookey PA, Schmidt NM, Aastrup P (2009) Ecological Dynamics Across the Arctic Associated with Recent Climate Change. Science 325:1355–1358

Quattrini AM, Nizinski MS, Chaytor JD, Demopoulos AWJ, Roark EB, France SC, Moore JA, Heyl T, Auster PJ, Kinlan B, Ruppel C, Elliott KP, Kennedy BRC, Lobecker E, Skarke A, Shank TM (2015) Exploration of the Canyon-Incised Continental Margin of the Northeastern United States Reveals Dynamic Habitats and Diverse Communities. PLoS One 10:e0139904

Quijon PA, Snelgrove PVR (2005) Spatial linkages between decapod planktonic and benthic adult stages in a Newfoundland fjordic system. J Mar Res 63:841–862

Rahbek C (2005) The role of spatial scale and the perception of large-scale species-richness patterns. Ecol Lett 8:224–239

Ramirez-Llodra E, Brandt A, Danovaro R, De Mol B, Escobar E, German CR, Levin LA, Arbizu PM, Menot L, Buhl-Mortensen P, Narayanaswamy BE, Smith CR, Tittensor DP, Tyler PA, Vanreusel A, Vecchione M (2010) Deep, diverse and definitely different: unique attributes of the world's largest ecosystem. Biogeosciences 7:2851–2899

Rex M, Stuart C, Hessler R, Allen J, Sanders H, Wilson G (1993) Global-Scale Latitudinal Patterns of Species-Diversity in the Deep-Sea Benthos. Nature 365:636–639

Rosenberg R, Agrenius S, Hellman B, Nilsson HC, Norling K (2002) Recovery of marine benthic habitats and fauna in a Swedish fjord following improved oxygen conditions. Marine Ecology Progress Series 234:43–53

Rosenzweig ML (1995) Species Diversity in Space and Time. Cambridge University Press

Rosenzweig M (1992) Species-diversity gradients - we know more and less than we thought. J Mammal 73:715–730

Rosenzweig ML, Sandlin EA (1997) Species diversity and latitudes: listening to area's signal. Oikos 80:172–176

Rowden AA, Schlacher TA, Williams A, Clark MR, Stewart R, Althaus F, Bowden DA, Consalvey M, Robinson W, Dowdney J (2010) A test of the seamount oasis hypothesis: seamounts support higher epibenthic megafaunal biomass than adjacent slopes. Marine Ecology 31:95–106

Ruiz GM, Fofonoff PW, Carlton JT, Wonham MJ, Hines AH (2000) Invasion of coastal marine communities in North America: Apparent patterns, processes, and biases. Annu Rev Ecol Syst 31:481–531

Sandwell DT, Müller RD, Smith WHF, Garcia E, Francis R (2014) New global marine gravity model from CryoSat-2 and Jason-1 reveals buried tectonic structure. Science 346:65–67

Sanford E and Bertness MD (2008) Latitudinal gradients in biological interactions. In: Witman J and Roy G (eds) Marine Macroecology. Oxford Press.

Schluter D, Pennell MW (2017) Speciation gradients and the distribution of biodiversity. Nature 546:48–55

Smith F, Witman JD (1999) Species diversity in subtidal landscapes: maintenance by physical processes and larval recruitment. Ecology 80:51–69

Smith CR, Baco AR (2003) Ecology of whale falls at the deep-sea floor. In: Gibson RN, Atkinson RJA (eds) Oceanography and Marine Biology, Vol 41. Taylor & Francis Ltd, London, p 311–354

Sogin ML, Morrison HG, Huber JA, Mark Welch D, Huse SM, Neal PR, Arrieta JM, Herndl GJ (2006) Microbial diversity in the deep sea and the underexplored "rare biosphere." Proc Natl Acad Sci U S A 103:12115–12120

Syvitski JPM, Farrow GE, Atkinson RJA, Moore PG, Andrews JT (1989) Baffin Island fjord macrobenthos: Bottom communities and environmental significance. Arctic 42:232–247

Tunnicliffe V (1981) High species diversity and abundance of the epibenthic community in an oxygen-deficient basin. Nature 294:354–356

Tunnicliffe V (1991) The Biology of Hydrothermal Vents - Ecology and Evolution. Oceanogr Mar Biol 29:319–407

Violle C, Enquist BJ, McGill BJ, Jiang L, Albert CH, Hulshof C, Jung V, Messier J (2012) The return of the variance: intraspecific variability in community ecology. Trends in Ecology & Evolution 27:244–252

Watts MC, Etter RJ, Rex MA (1992) Effects of spatial and temporal scale on the relationship of surface pigment biomass to community structure in the deep-sea benthos. In: Rowe GT, V Pariente (eds) Deep-Sea Food Chains and the Global Carbon Cycle. Dordrecht: Kluwer Academic Publishers, 245–254

Witman JD, Roy K (2009) Marine Macroecology. University of Chicago Press

Wlodarska-Kowalczuk M, Pearson TH (2004) Soft-bottom macrobenthic faunal associations and factors affecting species distributions in an Arctic glacial fjord (Kongsfjord, Spitsbergen). Polar Biol 27:155–167

Young CM, Tyler PA, Fenaux L (1997) Potential for deep sea invasion by Mediterranean shallow water echinoids: Pressure and temperature as stage-specific dispersal barriers. Mar Ecol-Prog Ser 154:197–209

Chapter 2 : Composition and functional diversity of macrofaunal assemblages on vertical walls of a deep northeast Pacific fjord

Note: This manuscript is currently being revised for a second submission to Marine Ecology Progress Series. The work was completed in collaboration with Di Wan, who analysed the ADCP data and provided edits in that portion of the manuscript.

ABSTRACT

Fjords are temperate zone coastal features with strong horizontal and vertical environmental gradients, but the composition and function of biota living on the confining walls are poorly documented due to relative inaccessibility. We present the results from remotely operated vehicle imagery of the subphotic (50-680 m depth) bedrock walls from three sites in Douglas Channel, a northeast Pacific fjord complex. We assess the composition and abundance of the wall fauna and relate these data to the water mass flux character of the fjord. Using a suite of morphological traits, we also identify areas of high function through habitat formation. This first record of hard substratum benthos in Douglas Channel reveals diverse assemblages marked by vertical zonation, dense animal cover (≥ 80 % areal cover in some areas), and some variation from fjord head to mouth. The deepest portions of the fjord at our most seaward site (≥ 400 m) harbor the most taxonomically and functionally rich assemblages, with multiple species exclusive to this zone, while there is a sharp increase in animal cover in shallow (≤ 150 m) areas; this rise in cover is caused by the appearance of dictyonine glass sponges and increases in articulate brachiopod, zoanthid, and encrusting sponge cover. Animal cover is positively correlated with winter kinetic energy density fluxes, indicating that a consistent oceanic influx augments biomass above 150 m most likely by increasing particle delivery rates. Our findings demonstrate fjord walls support high biomass, high

functioning, diverse, and expansive biosystems that warrant further study and consideration when developing coastal ocean management plans.

INTRODUCTION

Fjords are features of mid to high latitudes formed after the last glaciation that form coastal incisions sometimes hundreds of kilometers in length. As such, they serve as conduits for organisms that normally inhabit offshore regions to venture close to land, such as deep-water fish (Boje et al. 2014) and mammals (Keen et al. 2017). They provide the only close contact humans on land have with ocean depths that can reach 1000 m. In addition, these waterways can form passages for large vessels (e.g. tankers, cargo ships) to access secure inland ports. Fjordic walls often feature hard substrata where steep topography and low sediment loading facilitate settlement of sessile organisms. Deep fjordic areas below the photic zone (i.e. > ~50 m depth) are relatively inaccessible without guided camera systems or submersibles. For this reason, deep vertical bedrock substrata remain a poorly studied ecosystem, with most studies providing only qualitative descriptions of the biota (Wahl 2009).

In shallow (< 50 m) systems, vertical bedrock is dominated by a diverse suspension feeding fauna structured by larval recruitment (Smith & Witman 1999) and water column properties (e.g. ambient flow) that influence the delivery rate (Leichter & Witman 1997) and concentration (Lesser et al. 1994) of particulate organics. Where physical conditions permit, bedrock substrata are densely covered, and space competition becomes the dominant force shaping the diversity of the sessile fauna (Buss 1990). Miller and Etter (2011) showed that the abundance and diversity of organisms on vertical rock were higher than on adjacent horizontal surfaces in the subtidal Gulf of Maine; this

pattern was largely driven by intense competition for space between sessile invertebrates and phototrophs.

Similar processes influence subphotic hard substratum assemblages. Genin et al. (1992) describe high sponge and gorgonian cover on an abyssal rock cliff where local particle fluxes in a boundary current were enhanced. Submarine canyon walls provide refuge from deep-sea anthropogenic disturbances such as bottom trawling, and downslope carbon transport and internal water fluxes can support dense suspension-feeding communities absent from adjacent slopes (Huvenne et al. 2011). Similarly, some seamounts possess high biomass relative to adjacent bottoms, with a great proportion owing to increases in sessile filter-feeding invertebrates and their predators (Rowden et al. 2010). Haedrich and Gagnon (1991) also found a rich suspension feeding fauna covering deep rocky outcrops in a Newfoundland fjord, while muddy slopes and the fjord bottom were sparsely colonized.

The west coast of North America has more fjords than any other fjord province on the planet (Syvitsky et al. 1987), and studies here account for much of the work done on deep fjord epilithos (e.g. Levings et al. 1983). The fjordic environment can change spatially with terrestrial inputs at the landward head and oceanic inputs at the mouth creating steep horizontal gradients in variables such as salinity (Pickard 1961), sediment loading (Carney et al. 1999), larval supply (Quijon & Snelgrove 2005) and succession following disturbance (Moon et al. 2015) over relatively short distances. High productivity and associated sinking particle fluxes create steep gradients with depth in variables such as dissolved oxygen (Anderson & Devol 1973) and pH (Jantzen et al. 2013). Northeast Pacific fjords harbor large expanses of vertical bedrock substrata with

unusual and often dense assemblages along these gradients (Tunnicliffe 1981; Farrow et al. 1983).

The Douglas Channel complex incises the coast of northern British Columbia, Canada for about 95 km with depths to nearly 700 m; it has estuarine-driven circulation with both intermediate depth inflow and annual deep renewal (Macdonald et al. 1983). These features, and the presence of two sills that may influence water exchange, offer the opportunity to examine whether fjord wall communities reflect the vertical mass flux structure of the fjord. We present the results of remotely-operated vehicle (ROV) imaging surveys from three sites in Douglas Channel. Our primary objective was to examine the subphotic animal assemblages on the fjord walls to determine the distribution, abundance, and diversity of macrofauna with depth and location in the fjord, and relate these results to water properties; we tested the hypothesis that the abundance of suspension feeders on the fjord walls is augmented by current strength and direction using vertical current structure records from year-long deployments of two moorings in the inlet. We also assessed the functional diversity of the assemblages using a suite of biological effect traits (Naeem & Wright 2003) related to body morphology and thus, to biogenic habitat formation, to identify areas of high ecological function (Hooper et al. 2005). We expected, based on positive biodiversity-depth relationships on other fjord walls (Haedrich & Gagnon 1991) and the analogous abrupt topographies of submarine canyons (Vetter & Dayton 1998), to find an increase in functional diversity with depth. This study provides the first descriptions of the deep biota of Douglas Channel, where a diluted bitumen pipeline terminus and multiple liquid natural gas projects have been proposed for operation (Enbridge 2010; Hughes 2015). These projects would result in a

sharp increase in tanker traffic, and thus the chance of a hydrocarbon spill that could have long-lasting deleterious effects on the local biota (Webster et al. 1997; Dew et al. 2015). This work provides some baseline information on these previously unstudied assemblages.

MATERIALS & METHODS

Study site

Douglas Channel is part of a fjord complex on the northern coast of British Columbia, Canada, extending about 95 km from the upper estuary to Hecate Strait (Figure 2.1). Two sills approximately 200 m deep define a northern basin (to 400 m depth) and a southern basin reaching 680 m in Squally Channel. The depth ranges at our sites were 50-320 m at Maitland Island, 50-420 m at McKay Reach, and 170-680 m at Squally Reach.

Circulation in the fjord is driven primarily by wind forces and fresh water input from the Kitimat and Kemano rivers and scattered streams. The surface freshwater discharge peaks in May due to snowmelt and again in autumn-winter due to rain (Macdonald et al. 1983). This estuarine surface outflow is balanced by the compensating inflow immediately below the surface from Hecate Strait where the shallow bank constrains the intrusion to intermediate depth of 70-150 m (Wan et al. 2017). The incoming intermediate water from the continental shelf is storm-mixed in autumn and winter, importing nutrients into the fjord system that otherwise generates little *in situ.* Johannessen et al. (2015) describe strong connections in water properties of this layer between the Strait and the fjord throughout the year. An additional nutrient influx comes when wind-driven upwelling onto the Hecate Strait shelf drives annual deep-water

renewal in the fjord. Starting from mid-May to early June, dense shelf water intrudes under the bottom water of Douglas Channel over three months (Wan et al. 2017). After renewal, the temperature profiles are uniform below ~100 m and oxygen concentrations in the deep basins increase by ~1 mL/L to ~3.5 mL/L (Johannessen et al. 2015). The physical and chemical dynamics of Douglas Channel appear to be predictable over decadal time-scales (Macdonald et al. 1983; Wright et al. 2016).

Bedrock formations in Douglas Channel are metamorphic granitoids with gneissic diorite around Maitland and quartz monzonite and diorites in the McKay and Squally sections (Roddick 1970). Fjord structure and wall erosion formed by ice movement during Wisconsonian glaciation; ice retreat, then sea inundation, occurred after 13,000 BP (Clague 1985). As with all of the northeast Pacific coast, the deep fjord communities are post-glacial invasions.

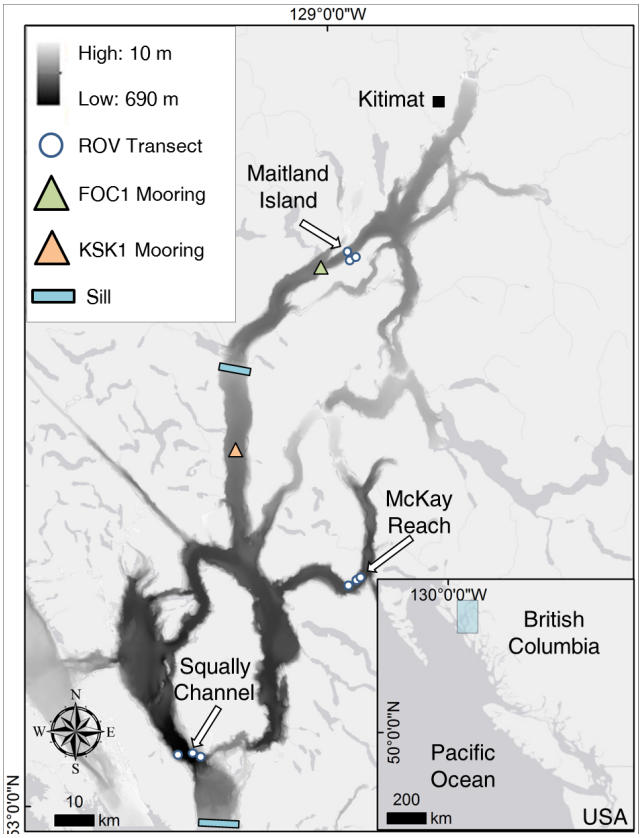

Figure 2.1. Distribution of ROV transects in the Douglas Channel fjord complex and geographic setting of the fjord (inset). Multi-beam bathymetry data are at 10 m grid cell resolution. Three transects were executed at each of three labeled sites starting on the bottom and ascending near-vertical walls. Locations of the two moorings with ADCPs are indicated. The northern sill is 200 m and the southern 140 m depth.

Kinetic energy flux

Kinetic energy flux per unit volume ($uE = \frac{1}{2}\rho \cdot u^3$, where u is the velocity and ρ is the water density; Kundu and Cohen 2008) can be used as a measure of the transport of the kinetic energy across a surface by integrating it over unit area to obtain the kinetic energy flux density ($\sum uE\,\Delta\, a = uEA$, where A is the unit area). The cubic velocity term (u^3) in kinetic energy flux density represents turbulence, and thus is relevant to suspension feeding organisms on the wall; particle encounter frequency increases unimodally with turbulence until drag forces at high current velocities impair the function of feeding appendages (Hart & Finelli 1999). We calculated the kinetic energy flux density (kg m^2 s^{-3}) from along-channel currents measured with Acoustic Doppler Current Profilers (ADCPs) and current meters during the July 2014-2015 deployment at FOC1 and KSK1 (Figure 2.1). The FOC1 mooring was chosen due to its close proximity to the Maitland Island site. KSK1, while located in a neighboring channel, has similar water properties and appears well connected to McKay Reach (Wan unpub. data).

At FOC1, there were single point current meters at 53 and 200 m, an upward looking ADCP at 39 m (300 kHz, 4 m bin size), and a downward looking ADCP at 100 m above the bottom (300 kHz, 4 m bin size). At KSK1, there was a single point current meter at 150 m, and upward looking ADCPs at 40 m depth (300 kHz, 2 m bin size) and at 11 m from the bottom (75 kHz, 16 m bin size). Summer values were calculated from May – September during which the basins underwent deep-water renewal processes, and winter values were calculated from the non-renewal months of October – April.

Wall transects

We selected three sites in areas where bathymetry indicated likely presence of steep to vertical slopes with bare bedrock. In late September 2015, we executed three transects at each of the Maitland Island, McKay Reach, and Squally Reach sites (Figure 2.1). These nine slow vertical ascents conducted with the ROV *ROPOS* formed our transects up the walls. High definition (HD) video, CTD (SBE 19plus V2; Sea-Bird Electronics Inc.) and oxygen probe (SBE43; Sea-Bird Electronics Inc.) data were recorded for each transect. The CTD and oxygen sensors were both mounted on the front of the ROV that maintained a distance of about 1 m from the wall. We collected navigation data on a per second basis using the ROV's internal high-precision ultra-short baseline system. The ROV ascended at ~0.1-0.3 knots (about 10 cm s^{-1}) while imaging the wall surface with a forward-mounted HD 1080i video camera; field of view was 1-2 m across measured by a pair of parallel horizontal lasers calibrated at 10 cm apart. A 12.1 megapixel Nikon D7000 digital camera captured high resolution photographs. Transects ended at about 40 m depth at Maitland and McKay, and at 175 m at Squally Reach where no cliffs occurred above this depth.

Video and image analyses

Image analysis incorporated two stages: i) initial full video scan to characterize the entire wall surface encountered and to generate estimates of faunal cover; and ii) detailed still frame analysis of overlaid quadrats on vertical walls. Thus, first, we annotated the video transects using VideoMiner (version 2.1.2.0; custom Fisheries and Oceans Canada video annotation software) to create: i) a second-to-second database of visually assessed habitat characteristics including the four dominant substratum types (sediment, bedrock, shell hash, and dead sponge), ii) percent cover estimates for dominant substrata and

vertical relief (i.e. estimated slope), and iii) estimates of the percentage of substratum occupied by organisms. Every ten seconds, we noted the presence of major taxonomic groups. Over the nine transects, the database includes over 78,000 non-overlapping records of substratum and biological observations, along with CTD data synchronized by timestamp (Table S1). Kinetic energy flux density values were generated in 1 m increments by spline interpolation between data points separated by 16 m; these 1 m values were then averaged into 10 m depth bands and related to faunal cover estimates via linear regressions.

For the second stage of analysis, we queried portions of the video with slope greater than 45º to isolate segments with vertical or near-vertical walls, low to moderate sediment drape, and bedrock as the primary substratum. Video framegrabs (n=5 or 6) in each 25 m depth band from the bottom up to 50 m provided the basis for a quadrat analysis using PhotoQuad software (Trygonis & Simi 2012). A grid of numbers from 1-100 was overlain on the framegrab; a 1 m^2 quadrat, overlain on the framegrab, was centered on a randomly chosen number or aligned with the nearest edge when the number was < 50 cm from the image border. All animals over 0.5 cm were measured for size and identified to the lowest possible taxonomic resolution using image matching with published and in-house guides plus past collections. Where possible, our identifications were verified using higher-quality digital photographs. In several cases, local experts corroborated our tentative identifications. Table S2 notes where species level is not possible and where two species are similar in appearance. We did not include hyperbenthic organisms (e.g. teleost fishes) if they were out of frame in the five seconds of video prior to, or after, the framegrab. This approach excluded passing organisms

attracted to the ROV lights (e.g. halibut), but included non-ephemeral mobile species (e.g. rockfish). We also excluded serpulid (Annelida) tubeworms, despite their near-ubiquity, from the quadrat analysis because it was not possible to confirm that the calcareous tubes contained living animals. Overall, this image analysis comprised 236 quadrats across the depth ranges of the three sampled sites.

Diversity analyses from quadrats

A "per depth band' species-abundance matrix was created from animal identifications and counts from still frames. Then, we calculated species richness and two taxonomic distinctness indices of Clarke and Warwick (2001) using the R package 'Vegan' (Oksanen et al. 2017); taxonomic distinctness indices included both an index that does ($s\Delta+$) and does not ($\Delta+$), incorporate species abundances during calculation.

Species count data from quadrat sampling were also analysed using the multivariate statistical software package PRIMER 6 (Clarke & Gorley 2006) with PERMANOVA (Anderson et al. 2008). Raw count data were square root transformed prior to analysis to account for the contribution of low-abundance taxa to assemblage structure without eliminating the signal from abundant species. Assemblages in the data were identified by hierarchical cluster analysis (CLUSTER) on the quadrat resemblance matrix with a similarity profile (SIMPROF) test (at $p = 0.05$). The percentage similarity (SIMPER) routine was employed to determine the taxa contributing to the differences between each SIMPROF assemblage. In order to determine the species contributions at the site level, we ran a SIMPER analysis for each site using count data; to reduce noise and include a larger species complement in each pairwise comparison, counts were binned into 25 m depth bands for the site analysis. We visualised patterns in the grouping of samples

by site and by SIMPROF-determined assemblage in two dimensions using canonical analysis of principal coordinates (CAP) plots.

A permutational multivariate analysis of variance (PERMANOVA) described the variability in assemblage structure between sites. Before the PERMANOVA, a distance-based homogeneity of multivariate dispersions (PERMDISP) test calculated with 999 permutations was employed to test for significant dispersion in the data; the deviations from centroid method was chosen to increase power and lessen the chance of Type I error (Anderson 2006). The PERMANOVA, with Type III (partial) sums of squares and 999 unrestricted permutations of raw data, included Site as the only factor in the design.

The degree to which environmental variables correlated with the assemblages was assessed with a distance-based linear model (DistLM) using all the quadrats in the fjord. Environmental variables were normalised (mean = 0 and unit variance) and assessed for covariance in PRIMER 6 using correlation matrices; if the Pearson correlation coefficient between two variables was greater than 0.9, one of the variables was removed (Anderson et al. 2008). Depth, temperature, dissolved oxygen, relief, areal animal cover, and areal bedrock cover were included in the null model. Final model selection was carried out using Akaike's Information Criteria (AICc) and a 999 permutation stepwise selection procedure. AICc was chosen as the most conservative method to create a parsimonious model, as it penalizes for excess model parameters (Burnham & Anderson 2004). A distance-based redundancy analysis (dbRDA) displayed the DistLM results in two dimensions, with quadrats identified by their SIMPROF-determined assemblage and vectors displaying individual contributions to the total variation for each variable.

We compiled a species-trait matrix from the quadrat analysis with functional trait modalities for six ordinal and factor traits (Table 1). For this analysis, we chose traits based on both pragmatism – given the paucity of behavioral and life-history data for our component species – and relevance to ecosystem properties through biogenic habitat formation (Hooper et al. 2005). The 'habitat provision' trait refers to whether a species likely provides a three-dimensional habitat (e.g. arborescent corals) or may possibly provide a habitat (e.g. shelled species) for other organisms. We analyzed our species-trait matrix in conjunction with a 'per depth band' species-abundance matrix in R (R Core Team 2013) using the 'FD' package (Laliberté & Legendre 2010) to calculate distance-based estimates of functional evenness (FEve; Villeger et al. 2008) and functional dispersion (FDis; Laliberté & Legendre 2010), along with a dendrogram to visualise the clustering of species by traits. The use of solely ordinal and factor traits precluded the calculation of functional richness using a convex-hull approach, and therefore was measured as the proportion of unique trait combinations in a given depth band over the number of unique trait combinations in the entire species pool (sUTC; Keyel & Weigand 2016).

Table 2.1. Functional traits scored for all species (n = 53) recorded in spaced still frame quadrats.

Functional Trait	**Type**	**Modalities**
Growth Form	Factor	Determinate (prone); Determinate (erect); Indeterminate (mound); Indeterminate (tree); Indeterminate (encrusting)
Preferred Substratum	Factor	Bedrock; Sedimented bedrock; Sediment
Motility	Factor	Sessile; Sedentary; Surface motile; Swimming
Habitat Structure	Factor	Tube; Free-living; Epizootic; Shelled
Log_{10} body size	Ordered Factor	Indexed from 0-2; log_{10} max body/colony size
Habitat Provision	Ordered Factor	Likely; Possible; None

RESULTS

In late September 2015, temperature at our study depths (50-680 m) decreased from 9º C to 7.5º C from 50 to ~175 m, then to fairly uniform temperatures (~ 7.2º C) below ~ 200 m at Maitland and McKay transects; temperatures at Squally were 0.5 to 1.0º C warmer (Figure 2.2). Dissolved oxygen generally remained above ~2.5 mL/L at all locations. The along-channel kinetic energy flux density plots (Figure 2.3) showed strong surface outflux with an underlying influx at both locations in both seasons, which correspond to previously described estuarine-driven two-layer circulation in the channel. In winter, at both instrumented locations, the influx spanned the range from about 40 to 120 m depth while summer influx was a narrower band with a bottom inflow evident near Maitland Island.

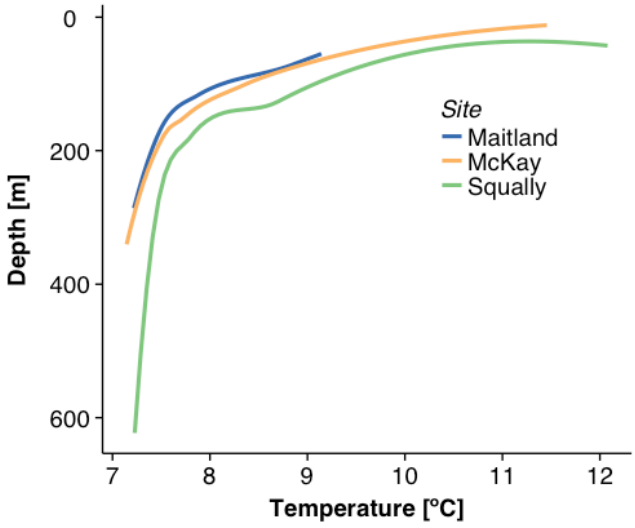

Figure 2.2. Temperature profiles taken during ROV descent at each site surveyed in Douglas Channel from ROV-mounted CTD in late September 2015. Each line is from one representative downcast, smoothed to remove noise caused by the ROV's variable descent rate. Profile shapes illustrate the steady temperature decrease from 40 to 150 m at the two northerly sites while Squally Reach temperatures are approximately a half-degree warmer at comparable depths.

Distribution of habitat

Substratum features varied by site in the fjord. At both Maitland Island and McKay Reach, the substratum was largely comprised of bare bedrock: 57% and 76% of the video records, respectively (Table A.1). At Squally Reach, sediment drape predominated in 71% of the records, largely due to the greater presence of low relief and stepped slopes. Biogenic substrata, which included shell hash composed of brachiopod/bivalve shells and glass sponge skeletons, were uncommon (<5% of records) at the Maitland and McKay sites and absent at Squally. Fauna appeared specific to the substratum type. Bare bedrock substrata were usually densely covered and dominated by sessile species, with colonial and encrusting forms as the main space competitors. Sedimented areas were more sparsely covered, with mobile species dominating the fauna. While shell hash was nearly devoid of animals save for the occasional mobile organisms, rockfish and crustaceans were common in the three-dimensional habitat of dead glass sponges.

Animal distributions in continuous video transects

A total of 53 taxa (>0.5 cm) from nine phyla were seen in the continuous transects, although it was not possible to identify all to species level (Figure A.2). Hexactinellid sponge species are distinguished by examination of spicules; thus, dictyonines included *Aphrocallistes vastus* and *Heterochone calyx,* and lyssacines included *Rhabdocalyptus dawsoni* and *Staurocalyptus dowlingi*. The glass sponge *Farrea occa* was seen in the continuous video but not in any of the subsequent quadrats. Tubes of the serpulid annelids *Serpula vermicularis* and *Protula pacifica* were present

throughout the fjord at all depths, but could not be confirmed alive or identified to the species level unless their branchial crowns were extended for feeding.

Animal assemblages on the walls ranged from scattered individuals on sediment-draped surfaces to near 100% cover on steep walls and overhangs to complex three-dimensional habitats formed by hexactinellid sponges as illustrated in Figure 2.4a. Differences in assemblage composition with depth and site are represented in Figure 2.5 based on presence/absence of major groups. Below we describe faunal distribution results as the data were collected – i.e., ascending from the bottom.

Serpulid worm tubes, asteroids, echinoids, decapods, non-hexactinellid sponges, and actinarians spanned the entire depth range sampled at all sites. Gastropods occurred at nearly all depths but decreased in the uppermost ~50 m of Maitland Island and McKay Reach. The comatulid crinoid *Florometra serratissima* (often associated with sponges) and cup corals of the genus *Caryophyllia* extended above 200 m in some areas, but were much more common deeper (Figure 2.4e). The brittle star *Ophiopholis aculeata* was limited to water below ~300 m, and was not seen in the Maitland transects. Other taxa with a deep-water affinity include lyssacine glass sponges that occurred sporadically from ~200 m to the bottom of the Squally Reach transects, and the articulate brachiopod *Laqueus vancouveriensis* that had a near-ubiquitous presence below 200 m (Figure 2.4c, 2.4e, 2.4f).

A few pairs of related taxa showed separation by depth. Above 200 m, the inarticulate brachiopod, *Novocrania californica*, was very common (Figure 2.4a) at these depths, and articulate brachiopods decreased. The shift from articulate to inarticulate brachiopod presence occurred at ~150-180 m at Maitland and McKay and ~300 m at

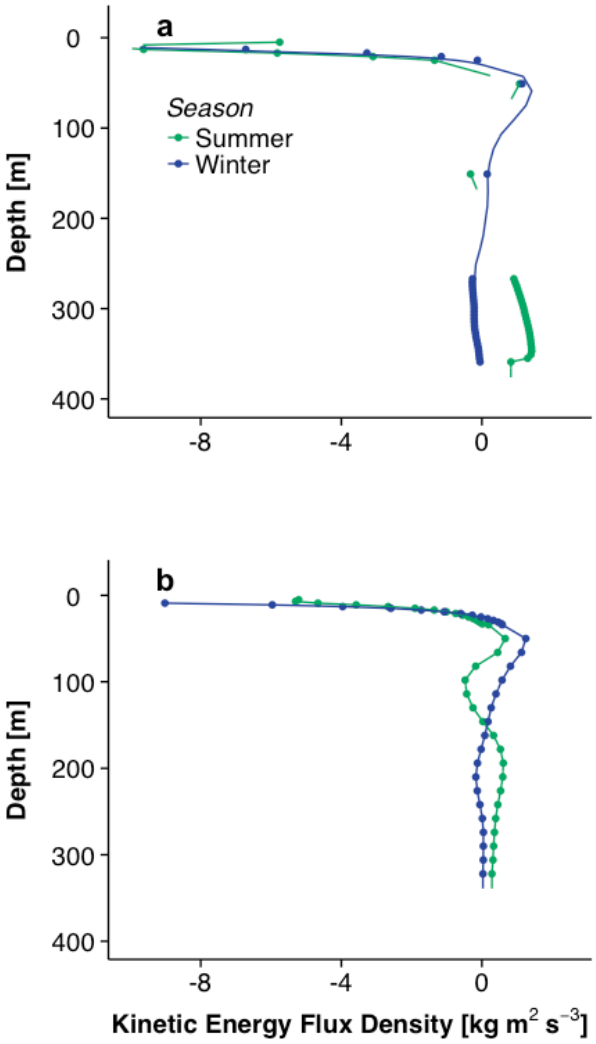

Figure 2.3. Along-channel kinetic energy flux density ($\frac{1}{2}\rho \cdot u^3$) calculated from a) FOC1 (near Maitland) & b) KSK1 ADCP moorings during July 2014-July 2015 deployments. Points are measured values with lines connected by spline interpolation. The negative flux is in the down-fjord direction, and the positive flux is in the up-fjord direction. Flow structure varies between summer (May to mid-September) and winter (October to April) due to a summer bottom renewal layer. In the upper 150 m, the energy flux density increases and peaks at the surface (outflow) and 50-70 m inflow, reflecting the estuarine circulation pattern.

Squally. Rockfish below 200 m occurred in topographically complex areas (e.g. locations with step-relief, overhangs, or dead glass sponge skeletons), but were more common in shallower areas where biogenic habitats were more abundant. Dictyonine glass sponges dominated many of the steep-wall assemblages above 150 m along with a unique co-occurring fauna that included relatively high densities of decapod crustaceans and rockfish (Figure 2.5a). Two numerous anthozoan taxa also had non-overlapping depth distributions; cup corals and zoanthids occurred mostly below and above ~200 m, respectively.

Mean animal cover estimates combined across all transects at the three sites were relatively low in the deeper reaches, then increased in variability around 250 m with a sharp increase at 150 m. Mean cover continued to increase incrementally above 100 m, and reached a maximum of 33% at 40-50 m (Figure 2.6a). In the 150-400 m depth ranges, no unique taxa were present, although arborescent corals were most commonly found here. While fewer taxonomic groups were present in the mid-depths than the deep reaches, cover was similar and ranged from ~3-10% per 10 m depth band (Figure 2.6a). Cosmopolitan groups such as articulate brachiopods, serpulid annelids, demosponges, actinarians, and gastropods dominated mid-depth walls. The sharp increase in cover seen at 150 m coincided with the appearance of dictyonine glass sponges, inarticulate brachiopods and zoanthid patches, all of which reached high densities above 150 m. Encrusting sponges also became more abundant and larger, contributing to the high cover.

Percent animal cover was positively correlated with winter kinetic energy flux densities (linear regression, $p < 0.001$, $r^2 = 0.75$, $F_{1,28} = 85.39$), with a predicted percent cover of 7.56 + 18.14 * flux density (Figure 2.6b) while summer fluxes were not ($p > 0.05$). The greatest landward (i.e. positive) fluxes occurred in the winter, while the strongest outflow fluxes were in summer (Figure 2.6b).

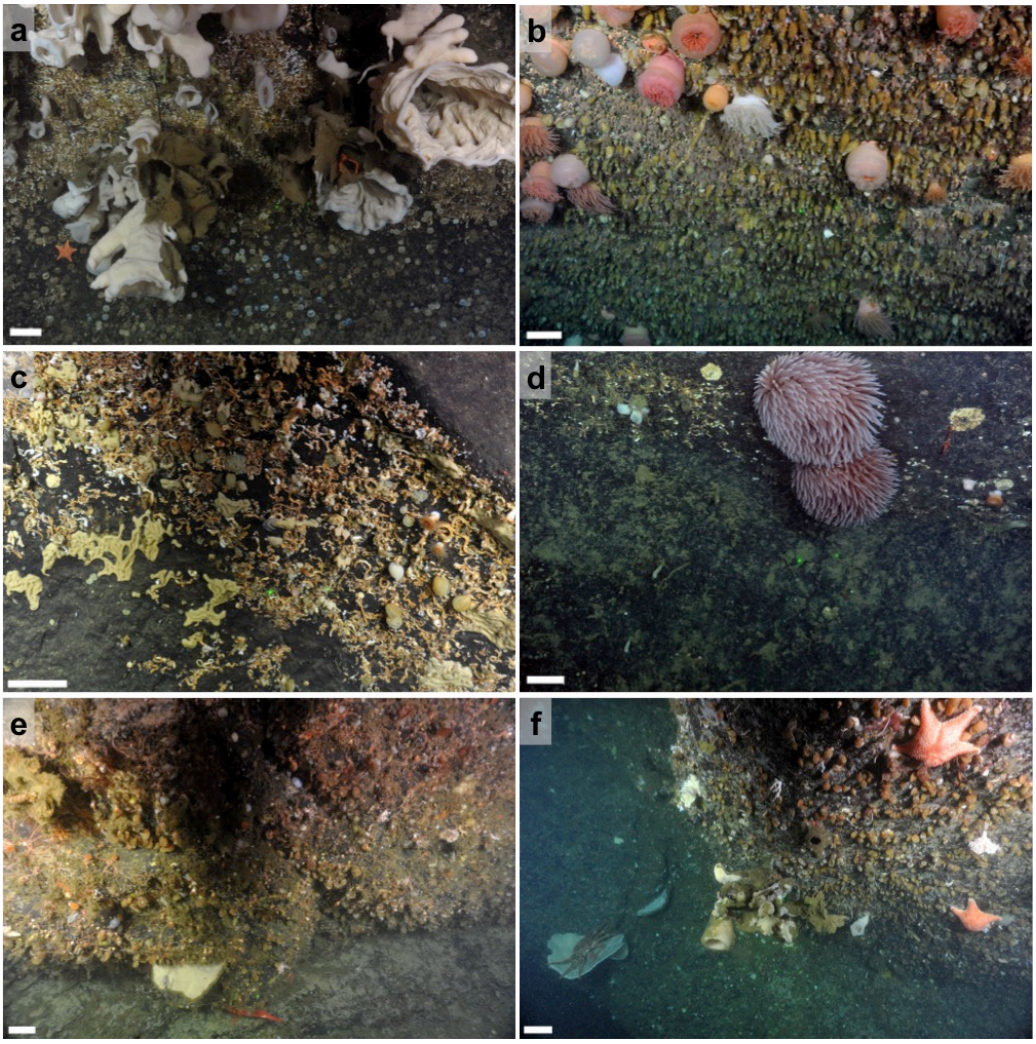

Figure 2.4. Douglas Channel assemblages representative of depth zonation: above 150 m (a and b), 150 to 400 m (c and d), and below 400 m (e and f). Scale bars are approximately 10 cm across. Image contrasts are increased to account for backscatter in water column.

a) Maitland Island: dense cover by hexactinellid sponges, serpulid tubes, and inarticulate brachiopods;

b) McKay Reach: zoanthid patches and anemones;

c) McKay Reach: articulate brachiopods, demosponges, and serpulid worms on slight overhang;

d) Maitland Island: lightly sedimented bedrock sparsely covered by demosponges and anemones;

e) Squally Reach: brittle stars, articulate brachiopods, cup corals, and a rockfish under a plate-like demosponge on a wall with accumulated sediment;

f) Squally Reach: asteroids, articulate brachiopods, brittle stars, a Dungeness crab, and an array of sponges on a deep wall

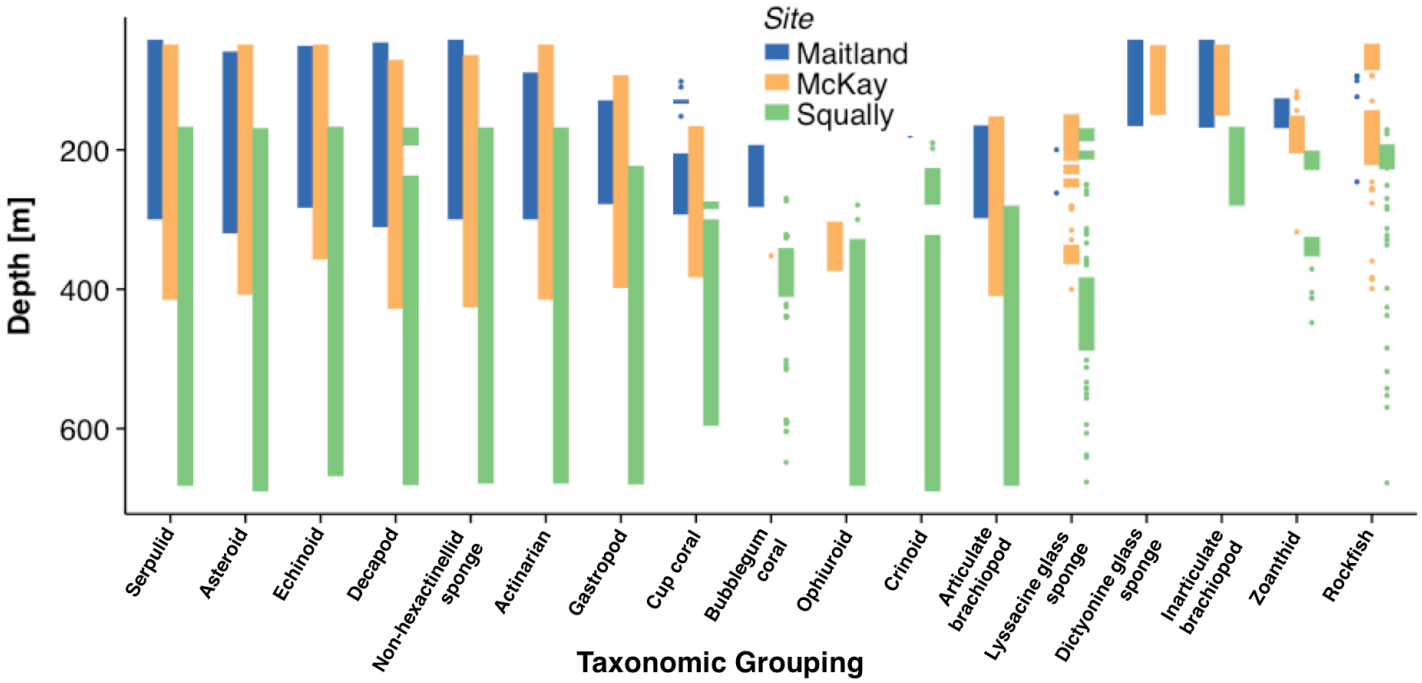

Figure 2.5. General distributions of major taxonomic groups at each of the sites in Douglas Channel from continuous video presence/absence records. For a list of species that belong to each taxonomic group, see Table A.2. The first seven groups are nearly ubiquitous at the observed depths of all sites while cup corals to lyssacine glass sponges are more common in deeper water. Dictyonine glass sponges to rockfish are more commonly observed in shallower areas. The glass sponge groups separate by depth, as do the articulate and inarticulate brachiopods.

Animal distributions in spaced still frames

Depth zonation was also evident in records of species abundances in one square meter quadrats (Figure 2.7). Both the sponge *Auletta krautteri* and the pom-pom anemone *Cribrinopsis fernaldi* occurred throughout the depth range at low mean abundances when present (3.0 and 1.4 m^{-2}, respectively), with highest densities below 200 m. Arborescent corals were sparsely distributed; the small *Antipathes,* present only in Squally Reach quadrats, reached the highest densities at 189 m depth, and only *Primnoa pacifica* occurred in quadrats above 150 m. A small number of species contributed to increasing densities in shallower water (Figure 2.7). The brachiopod *L. vancouveriensis* was most

abundant at 250 m, decreasing to low density patches (≤5 m^{-2}) above 150 m in cryptic environments (e.g. overhangs), while the inarticulate brachiopod *N. californica* densities below 200 m (≤ 30 m^{-2}) increased three-fold above ~180 m at Maitland and McKay. Dense patches of the zoanthid *E. scotinus* occurred primarily above 180 m further up the fjord. The encrusting sponges *Clathrina* cf. *coriacea* and *Plakina atka,* both nearly ubiquitous from 680 m upward, achieved their highest densities up the upper 150 m (Figure 2.7); *P. atka* covered more than 25 percent of the available space in some areas. *Hexadella spp.*, another encrusting sponge, showed similar space occupation with a peak around 200 m. Highest coverage by dictyonine glass sponges occurred in the shallowest portions of the transects as seen in the continuous assessment (Figure 2.5).

Distinct species assemblages

PERMDISP analysis of quadrats showed no significant dispersions for the 'Site' factor ($F_{2,232}$ = 0.42553, p[perm]=0.647). Although the subsequent PERMANOVA results indicate that animal assemblages were significantly structured by Site (df=2, SS=68,289, MS=34144, Pseudo-F=11.467, p[perm]=0.001), CAP-visualization of our cluster analysis displayed substantial overlap among the assemblages at the three sites with little apparent pattern of clustering in the site-level structure of quadrat assemblages (Figure 2.8a). However, clustering was more apparent from 175-300 m, where the three sites overlap (Figure 8b).

Cluster analysis and the subsequent SIMPER test identified the taxa that contributed most to the similarity between 25 m depth bands at each site (Table 2.2). The demosponge *P. atka* contributed the most to the among-depth-band similarity at McKay and Squally, while the inarticulate brachiopod, *N. californica*, was the largest contributor for Maitland quadrats.

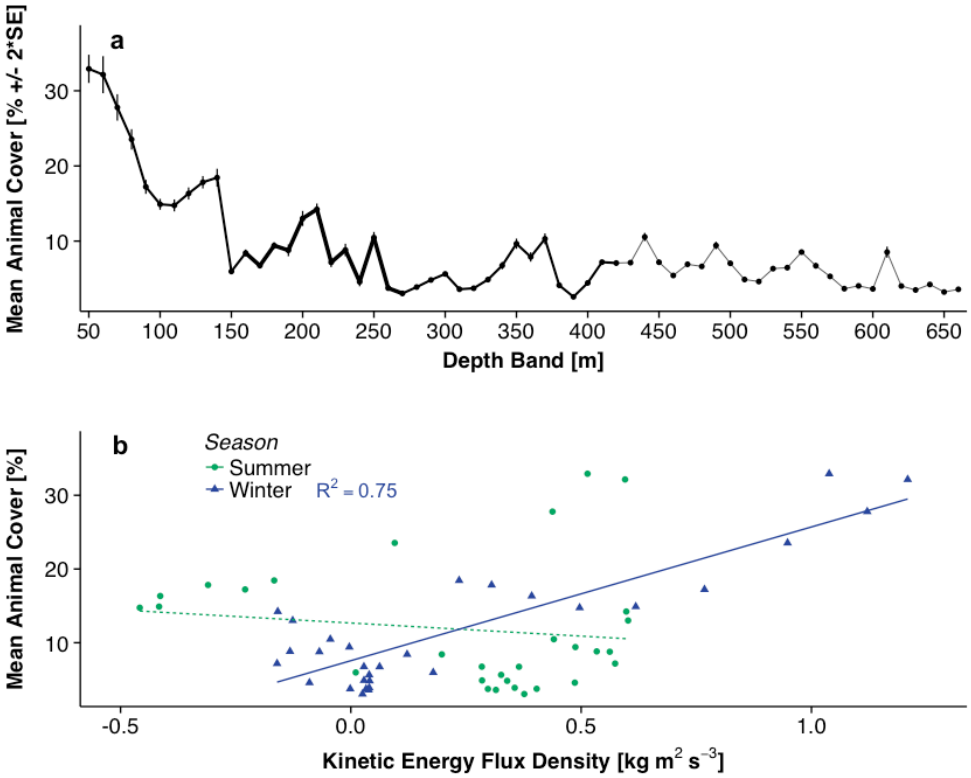

Figure 2.6. a) Mean animal % cover by 10 m depth band composited across all sites estimated in every 10-second interval in the continuous video transects. Line weight increases with number of sites included in the depth band, with one being the thinnest line and three being the thickest. Standard error calculated from all transects available for a given depth band. Cover is relatively constant at all depths below 150 m, but increases shallower than 150 m.

b) Mean animal % cover versus mean seasonal kinetic energy flux density for each 10 m depth band. Kinetic energy flux values are from mooring KSK1; mean fluxes per 10 m depth band were calculated by averaging values in 1 m increments along spline interpolated line (see Figure 3b) into 10 m bands. Solid and dashed lines show significant ($p<0.05$) and non-significant ($p>0.05$) linear regressions, respectively.

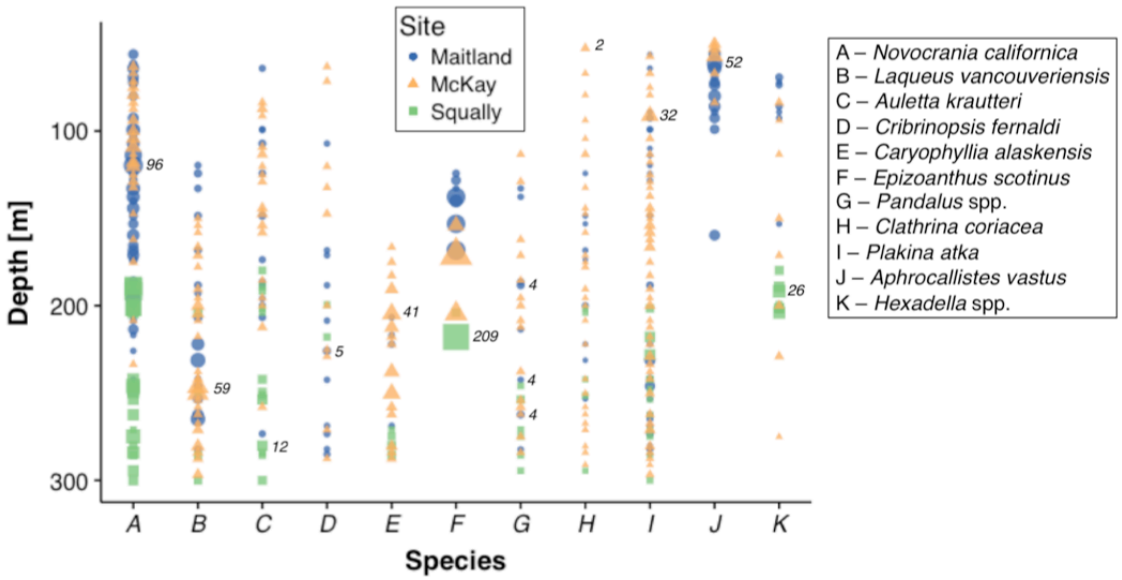

Figure 2.7. Depth distributions of the eleven most common taxa above 300 m from still frame quadrats. Symbol size denotes abundance plotted as counts per quadrat for solitary organisms (A-G) and mean cover per quadrat for colonial/encrusting organisms (H-K). Peak m^{-2} densities, represented as counts or percent cover, are annotated for each species.

The SIMPROF analysis displayed six unique assemblages in quadrats across the three sites (Figure 2.8b), and the consequent SIMPER analysis described the taxa comprising each group (Table 2.3). Similarity within assemblage VI, the most common in the fjord, was driven by the near-ubiquitous *P. atka* and species that occurred from mid-depths down. Assemblage V, the second most common, was dominated by *N. californica*, the inarticulate brachiopod that primarily occurred above ~150 m. No assemblages were unique to one site, although assemblage I, composed primarily of mobile species, was not present at Maitland Island. The uncommon I and III assemblages were associated with sparse cover and composed of few species. More than eighty

percent of the similarity among quadrats within the II, IV, and V assemblages was driven by a single species (*Hexadella spp., E. scotinus,* and *N. californica*, respectively).

The best DistLM model included all but one of the null model environmental parameters ($R^2 = 0.22$, RSS = $5.94x10^5$; in order of decreasing explanations of variance: depth, animal cover, temperature, relief and dissolved oxygen; Table 2.4). A dbRDA plot (Figure 2.8c) shows the contributions of each variable to the model, in which Assemblage VI associated most closely with the depth vector. All other assemblages displayed no apparent trend along the environmental variable vectors.

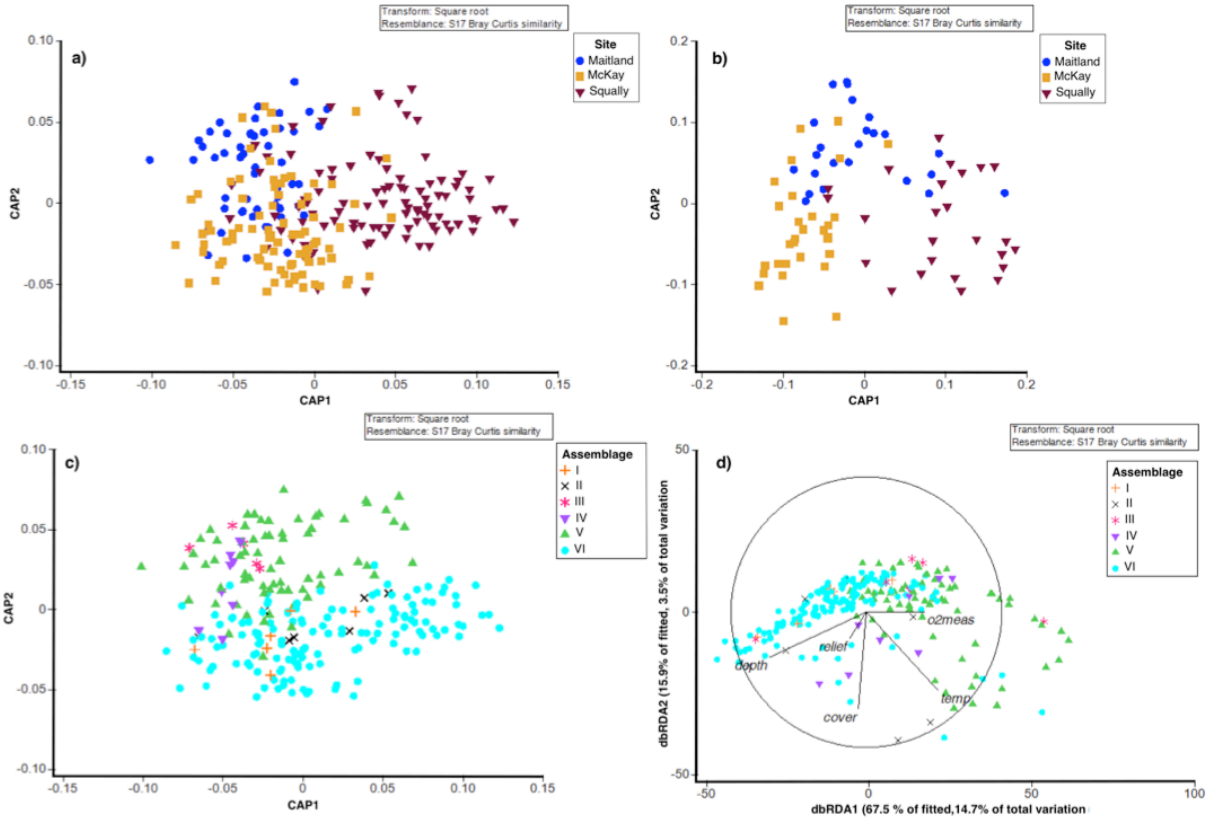

Figure 2.8. Canonical analysis of principal coordinates (CAP) plots of quadrat samples examined by:
a) site (all depth ranges), and
b) site (overlapping depth ranges, i.e. 175 – 300 m)
c) SIMPROF-determined assemblages (I-VI; see Table 2.2).
d) Distance-based redundancy analysis (dbRDA) plot of DistLM results in two dimensions using assemblages I to VI. Length of variable vector is proportional to contribution to the total explained variance (see Table 2.3).

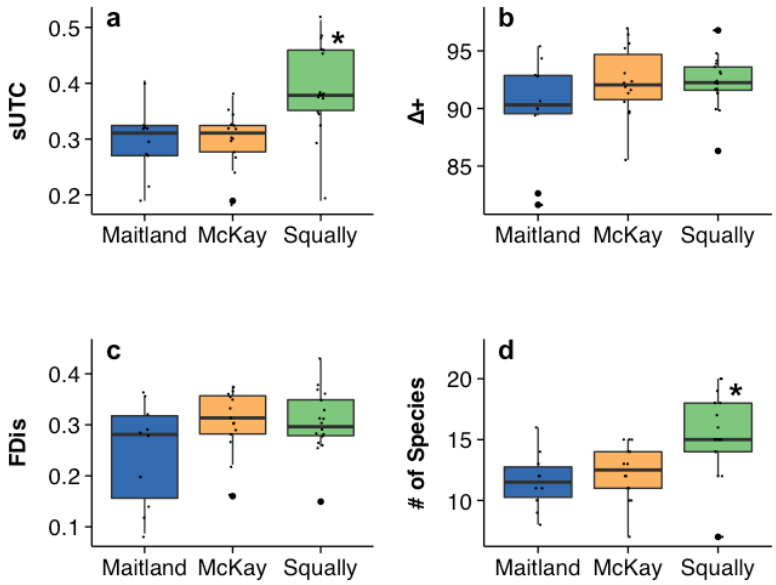

Figure 2.9. Boxplots showing site-by-site comparisons of taxa scored in quadrats. Variables were calculated for 25 m depth bands. Bolded black lines represent median values, while the upper and lower edges of the boxes show second and third quartiles of the data, respectively. Whiskers represent the edges of the first and fourth quartiles and large dots are outliers. Asterisks indicate significant differences between sites as determined by Welch's ANOVA ($p < 0.05$).
a) unique trait combinations in a sample versus the entire species pool (sUTC);
b) taxonomic distinctness (Δ+);
c) functional dispersion (FDis);
d) number of species.

Table 2.2. Taxon composition by SIMPER for 25 m depth band comparisons among and between sites. Group similarity is among 25 m depth bands at each site. Pairwise similarity is between 25 m depth bands between sites. The cut-off for cumulative percentage to group similarity is 95%. Species contributing over 10% are brachiopods (*N. californica* and *L. vancouveriensis*), sponges (*P. atka* and *C.* cf. *coriacea*) and the cup coral, *C. alaskensis*.

Assemblage	Average Pairwise Similarity (%)	Group Similarity (%)	Taxa (contributing % similarity)
Maitland	McKay – 18.1 Squally – 17.3	25.4	*N. californica* (61.9), *P. atka* (14.9), *L. vancouveriensis* (6.4), dictyonines (3.4), *A. krautteri* (3.1), *C. fernaldi* (2.0), *E. scotinus* (1.4), *S. pallidus* (1.0), *C. coriacea* (1.0)
McKay	Squally – 21.5	23.9	*P. atka* (44.5), *L. vancouveriensis* (16.2), *C. coriacea* (13.9), *N. californica* (7.0), *C. alaskensis* (6.5), *A. krautteri* (3.1), *Pandalus* (3.0), *S. pallidus* (1.1)
Squally	-	26.2	*P. atka* (24.9), *C. alaskensis* (13.9), *C. coriacea* (10.4), *N. californica* (10.1), *L. vancouveriensis* (6.6), *O. aculeata* (6.4), *Hexadella* (4.9), *A. krautteri* (4.7), *C. platinum* (4.1), *Antipathes* (3.8), Porifera1 (3.6), *Pandalus* (2.4)

Table 2.3. Taxon composition by SIMPER for the SIMPROF-determined assemblages (a-f). Group similarity is between quadrats within the assemblage group. The cut-off for cumulative percentage to group similarity is 95%.

Assemblage	Group Similarity (%)	Taxa (contributing % similarity)
I	32.0	*Pandalus* (71.2), *F. oregonensis* (11.5), *C. alaskensis* (6.5), *O. aculeata* (5.8)
II	33.5	*Hexadella* (86.2), dictyonines (3.3), *C. alaskensis* (2.1), *C. fernaldi* (1.4)
III	50.0	*C. fernaldi* (78.1), *N. californica* (21.9)
IV	48.5	*E. scotinus* (80.8), *N. californica* (11.1), *L. vancouveriensis* (2.5), *P. atka* (1.8)
V	40.9	*N. californica* (80.7), *P. atka* (7.0), *A. krautteri* (4.6), *C. coriacea* (1.4), *S. pallidus* (1.1), dictyonines (1.0)
VI	30.6	*P. atka* (42.5), *L. vancouveriensis* (16.4), *C. coriacea* (12.8), *C. alaskensis* (11.8), *O. aculeata* (3.3), *C. platinum* (2.5), *A. Krautteri* (2.5), *Pandalus spp.* (1.7), Porifera1 (1.30), *Hexadella* (1.1)

Table 2.4. DistLM Pseudo-*F* values and the amount of variance explained by each variable selected by DistLM as part of the best model.

Environmental variable	Pseudo-*F* value	Proportion of explained variance	Cumulative explained variance
Depth	32.53	0.12	0.12
% Animal Cover	9.43	0.034	0.16
Temperature	9.42	0.033	0.19
Relief	4.36	0.015	0.20
Dissolved Oxygen	3.78	0.013	0.22

Functional and taxonomic diversity

Significant differences between sites in the 25 m depth bands were shown for mean sUTC (Welch's ANOVA, $p < 0.01$, df = 2, 22.51, F = 7.96) and species richness (Welch's ANOVA, $p < 0.01$, df = 2, 23.70, F = 6.84); Squally Reach had a significantly greater mean value than the other sites for both sUTC and species richness (Games-Howell post-hoc test, $p < 0.05$ for both; Figure 2.9a and 2.9d). Taxonomic distinctness (Δ+), on the other hand, was not significantly different between sites (Welch's ANOVA; $p > 0.05$), and had high (> 90%) median values at each site (Figure 2.9b). Neither FDis (Figure 9c) nor FEve differed significantly between sites (Welch's ANOVA, $p > 0.05$), although FDis was more varied at Maitland. Taxonomically related species often did not cluster together, and mobile species clustered separately from sessile species (Figure A.3.)

There were no obvious trends with depth for FEve, FDis, and Δ+, but sUTC and sΔ+ decreased sharply above ~325 m at Squally Reach (Figure 2.10a). sUTC and sΔ+ were similar between Maitland and McKay at all depth bands deeper than 100-125 m. Both steadily decreased at McKay above 175 m with an increase in the uppermost 50-75 m depth band. Quadrats shallower than 200 m had significantly lower values for both sUTC and sΔ+ (ANOVA; $F_{1,39} = 8.38$ & 7.51, respectively; $p < 0.01$ for each; Figure S1). There were no apparent trends with depth for FEve or FDis, but three of the four depth bands with Δ+ below the calculated 'expected value' of Δ+ (i.e. under the assumption of random assembly from the entire species pool) were above 100 m (Figure A.2). The relatively low mean FDis (~0.3) suggests that, per depth band, the abundance-weighted divergences in species traits within assemblages were relatively small. sUTC and the

number of species per 25 m depth band were significantly positively correlated, indicating a low level of functional redundancy on the depth band scale (Spearman's Rank Correlation = 0.96, $p < 0.01$; Figure 2.10b).

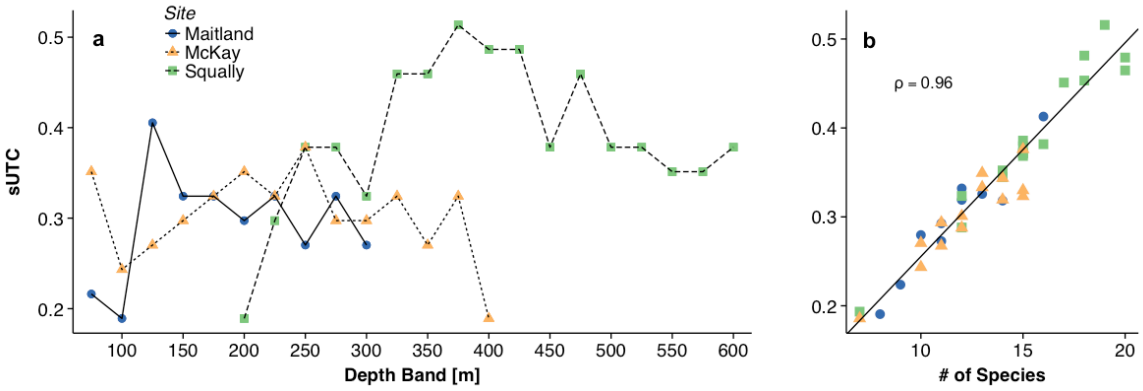

Figure 2.10. a) Line plot of proportions of unique trait combinations (sUTC) by depth band and location. Depth labels represent the base of each band. Both sUTC and taxonomic distinctness • richness (sΔ+, not shown) identify greater diversity below 300 m in Squally Reach than at all other depths in the fjord.
b) Relationship between sUTC and number of species in each 25 m depth band. The linear relationship proceeds throughout the entire range of species richness, indicating low functional redundancy at the depth band scale at all sites.

DISCUSSION

This first record of the deep hard substratum fauna in the Douglas Channel complex reveals a suite of diverse assemblages marked by vertical zonation, expanses with dense cover, and variation along the fjord head-mouth axis. We recorded 53 species (or species groups) representing nine phyla and 38 orders from the nine transects. The spatial dominance by large sessile invertebrates and the lack of evidence for recent mass recruitments indicate that these assemblages are primarily composed of perennial species, and thus are shaped over long timescales.

Vertical walls form a substantial component of the total benthic habitat in fjordic environments. We estimate, using the mean depth and coastline length of Douglas Channel from Macdonald et al. (1983), that walls represent ~20 % of the fjord's total benthic area; the majority of these cliffs surveyed in the current study were unsedimented (Table A1), and thus available for colonization. Although this estimate may be high due to our site selection for steep topography, most low-relief walls with moderate-to-heavy sediment drape were colonized by organisms while adjacent flat areas were not. Guided submersible systems are required to investigate these steep bedrock substrata, as standard deep-sea sampling techniques (e.g. grabs, towed camera systems, etc.) do not suffice. For this reason, the contribution of deep wall habitats to ecosystem diversity and function remains nearly unknown.

Depth-related distributions

Most of the mobile species and larger sessile animals documented were eurybathic, but some taxa (six of the 17 documented groups) were primarily seen below 400 m. As only Squally Reach extended below 400 m, it is possible that these taxa were also constrained by site (near the fjord mouth) as well as depth. The bubblegum coral *P. arborea* and crinoid *F. serratissima*, for example, were primarily seen from 200 m to below 600 m and at Squally Reach, but records of these species exist in shallower waters (e.g. Stone 2014), including elsewhere in Douglas Channel (Gasbarro unpub. data).

Mean animal cover above 150 m reached a peak at 40-50 m nearly three times that of the average cover across all depths. High densities of glass sponges in the upper 150 m are similar to those in Leys et al. (2004), who surveyed 11 BC fjords and found the highest densities of glass sponges from 50-150 m in Jervis Inlet. Amongst solitary

epilithos, only the inarticulate brachiopod, *N. californica*, noticeably increased in the upper 150 m. Tunnicliffe and Wilson (1988) also found a shallow water distinction and high densities of *N. californica* in nearby Dean and Burke Channels. As the lower valve of craniid brachiopods cements to the wall, feeding takes place very low in the boundary layer compared to terebratulids; thus, access to suspended particles in turbulent flow may affect this distribution.

The increase in animal cover with kinetic energy flux density above 150 m indicates that these animals benefit from increased particle delivery due to consistent estuarine inflow. Enhanced turbulence at these intermediate depths will also increase substratum contact frequency by settling larvae (Abelson & Denny 1997) without impeding suspension feeding functions, as inflow velocities rarely exceed 20 cm s^{-1} (Wan et al. 2017). The positive correlation with winter flux density suggests that incoming oceanic water may be more important for suspension-feeder growth than outflowing water that contains greater concentrations of low-nutrient riverine particulates (Johannessen et al. 2015). However, in the summer, higher density diel vertical zooplankton migrations are another important component of the seston pool available to suspension feeders, and their daytime descents are also limited to the upper ~150 m of the fjord (Keen et al. 2017). Thus, the physical dynamics of the fjord appear to exert a strong influence on the wall assemblages, likely with enhanced food delivery shallower than 150 m supporting higher biomass.

Sharp increases in kinetic energy flux density, overall animal cover and food-limited species all suggest a switch from the food-limited assemblages below ~150 m to assemblages that primarily compete for space where cover reached > 80% in some areas.

These densities rival those of productive ecosystems such as coral reefs, where competition for space is fierce (Chadwick & Morrow 2011). Overgrowth competition is prevalent on hard substrata, and a lack of unambiguous dominants can maintain epilithic diversity (Buss 1990). Despite the lack of an apparent trend in animal cover and both sUTC and species richness, quadrats with ≥ 50 % animal cover never contained fewer than three species, even when a single organism primarily occupied the space. Indeterminate lateral growth and clonal strategies (Sebens 1987) were common amongst the high-space-occupiers (e.g. encrusting sponges, zoanthids). Solitary species that form dense monospecific aggregations also prevent overgrowth from other species (Jackson 1977), such as serpulid worms and inarticulate brachiopods in Douglas Channel. Glass sponges and some demosponges escape from competition by growing off the substratum (Sebens 1982). Behavioral aggression (Bruno & Witman 1996), overgrowth survival (Dalby & Young 1993) and chemical defenses (Slattery et al. 1995) are also employed by solitary species to persist amongst stronger space competitors, but these mechanisms are not easily identifiable from video surveys.

Site differences

While the PERMANOVA revealed a significant site effect, effect size was somewhat small, indicating relatively mild differences between sites along the fjord axis. The most obvious difference between sites was due to the great densities of inarticulate brachiopods at Maitland that drove the multivariate community structure here, while the encrusting demosponge *P. atka* was dominant at the other sites (Table 2.2). Brachiopods maintain high densities at the heads of other BC fjords where high sedimentation rates exclude less tolerant epifauna (Tunnicliffe & Wilson 1988; Farrow et al. 1983). Although

terrigenous input into Douglas Channel is lower relative to glacially fed BC inlets (Macdonald et al. 1983), some epifauna are likely intolerant of settling sediment disturbance at the fjord head, to the benefit of *N. californica*. The spring freshet causes sinking particle pulses of up to 5 g m^{-2} d^{-1} (Johannessen et al. 2015). While less than the average inputs into fjords that drain ice fields (Farrow et al. 1983), these pulses may represent significant periodic disturbances that shape the animal assemblages near the fjord head.

The increase in species richness at the seaward end of the fjord may be driven by greater concentrations of chl-a and zooplankton in the outer fjord basin (Keen et al. 2017). Proximity to the outer sill may enhance larval delivery to Squally Reach from Hecate Strait, as found by Quijon and Snelgrove (2005) in a Newfoundland fjord system. Alternatively, the greater richness at Squally may be due to the addition of echinoderms and corals with affinities to the greater depth at this site.

Functional Diversity

As body form diversity is an important feature of suspension feeder assemblages, it can serve as a proxy for trophic structure (Gili & Coma 1998). The low functional redundancy within quadrats (Figure 2.10b) indicates that even where many species occupied the walls, body forms were varied. The lack of functional redundancy was also evident in the taxonomic distinctness * richness (sΔ+) index that mirrored the sUTC index; where species increased, so did functional richness and sΔ+. The high taxonomic distinctness at the depth-band scale throughout the fjord (Figure A.2) also highlights the diversity of lineages that have adopted the suspension-feeding mode, along with a variety of mobile predators. This morphological diversity may allow for resource partitioning by

consumption of varied particle sizes (Abelson et al. 1993), with the multiple modes of suspension feeding by zoobenthos (Riisgård & Larsen 2000) leading to wide differences in foraging efficiency, energetics, and consumed seston fractions (Coma et al. 2001).

The distinct deep 'VI' assemblage at Squally Reach encompassed traits that reflect habitat formation including various arborescent and cup corals with high abundances of ophiuroids, and both free-living and epizootic crinoids. These organisms had unique trait combinations that were absent or rare on mid-depth walls where encrusting organisms dominated. They also all either create three-dimensionality off the walls, or, in the case of the ophiuroids, favor areas where significant three-dimensionality is present. While not numerically dominant, glass sponges (Marliave et al. 2009) and arborescent corals (Stone 2014) are important habitat formers where relatively high densities of rockfish and decapod crustaceans occur.

Ecological relevance of fjord walls

Fjords provide sheltered waters with expanses of near vertical, unsedimented bedrock across large depth ranges that can be readily colonized. These cliffs can foster high-biomass assemblages that are distinct from the sedimented fjord floor. Habitat complexity is increased by the erect morphologies of many of the sessile organisms, and the microhabitats they provide are used by commensals as refuges; in some cases, these interactions are even mutualistic (Buhl-Mortenson 2010). Crinoids and zoanthids were seen attached to various erect sponges, while brittle stars, echinoids, decapods, and rockfish occurred at greater densities where three-dimensional biological structures were present.

Fjords provide habitat for a variety of organisms known mostly in offshore deep water settings. The Brachiopoda, once dominant in Paleozoic subtidal assemblages, are rare components of Holocene ecosystems, yet they are nearly ubiquitous in British Columbian fjords such as Douglas Channel (Tunnicliffe & Wilson 1988), and maintain dense populations in the fjords of Chile (Baumgarten et al. 2014) and New Zealand (Richardson 1981). Glass sponges are mostly deep-sea taxa, but occur at shallow depths throughout the BC coast/shelf and form extensive reefs in some areas (Leys et al. 2004). Southward and Southward (1992) report a pogonophoran tubeworm from 200-300 m in two northern BC fjords that was previously known from deep-sea environments. Fjord biota are also reservoirs of genetic diversity (Turan et al. 1998; Drengstig et al. 2000; Le Goff-Vitry et al. 2004); allopatric speciation (Suneetha & Naevdal 2001) and pre-acclimation to ocean acidification (Fillinger & Richter 2013) may occur in isolated fjordic populations.

Bentho-pelagic coupling, while not directly measured in this study, likely exerts a strong influence over the carbon flow and productivity of the fjord. The high suspension feeder abundance, especially in the upper 150 m, transforms sinking organic matter and plankton into benthic biomass, some of which becomes available to larger predators. Subsequent release to the pelagic system of waste products, gametes, and larvae maintains organic cycling within the fjord before final loss to bottom sediments (Perea-Blázquez et al. 2012) or flushing. Our results suggest that the breadth of biofiltration may be greatest in the deepest portion of the fjord where there is an array of body forms, but that nutrient fluxes likely increase above ~150 m where abundances, especially sponges, were greatest. Sponges have some of the highest capture rates measured for any

suspension feeding taxa, and thus are significant regulators of seston in the water column (Gili & Coma 1998; Yahel et al. 2007; Kahn et al. 2015). More specific measurements of community filtration rates would be useful for further functional characterization of the wall fauna.

Numerous development projects, including the proposed diluted bitumen (dilbit) pipeline terminus at the fjord head, would bring heavy tanker traffic into Douglas Channel (Enbridge 2010). Better understanding of the consequences of a dilbit spill in aquatic environments requires baseline benthic studies (Lee et al. 2015). A 2010 Kalamazoo River spill demonstrated the potential ecological consequences when sinking dilbit had toxicological effects on organisms from microbes to chordates, and cleanup required years of dredging, arguably causing ecological impacts as great as the original spill (Dew et al. 2015). A dilbit spill in Douglas Channel would also have the potential to sink (Wu et al. 2016). In 2016, a ban on oil tankers came into effect (House of Commons Canada 2017). Thus, such risk will remain low as long as the ban is maintained.

These first surveys of the deep wall fauna of Douglas Channel augment our understanding of the distribution of northeast Pacific coastal diversity. Differences are emerging in faunal composition and environmental forcing along the coast. Douglas Channel is relatively oligotrophic (Wright et al. 2016), and nutrient regeneration largely comes from adjacent shelf water, concentrating nutrients at depth (Johannessen et al. 2015). Oxygen in the fjord was comparable to Jervis Inlet, where low productivity and a deep basin prevent large fluxes of organic matter from depleting bottom oxygen (Timothy et al. 2003). Conversely, high productivity southern fjords such as Saanich Inlet and the inner basin of Howe Sound support dense vertical-wall communities even under

periodic oxygen depletion (Tunnicliffe 1981; Levings et al. 1983). Douglas Channel and other northern BC fjords host inarticulate brachiopods, zoanthids, pom-pom anemones. crinoids and brittle stars in great abundances, whereas they are rare or absent in southern BC and Vancouver Island fjords (Levings et al. 1983). Southern fjords also have high densities of an articulate brachiopod, *Terebratulina unguicula* (Tunnicliffe & Wilson 1988) and ascideans (Tunnicliffe 1981); the former was absent and the latter rare in Douglas Channel. While the taxa in Douglas Channel matched those seen in nearby inlets and none appeared to be exclusive to the fjord, the overall species diversity was lower than that seen in other northern (Tunnicliffe unpub. data.) and southern (Levings et al. 1983) BC fjords.

The distinct assemblage profiles and environmental uniqueness of fjords, along with the high animal densities highlight the importance of this fjordic wall fauna to the coastal diversity of the northeast Pacific. Furthermore, several taxa listed as 'vulnerable' (e.g. glass sponges and tree corals; Fisheries & Oceans Canada 2010) are present on the Douglas Channel cliffs. Fjord walls are high biomass, high functioning, and expansive systems that may act as biodiversity reservoirs in a changing ocean, warranting consideration when developing management profiles for coastal oceans.

Literature Cited

Abelson A, Denny M (1997) Settlement of Marine Organisms in Flow. Annual Review of Ecology and Systematics 28:317–339

Abelson A, Miloh T, Loya Y (1993) Flow patterns induced by substrata and body morphologies of benthic organisms, and their roles in determining availability of food particles. Limnol Oceanogr 38:1116–1124

Anderson MJ (2006) Distance-based tests for homogeneity of multivariate dispersions. Biometrics 62:245–253

Anderson JJ, Devol AH (1973) Deep water renewal in Saanich Inlet, an intermittently anoxic basin. Estuarine and Coastal Marine Science 1:1–10

Anderson M, Gorley R, Clarke KP (2008) for PRIMER: guide to software and statistical methods. PRIMER-E, Plymouth, UK.

Baumgarten S, Laudien J, Jantzen C, Haeussermann V, Foersterra G (2014) Population structure, growth and production of a recent brachiopod from the Chilean fjord region. Mar Ecol-Evol Persp 35:401–413

Boje J, Neuenfeldt S, Sparrevohn CR, Eigaard O, Behrens JW (2014) Seasonal migration, vertical activity, and winter temperature experience of Greenland halibut *Reinhardtius hippoglossoides* in West Greenland waters. Mar Ecol-Prog Ser 508:211–222

Bruno JF, Witman JD (1996) Defense mechanisms of scleractinian cup corals against overgrowth by colonial invertebrates. J Exp Mar Biol Ecol 207:229–241

Buhl-Mortensen L, Vanreusel A, Gooday AJ, Levin LA, Priede IG, Buhl-Mortensen P, Gheerardyn H, King NJ, Raes M (2010) Biological structures as a source of habitat heterogeneity and biodiversity on the deep ocean margins. Marine Ecology 31:21–50

Burnham KP, Anderson DR (2004) Multimodel inference: understanding AIC and BIC in model selection. Sociological Methods & Research 33:261–304

Buss L (1990) Competition within and between encrusting clonal invertebrates. Trends Ecol Evol 5:352–356

Carney D, Oliver JS, Armstrong C (1999) Sedimentation and composition of wall communities in Alaskan fjords. Polar Biology 22:38–49

Chadwick NE, Morrow KM (2011) Competition Among Sessile Organisms on Coral Reefs. In: Dubinsky Z, Stambler N (eds) Coral Reefs: An Ecosystem in Transition. Springer Netherlands, Dordrecht, p 347–371

Clague JJ (1985) Deglaciation of the Prince Rupert – Kitimat area, British Columbia. Can J Earth Sci 22:256–265

Clarke KR, Gorley RN, (2006) PRIMER V6: user manual-tutorial. Plymouth Marine Laboratory.

Clarke KR, Warwick RM (2001) A further biodiversity index applicable to species lists: variation in taxonomic distinctness. Mar Ecol-Prog Ser 216:265–278

Coma R, Ribes M, Gili JM, Hughes RN (2001) The ultimate opportunists: consumers of seston. Mar Ecol-Prog Ser 219:305–308

Dalby J, Young C (1993) Variable effects of sscidian competitors on oysters in a Florida epifaunal community. J Exp Mar Biol Ecol 167:47–57

Dew WA, Hontela A, Rood SB, Pyle GG (2015) Biological effects and toxicity of diluted bitumen and its constituents in freshwater systems. J Appl Toxicol 35:1219–1227

Drengstig A, Fevolden SE, Galand PE, Aschan MM (2000) Population structure of the deep-sea shrimp (*Pandalus borealis*) in the north-east Atlantic based on allozyme variation. Aquat Living Resour 13:121–128

Enbridge (2010) Volume 8A:overview and general information — marine transportation; Volume 8B:environmental and socio-economic assessment (ESA) — marine transportation. Enbridge Northern Gateway Project Sec. 52 Application. Northern Gateway Piplines Inc., Calgary

Farrow G, Syvitski J, Tunnicliffe V (1983) Suspended particulate loading on the macrobenthos in a highly turbid fjord - Knight Inlet, British-Columbia. Can J Fish Aquat Sci 40:273–288

Fillinger L, Richter C (2013) Vertical and horizontal distribution of *Desmophyllum dianthus* in Comau Fjord, Chile: a cold-water coral thriving at low pH. PeerJ 1:e194

Fisheries & Oceans Canada (2010) Pacific region cold-water coral and sponge conservation strategy: 2010-2015.

Genin A, Paull C, Dillon W (1992) Anomalous abundances of deep-sea fauna on a rocky bottom exposed to strong currents. Deep-Sea Research Part a-Oceanographic Research Papers 39:293-

Gili J-M, Coma R (1998) Benthic suspension feeders: their paramount role in littoral marine food webs. Trends in Ecology & Evolution 13:316–321

Hart DD, Finelli CM (1999) Physical-biological coupling in streams: the pervasive effects of flow on benthic organisms. Annu. Rev. Ecol. Syst. 30:363-395

Haedrich R, Gagnon J (1991) Rock wall fauna in a deep Newfoundland fjord. Cont Shelf Res 11:1199–1207

Hooper DU, Chapin FS, Ewel JJ, Hector A, Inchausti P, Lavorel S, Lawton JH, Lodge DM, Loreau M, Naeem S, Schmid B, Setälä H, Symstad AJ, Vandermeer J, Wardle DA (2005) Effects of biodiversity on ecosystem functioning: a consensus of current knowledge. Ecological Monographs 75:3–35

House of Commons Canada (2017) Bill C-48: Oil Tanker Moratorium Act. 1st Reading May 12, 2017, 42nd parliament, 1st session. Retrieved from the Parliament of Canada website: http://www.parl.ca/DocumentViewer/en/42-1/bill/C-48/first-reading

Hughes, JD (2015) A clear look at BC LNG: energy security, environmental implications and economic potential. Canadian Centre for Policy Alternatives, BC Office. Retrieved from the Northwest Insitute for Bioregional Research website: northwestinstitute.ca/index.php/lng

Huvenne VAI, Tyler PA, Masson DG, Fisher EH, Hauton C, Hühnerbach V, Bas TPL, Wolff GA (2011) A picture on the wall: innovative mapping reveals cold-water coral refuge in submarine canyon. PLOS ONE 6:e28755

Jackson J (1977) Competition on marine hard substrata - adaptive significance of solitary and colonial strategies. Am Nat 111:743–767

Jantzen C, Haeussermann V, Foersterra G, Laudien J, Ardelan M, Maier S, Richter C (2013) Occurrence of a cold-water coral along natural pH gradients (Patagonia, Chile). Mar Biol 160:2597–2607

Johannessen SC, Wright CA, Spear DJ (2015) Seasonality and physical control of water properties and sinking and suspended particles in Douglas Channel, British Columbia. Canadian Technical Report of Hydrography and Ocean Sciences. 308

Kahn AS, Yahel G, Chu JWF, Tunnicliffe V, Leys SP (2015) Benthic grazing and carbon sequestration by deep-water glass sponge reefs. Limnol Oceanogr 60:78–88

Keen EM, Wray J, Meuter H, Thompson K-L, Barlow JP, Picard CR (2017) “Whale wave”: shifting strategies structure the complex use of critical fjord habitat by humpbacks. Mar Ecol-Prog Ser 567:211–233

Keyel AC, Wiegand K (2016) Validating the use of unique trait combinations for measuring multivariate functional richness. Methods Ecol Evol 7:929–936

Kundu PK, and IM Cohen, (2008) Fluid Mechanics. 4th ed. Academic Press, Amsterdam, 871 pp.

Laliberte E, Legendre P (2010) A distance-based framework for measuring functional diversity from multiple traits. Ecology 91:299–305

Le Goff-Vitry MC, Pybus OG, Rogers AD (2004) Genetic structure of the deep-sea coral *Lophelia pertusa* in the northeast Atlantic revealed by microsatellites and internal transcribed spacer sequences. Mol Ecol 13:537–549

Lee K, Boufadel M, Chen B, Foght J, Hodson P, Swanson S, Venosa A (2015). Expert panel report on the behaviour and environmental impacts of crude oil released into aqueous environments. Royal Society of Canada, Ottawa, ON.

Leichter JJ, Witman JD (1997) Water flow over subtidal rock walls: Relation to distributions and growth rates of sessile suspension feeders in the Gulf of Maine - water flow and growth rates. J Exp Mar Biol Ecol 209:293–307

Lesser M, Witman J, Sebens K (1994) Effects of flow and seston availability on scope for growth of benthic suspension-feeding invertebrates from the Gulf of Maine. Biol Bull 187:319–335

Levings C, Foreman R, Tunnicliffe V (1983) Review of the benthos of the Strait of Georgia and contiguous fjords. Can J Fish Aquat Sci 40:1120–1141

Leys SP, Wilson K, Holeton C, Reiswig HM, Austin WC, Tunnicliffe V (2004) Patterns of glass sponge (Porifera, Hexactinellida) distribution in coastal waters of British Columbia, Canada. Mar Ecol-Prog Ser 283:133–149

Macdonald RW, Bornhold BD, and Webster I (1983) The Kitimat fjord system: an introduction. *In* Proceedings of a Workshop on the Kitimat Marine Environment. Canadian Technical Report of Hydrography and Ocean Sciences 18:3–13

Marliave JB, Conway KW, Gibbs DM, Lamb A, Gibbs C (2009) Biodiversity and rockfish recruitment in sponge gardens and bioherms of southern British Columbia, Canada. Mar Biol 156:2247–2254

Miller RJ, Etter RJ (2011) Rock walls: small-scale diversity hotspots in the subtidal Gulf of Maine. Mar Ecol-Prog Ser 425:153–165

Moon H-W, Hussin WMRW, Kim H-C, Ahn I-Y (2015) The impacts of climate change on Antarctic nearshore mega-epifaunal benthic assemblages in a glacial fjord on King George Island: responses and implications. Ecol Indic 57:280–292

Naeem S, Wright JP (2003) Disentangling biodiversity effects on ecosystem functioning: deriving solutions to a seemingly insurmountable problem. Ecology Letters 6:567–579

Oksanen J, Blanchet FG, Friendly M, Kindt R, Legendre P, McGlinn D, Minchin PR, O'Hara RB, Simpson GL, Solymos P, Stevens MH, Szoecs E, Wagner H (2017). vegan: Community Ecology Package. R package version 2.4-4. https://CRAN.R-project.org/package=vegan

Ostroumov S (2005) Suspension-feeders as factors influencing water quality in aquatic ecosystems. In: Dame RF, Olenin S (eds) Comparative Roles of Suspension-Feeders in Ecosystems. Springer, Dordrecht, p 147–164

Pickard G (1961) Oceanographic features of inlets in the British Columbia mainland coast. Journal of the Fisheries Research Board of Canada 18:907–999

Perea-Blázquez A, Davy SK, Bell JJ (2012) Estimates of particulate organic carbon flowing from the pelagic environment to the benthos through sponge assemblages. PLOS ONE 7:e29569

Quijon PA, Snelgrove PVR (2005) Spatial linkages between decapod planktonic and benthic adult stages in a Newfoundland fjordic system. J Mar Res 63:841–862

R Development Core Team (2013) R: a language and environment for statistical computing. R Foundation for Statistical Computing, Vienna, www.R-project.org/

Richardson JR (1981) Recent brachiopods from New Zealand — background to the study cruises of 1977–79. New Zealand Journal of Zoology 8:133–143

Riisgård H., Larsen P. (2000) Comparative ecophysiology of active zoobenthic filter feeding, essence of current knowledge. Journal of Sea Research 44:169–193

Roddick JA (1970) Douglas Channel-Hecate Strait map-area, British Columbia. Geological Survey of Canada 70-41

Rowden AA, Schlacher TA, Williams A, Clark MR, Stewart R, Althaus F, Bowden DA, Consalvey M, Robinson W, Dowdney J (2010) A test of the seamount oasis hypothesis: seamounts support higher epibenthic megafaunal biomass than adjacent slopes. Marine Ecology 31:95–106

Sebens K (1982) Competition for space - growth-rate, reproductive output, and escape in size. Am Nat 120:189–197

Sebens K (1987) The Ecology of Indeterminate Growth in Animals. Annu Rev Ecol Syst 18:371–407

Slattery M, Mcclintock J, Heine J (1995) Chemical defenses in Antarctic soft corals - evidence for antifouling compounds. J Exp Mar Biol Ecol 190:61–77

Smith F, Witman JD (1999) Species diversity in subtidal landsapces: maintenance by physical processes and larval recruitment. Ecology 80:51–69

Southward A, Southward E (1992) Distribution of Pogonophora (tube-worms) in British-Columbian fjords. Mar Ecol-Prog Ser 82:227–233

Stone RP (2014) The ecology of deep-sea coral and sponge habitats of the central Aleutian Islands of Alaska. NOAA Professional Paper NMFS 16:1-52

Suneetha KB, Naevdal G (2001) Genetic and morphological stock structure of the pearlside, Maurolicus muelleri (Pisces, Sternoptychidae), among Norwegian fjords and offshore areas. Sarsia 86:191–201

Syvitski JPM, Burrell DC, Skei JM (1987) Fjords: processes and products. Springer-Verlag, New York

Timothy DA, Soon MYS, Calvert SE (2003) Settling fluxes in Saanich and Jervis Inlets, British Columbia, Canada: sources and seasonal patterns. Prog Oceanogr 59:31–73

Trygonis V, Sini M (2012) photoQuad: A dedicated seabed image processing software, and a comparative error analysis of four photoquadrat methods. J Exp Mar Biol Ecol 424:99–108

Tunnicliffe V (1981) High species diversity and abundance of the epibenthic community in an oxygen-deficient basin. Nature 294:354–356

Tunnicliffe V, Wilson K (1988) Brachiopod populations - distribution in fjords of British-Columbia (Canada) and tolerance of low oxygen concentrations. Mar Ecol-Prog Ser 47:117–128

Turan C, Carvalho GR, Mork J (1998) Molecular genetic analysis of Atlanto-Scandian herring (*Clupea harengus*) populations using allozymes and mitochondrial DNA markers. J Mar Biol Assoc UK 78:269–283

Vetter EW, Dayton PK (1998) Macrofaunal communities within and adjacent to a detritus-rich submarine canyon system. Deep Sea Research Part II: Topical Studies in Oceanography 45:25–54

Villeger S, Mason NWH, Mouillot D (2008) New multidimensional functional diversity indices for a multifaceted framework in functional ecology. Ecology 89:2290–2301

Wahl M (Ed) (2009) Marine hard bottom communities: patterns, dynamics, diversity and change. Springer, Berlin

Wan D, Hannah CG, Foreman MGG, Dosso S (2017) Subtidal circulation in a deep-silled fjord: Douglas Channel, British Columbia. J Geophys Res Oceans, 122, doi:10.1002/2016JC012022

Wright CA, Vagle S, Hannah C, Johannessen SC, Spear D, Wan D (2016) Physical, chemical and biological oceanographic data collected in Douglas Channel and the approaches to Kitimat, October 2014-July 2015. Canadian Data Report of Hydrography and Ocean Sciences. 200:viii+74pp

Webster L, Angus L, Topping G, Dalgarno EJ, Moffat CF (1997) Long-term monitoring of polycyclic aromatic hydrocarbons in mussels (*Mytilus edulis*) following the Braer oil spill. Analyst 122:1491–1495

Wu Y, Hannah CG, Law B, King T, Robinson B (2016). An estimate of the sinking rate of spilled diluted bitumen in sediment laden coastal waters. Proceedings of the thirty-ninth AMOP Technical Seminar, Environment and Climate Change Canada, Ottawa, ON. p 331-347

Yahel G, Whitney F, Reiswig HM, Eerkes-Medrano DI, Leys SP (2007) In situ feeding and metabolism of glass sponges (Hexactinellida, Porifera) studied in a deep temperate fjord with a remotely operated submersible. Limnol Oceanogr 52:428–440

Chapter 3 : Epibenthic megafaunal response to a prolonged hypoxic event: community structure patterns and oxygen thresholds

INTRODUCTION

The loss of oxygen in the global oceans is accelerating (Keeling et al. 2010). Under predicted climate scenarios, upper-ocean warming will lower oxygen solubility, strengthen stratification, decrease ventilation and disrupt thermohaline circulation patterns, leading to a decrease of up to seven percent in the ocean's overall dissolved oxygen content (Keeling et al. 2010). In addition, expansion and/or intensification of major oceanographic features such as oxygen minimum zones (Stramma et al. 2010), eutrophic dead zones (Diaz & Rosenberg 2008), and eastern-boundary upwelling regimes (Wang et al. 2015) all contribute to an increase in oceanic regions of low-oxygen, or hypoxia.

Resolving the ecological consequences of dissolved oxygen loss on marine ecosystems remains an active field of research. Behavioral changes, decreased growth, metabolic effects, oxidative stress and finally mortality are all induced (Gray et al. 2002) at varying oxygen levels according to taxon. As the intensity and frequency of hypoxic events grow, many ecosystems move toward microbial energetic pathways (Diaz & Rosenberg 2008), and this shift can be accelerated by alterations in predatory-prey interactions (Breitburg et al. 1997). Furthermore, expanding hypoxia will lead to a loss of suitable habitat and contraction of communities in space (Stramma et al. 2012). Competitive interactions may be increased in these contracted habitats, leading to losses in biodiversity and ecosystem functioning (Stramma et al. 2010). Low-oxygen effects reach across life-history stages as well. For example, larval fish biomass decreases in

concert with oxygen (Johnson-Colegrove et al. 2015). Many taxa will be impacted by deoxygenation, while those pre-acclimated to low oxygen lifestyles are most likely to fare better (Rosa & Seibel 2008; Grego et al. 2014). Benthic habitats may be particularly prone to the adverse effects of deoxygenation as they are the most distant from atmospheric oxygen sources and their sediments are enriched from falling organic matter (Vaquer-Sunyer & Duarte 2008).

Notably strong gradients in dissolved oxygen can exist in fjordic basins with seasonal deep-water renewal, often alongside other environmental gradients (Levings et al. 1983; Rosenberg 2002). These oxyclines facilitate study of benthic community responses to low-oxygen pulses (e.g. Chu & Tunnicliffe 2015a). Threshold changes in species composition and abundances occur at various dissolved oxygen levels globally according to species physiological tolerances (Deutsch et al. 2015) and can have major long-lasting impacts on seafloor ecosystems (Moffitt et al. 2015). While the most commonly used threshold for sublethal hypoxia is 1.4 ml L^{-1}, the response varies by taxon, temperature and ocean basin (Vaquer-Sunyer & Duarte 2008; Vaquer-Sunyer & Duarte 2011; Chu & Gale 2017). As deoxygenation continues to be one of the major global drivers of ocean change, especially in the northeast Pacific (Somero et al. 2016), case studies documenting biotic responses to low-oxygen stress are necessary to develop a mechanistic understanding of deoxygenation effects, and to use this understanding to predict changes in biogeography and ecosystem functioning.

Chu & Tunnicliffe (2015a) found a strong benthic megafaunal response to seasonal hypoxia in the Saanich Inlet, British Columbia in which species distributions coalesced during summer hypoxia and recovered following deep-water replenishment in

2013. In addition, up-slope movements of three mobile species were noted beginning in the 1 - 1.15 ml L^{-1} oxygen range, suggesting that the northeast Pacific threshold of 0.88 ml L^{-1} found by review of species critical oxygen tensions (Chu & Gale 2017) may better predict hypoxia responses in this region than the commonly used global threshold of 1.4 ml L^{-1}. The Northeast Pacific experienced record-high surface temperatures in the two years (i.e. 2014-15) following their study due to the confluence of strong El Niño conditions and an anomalous warm water mass that eventually mixed downward in early 2016 (Ross 2017). These meteorological events also affected the subsurface waters, as seafloor cabled observatories show abnormal temperature spikes and oxygen losses in the same timeframe (Dewey et al. 2015), with relatively weak deep-water replenishment in the Strait of Georgia (Sastri et al. 2016) leading to record oxygen minima in adjacent restricted waters.

Here we document the response of epibenthic megafauna in Saanich Inlet to an extended hypoxic event in 2016 to determine whether the 2013 disassembly and recovery response to seasonal hypoxia described by Chu & Tunnicliffe (2015a) varies with changes in the duration and spatial extent of hypoxia. In spring, summer and fall at approximately the same times of year in both 2013 and 2016, we flew the same benthic video transect; this enabled direct comparisons of seasonal bottom oxygen and community structure between the years. Given the successive weak oxygen renewal events in 2016, we predict notable shoaling of both hypoxia and species distributions. Additionally, we examine community transitions along the dissolved oxygen gradient in both years in order to detect local community-level hypoxia thresholds and to test the null hypothesis that the thresholds did not change between years despite changes in the

oxygen cycle. We also present a novel adaptation of the Fisher Information statistic – an information theory metric used in ecological studies as a warning signal for temporal community shifts (Fath et al. 2003; Karunanithi et al. 2008) – converted to detect transitions along environmental gradients. Then, we validated the Fisher Information results against those obtained with a multivariate regression tree and to species accumulation curves along the oxygen gradient. Finally, we determined whether the long-term negative trend in Saanich Inlet dissolved oxygen from 2006-2014 described by Chu & Tunnicliffe (2015a) from cabled observatory data intensified following the change in oceanographic conditions from 2014-2016. Taken together, we show that interruptions in the timing and intensity of an annual oxygen depletion-renewal cycle have the capacity to rapidly change benthic communities.

MATERIALS & METHODS

Study site

Saanich Inlet is a reverse estuarine fjord with depths down to 230 m and limited exchange with waters from the Strait of Georgia due to a 75 m sill at its mouth. This limited exchange, coupled with high primary productivity in the spring and summer months that fuels microbial respiration at depth (Grundle et al. 2009; Zaikova et al. 2010), causes seasonal hypoxia/anoxia to develop in the mid-to-late summer (Herlinveaux, 1962). Oxygen is renewed annually in the fall as dense, well-oxygenated water from the Strait of Georgia enters over the sill, descending into the bottom layers of the inlet causing the anoxic water to shoal upward (Anderson & Devol, 1973; Tunnicliffe 1981). Another oxygen injection sometimes occurs in spring at intermediate depths from 90-160 m (Manning et al. 2010). Although the oxygen depletion-recovery cycle is

predictable and well chronicled, the timing and extent of both depletion and renewal vary (Matabos et al. 2012; Chu & Tunnicliffe 2015a).

Benthic ROV transect & video analysis

Since 2005, benthic surveys with remotely operated vehicles (ROVs) outfitted with dissolved oxygen sensors and high-definition video cameras have repeated the same transect (n=13) in Patricia Bay, Saanich Inlet, B.C (Yahel et al. 2008; see Chu & Tunnicliffe 2015a for transect map). This transect transitions through near-bottom zones of low to high oxygen along a shallow depth gradient (180-40 m) and allows for comparisons of bottom oxygen and epibenthic megafaunal abundances between years, creating a one-of-a-kind ecological time-series. The transect was flown three times in 2013 and documented the influence of seasonal hypoxia expansion on the epibenthic community (Chu & Tunnicliffe 2015a; see their Figure 1 for transect location). Three transects were flown in 2016 at approximately the same times of year (i.e. spring, summer, and fall); the respective transect dates were May 4th, August 5th, and October 5th. The fall 2016 transect was truncated (140-40 m) due to logistical constraints, but still captured the full range of oxygen typical of the transect (i.e. ~ 0 – 4.5 ml L^{-1}).

The spring 2013, spring 2016 and fall 2016 transects were flown using the ROV Oceanic Explorer, while the summer 2013, fall 2013 and summer 2016 transects were flown with the ROV ROPOS. The ROV flew <1 m above the bottom at ~0.5 knots. An approximately downward-pointing video camera recorded the seabed in 1080i high-definition. A Sea-Bird SBE 19plus conductivity-temperature-depth (CTD) and an SBE43 oxygen sensor, with intakes ~0.5 m above the ROV bottom, recorded CTD and oxygen data at 4 hz; these data were averaged to one-second intervals before all analyses. The

accuracy of the oxygen sensor is 2% of surface saturation which is 0.13 mL L^{-1} for a solubility of 6.5 mL L^{-1} at 32 PSU and 10 °C; the sensor precision is 0.023 mL L^{-1} and has a response time < 1 s. Navigation data were recorded on all ROPOS-flown transects with its ultra-short baseline system, while navigation data for Oceanic Explorer-flown transects were interpolated *post hoc* using bathymetric data and the x/y coordinates of the transect line at the bottom depths recorded from the CTD.

Individual animals (> ~5 cm) were identified and counted for each second of video with and presence/absence of two sponge species were also recorded. Abundances and identifications were verified through multiple playbacks of the video in densely populated areas. All animals were counted as they crossed the bottom of the oblique image to increase the accuracy of their correspondence with environmental and navigation records. Animals that exited off the side of the image were only counted if they did so in the lower-half of the image in order to reduce false replicate counts from species exiting and re-entering the frame. Paired horizontal scaling lasers at 10 or 11 cm spacing were used to determine the width of the field of view, which varied from ~1-4 m on average. The area surveyed per second was determined using the field of view and the ROV speed (~ 0.2 m s^{-1}). All environmental, navigational, and biological data were synchronized into matrices by timestamp prior to analysis in R (R Core Team 2017).

Community structure along oxygen gradient

In order to standardize benthic community abundances by area, transect lines were divided into ~20 m^2 quadrats (n=538, 367 respectively for 2013, 2016); a smaller field of view in ROV Oceanic Explorer flown transects, along with the truncation of the bottom half of the Fall 2016 transect, account for the disparity in total number of quadrats

between years. Animal counts were summed and environmental data were averaged per quadrat. Kernel density plots were used to visually assess changes in species abundances and oxygen distributions between seasons and years for the 14 most abundant mobile megabenthos.

Binary presence-absence matrices of these 14 mobile species were then compiled for both 2013 and 2016 with each row representing a species and each column a quadrat. Species were selected based on consistent presence across seasons/years and varying interspecific oxygen distributions in order to represent the community response along the entire natural oxygen gradient. Some abundant fish species including Pacific hake, shiner perch, and walleye pollock were not included in analyses due to their attraction to ROV lights and non-benthic behavior.

We then performed a null model analysis using the R package EcoSimR (Gotelli et al. 2015) in order to generate community co-occurrence or 'c-scores' (Stone & Roberts 1990) for each year to determine whether changes in the oxygen regime were reflected in the degree of community segregation. The c-score quantifies community segregation by multiplying the number of sites in which each species occurs minus the number of sites shared with the next species. This process is iterated for all species pairs until a community-level c-score is obtained. The sim4 'fixed-proportional' algorithm, in which species totals in the original matrix are preserved and site totals have probabilities assigned in proportion to the totals in the original matrix, was chosen because it preserves species-site heterogeneity and is conservative (i.e. has a relatively low Type I error rate when compared to other algorithms) in distinguishing non-randomness in the observed

data matrices (Gotelli 2000). The average covariance in association between species pairs (V-ratio; Schluter 1984) was also calculated for each year.

Changes in pairwise species associations in the same 14 species between 2013 and 2016 were then assessed using the FORTRAN program 'Pairs' (Ulrich 2008). Both observed and expected scores were standardized into 22 c-score groups ranging from 0 to 1 in which observed scores for each unique species pair in each year were compared to a Bayesian distribution of expected scores (95% CI) created from 100 randomized matrices in each year. Z-transformed scores (Observed-Expected/St. Dev.), with a false-error rate correction (Benjamini & Yekutieli 2001), were then calculated for species pairs in groups with observed frequencies above or below the null expectation. We then noted significantly associated species pairs (i.e. species either more aggregated or segregated than expected by chance). For each significant pairwise association in each year, bootstrap re-sampled distributions (n=1000) of oxygen occurrences for each species were compared for significant differences using Welch's two-sample t tests.

Assemblage transitions

Breaks in community structure corresponding to environmental and temporal variables were first examined by creating a multivariate regression tree (MRT) using the R package "mvpart" (De'ath 2002). Density data from the same fourteen mobile animals were used to make a species-abundance matrix; these data were 4^{th}-root transformed prior to MRT analysis in order to incorporate contributions from the rarer taxa without eliminating the signal from the most abundant species (e.g. slender sole and squat lobsters). Using normalised environmental data including dissolved oxygen, temperature, salinity, and depth as explanatory variables along with year, the tree split the dataset into

groups chosen to maximize the explanatory power of the tree while minimizing cross-validation error. The MRT provided the number of samples (quadrats) in each mutually exclusive group, along with a global error and R^2 for the entire tree. Barplots of species density at each node were also shown.

Fisher Information (FI) is an information theory metric used to analyze patterns in data, particularly in tracking the stability of data-rich systems (e.g. Ahmad et al. 2016); it provided the basis for a second analysis of community structure along the dissolved oxygen gradient. We used the derivation of FI developed by Fath et al. (2003) adapted to analyze breakpoints over a range of dissolved oxygen windows rather than the time windows typically employed in FI studies.

The steps for computing our FI were adapted from Eason & Cabezas (2012); quadrats were binned into 0.25 mL L^{-1} "O_2 windows" ranging from 0-4 ml L^{-1} using the mean oxygen level of the quadrat. All quadrats with mean oxygen levels above 4.00 mL L^{-1} were binned due to a paucity of data in this upper range and because the chosen component species are not biologically limited by oxygen in this range (Chu & Tunnicliffe 2015a). Mean densities for the 14 species in each oxygen window were then calculated and compiled into an O_2 window-density matrix that was used to calculate the Fisher Information score for each window using the Python library provided by Ahmad et al. (2016). We ran the analysis for all quadrats in both 2013 and 2016. A null distribution of 500 FI scores using mean species densities from 50 randomly selected quadrats, regardless of year, allowed for comparisons of the observed FI scores in each dissolved oxygen window to those expected by chance in the same system. We also created species

accumulation curves in each 0.25 ml L^{-1} oxygen window using combined data from both years in order to compare the changes in FI to those seen in species diversity.

Long-term dissolved oxygen record

Ocean Network Canada's VENUS cabled subsea observatory has maintained a Saanich Inlet node since 2006; this node is located ~200 m south of our transect at 95 m depth, measuring fluctuation in dissolved oxygen levels throughout the annual hypoxia cycle. The open source VENUS time-series (available at www.oceannetworks.ca) of *in situ* dissolved oxygen provides real-time data at one-minute intervals dating back to February 2006, allowing for unique insights into the seasonal and long-term dynamics of dissolved oxygen in the area. We analyzed these data, averaged from one-minute into one-hour intervals, from April 2006 to April 2017 with linear regression in order to determine if the long-term negative trend in dissolved oxygen from 2006-2014 described by Chu and Tunnicliffe (2015a) had changed. All gaps in the data (~7 % of the data set) were filled via linear interpolation prior to analysis. We analyzed the data using the 'xts' (Ryan & Ulrich 2017) and 'zoo' (Zeileis & Grothendieck 2017) R time-series packages and used the R function rollapply to calculate running one-year mean and variance in oxygen. Long-term trends in dissolved oxygen and yearly mean dissolved oxygen were analyzed with linear regressions.

RESULTS

Benthic oxygen profiles

Along-bottom oxygen profiles were notably different in 2016 than 2013; both hypoxia (O_2 < 0.88 mL L^{-1} using the East Pacific hypoxia threshold suggested by Chu & Gale 2016) and anoxia extended shallower in all seasons (Figure 3.1). The difference in

the spatial extent of anoxia between 2013 and 2016 was most evident in the fall transects; anoxia (O_2 < oxygen sensor sensitivity threshold) extended 40 m shallower in fall 2016 and covered 59% of the transect versus 31% in 2013. The 2016 profiles, particularly in spring and fall, display sharp boundaries between hypoxia and normoxia, while oxygen increased more gradually with depth in 2013 (Figure 3.1); a smaller proportion of the transect experienced oxygen between 1.1 and 1.8 ml L^{-1} in all seasons in 2016 (Table 3.1). While the extent of the slope covered in hypoxia decreased and the extent in normoxia increased post-summer in 2013, this was less apparent in 2016 (Table 3.1). The maximum depth of occurrence for slender sole along the transect was also shallower in each season compared to 2013 (Figure 3.1). Again, the difference between 2013 and 2016 was most notable between the fall transects, where the deepest slender sole was seen at ~95 m in 2016 versus ~155 m in 2013.

Table 3.1. Length of bottom transect that experienced hypoxic, transitional and normoxic dissolved oxygen levels in 2013 and 2016 transects. The extent of transitional oxygen ranges indicates a steepening of the hypoxia-normoxia gradient in 2016. Note that the fall 2016 length in hypoxia is artificially low because the bottom quarter of the transect was not surveyed; an extrapolated length is provided in parentheses.

Oxygen range	**2013 extent [m]**			**2016 extent [m]**		
	Spring	**Summer**	**Fall**	**Spring**	**Summer**	**Fall**
Hypoxia (< 1.1 ml L^{-1})	1088	2153	1349	1224	2031	1246 (1800)
Transitional (1.1 – 1.8 ml L^{-1})	223	814	322	33	158	31
Normoxia (> 1.8 ml L^{-1})	813	813	663	770	285	315

2013 vs. 2016 community structure

Over the six transects, we mapped 35980 animal counts, 25262 in 2013 and 10718 in 2016, from 55 species to their oxygen occurrence. In addition, we recorded the presence of bacterial mats (*Beggiatoa* spp.) and two species of demosponges, totaling over 17,000 additional records.

The effects of the increase in spatial and temporal hypoxia coverage varied by species. The major peaks in both mobile animal abundance extended to lower oxygen in 2016 (Figure 3.3), with notable increases in the number of organisms experiencing severe (<0.5 ml L^{-1} O_2) hypoxia in all seasons (Table 3.2; Table 3.3). Species that normally

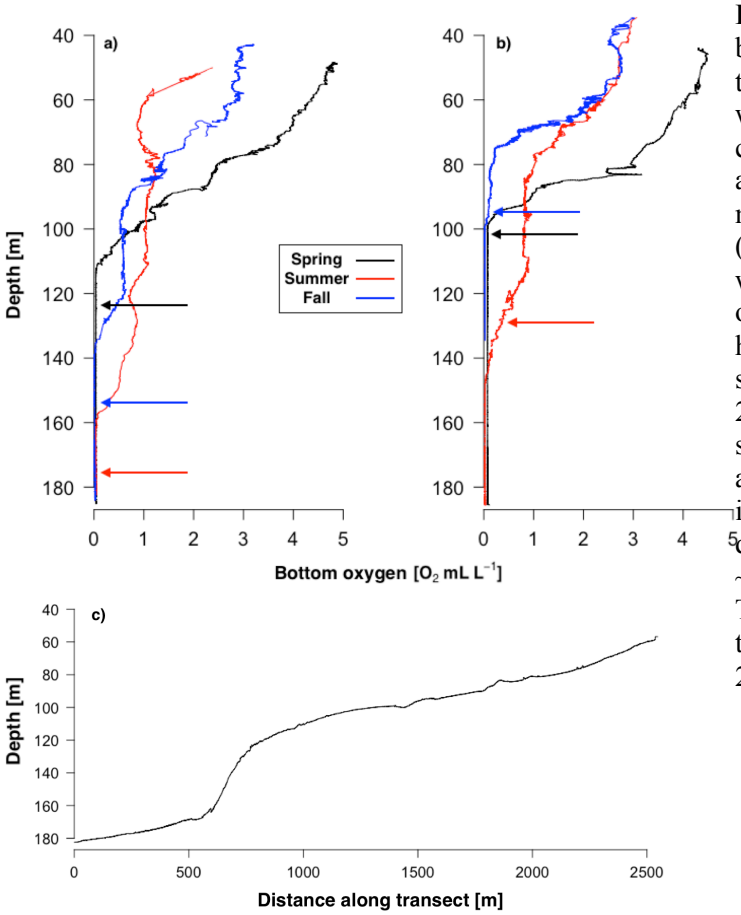

Figure 3.1. Seasonal along-bottom oxygen profiles show the oxygen renewal cycle within years and habitat compression between a) 2013 and b) 2016. Arrows show the maximum depth of slender sole (*Lyopsetta exilis*) occurrence, which indicates the limit of oxygenated megafaunal habitat. Anoxia extended shallower in all seasons in 2016 versus 2013. The deepest slender sole occurrence was also shallower in every season in 2016, with a maximum difference between years of ~60 m in fall transects. c) Typical deep-to-shallow transect profile from Summer 2016.

inhabit low-oxygen waters tended to show the least differences between 2013 and 2016. The distributions relative to oxygen of slender sole (*Lyopsetta exilis*) and squat lobster (*Munida quadrispina*), the two most abundant megafaunal species, were largely unchanged in the spring and summer seasons (Figure 3.2a, 3.2b) outside of a dense cluster of squat lobsters in spring 2016 that may have been a mating aggregation (Doya et al. 2016). Both species declined and occurred at comparatively low oxygen in Fall 2016. Conversely, the commercial spot prawn, *Pandalus platyceros*, occupied a narrow range (0.81-1.94 mL L^{-1}) of oxygen in spring 2016 and was completely absent in fall 2016 without evidence for a mortality event. Spot prawn occurred at relatively low oxygen in spring 2016. Additionally, low densities in summer preceded the fall 2016 disappearance of spot prawn; we also found low densities of slender sole and squat lobster in fall 2016 (Table 3.2).

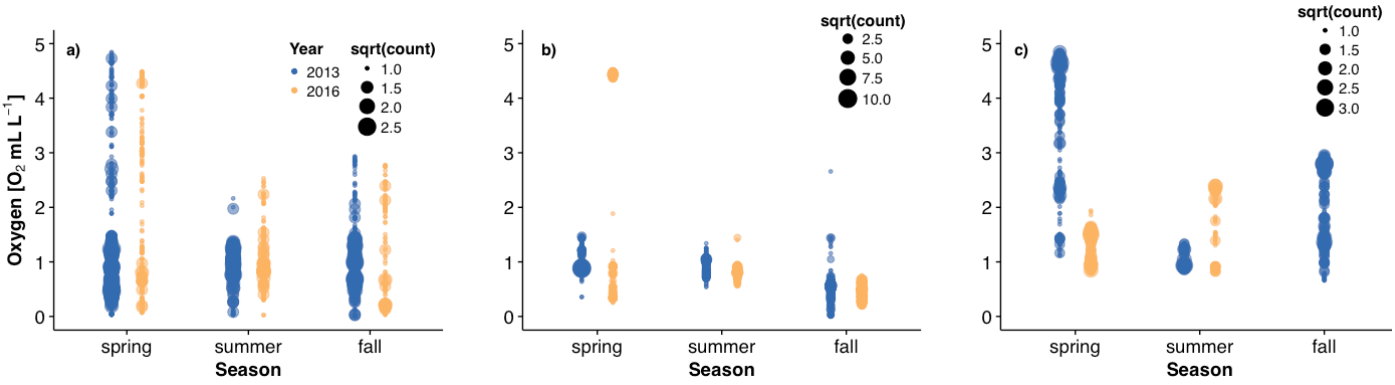

Figure 3.2. Distribution of abundance with oxygen for the three most abundant mobile species in Saanich Inlet in 2013 versus 2016 sampling season. Counts s^{-1} from video analysis were square-root transformed in order to lessen the visual effect of outliers (i.e. dense aggregations) but note the differing scales across species. Distributions of a) slender sole and b) squat lobster, the most abundant and hypoxia-tolerant of the mobile megabenthos, were largely unaffected by the increased extent of hypoxia while c) the hypoxia-sensitive spot prawn was seen at much lower oxygen in spring 2016 than 2013, and was absent in fall 2016.

The striped nudibranch, *Armina californica*, was notably abundant in the shallow well-oxygenated segments of the summer (n=68) and fall (n=167) transects usually occupied by spot prawns. This species was seen infrequently (n < 5) in all previous transect years (Chu & Tunnicliffe 2015b). In addition, the white sea cucumber, *Pentamera calcigera*, was observed for the first time in fall 2016 and in high abundances (n=63); this species occupied a narrow and low range of oxygen (0.12-0.2 mL L^{-1}). The seawhip, *Halipteris willemoesi,* historically the most abundant animal on the transect (Chu & Tunnicliffe 2015a), declined greatly in fall 2016 (Table 3.3). We observed many freshly fallen seawhips with soft tissue still present.

Both the observed and expected c-scores, reflecting community segregation for the 14 species assemblage, were higher in 2013 than 2016; scores were 1077 versus 386. The 2013 score differed from the null model 95 % CI (Figure 3.5), indicating non-random assemblages assembly ($p < 0.01$) and significant segregation. In contrast, significant assemblage-wide segregation was not observed in 2016, suggesting a more homogenized community than in 2013. Species-pair covariance shows a similar trend towards aggregation, as the V-ratio increased from 3.09 in 2013 to 3.54 in 2016.

PAIRS analysis shows that no species pairs were either always or never co-occurring in 2013 (Fig. 3.5a), while three species pairs displayed complete overlap (c-score = 0) and seven pairs had complete segregation (c-score=1) in 2016 (Fig 3.5b). In addition, the observed number of species-pairs in both a highly aggregated ($0.925 < c < 0.975$) and highly segregated ($0.175 < c < 0.225$) c-score bin in 2016 exceeded the 95% confidence interval from an empirical Bayesian distribution. In 2013, two highly

segregated bins (c < 0.2) had more species pairs than expected, while zero highly aggregated bins (c > 0.8) did so.

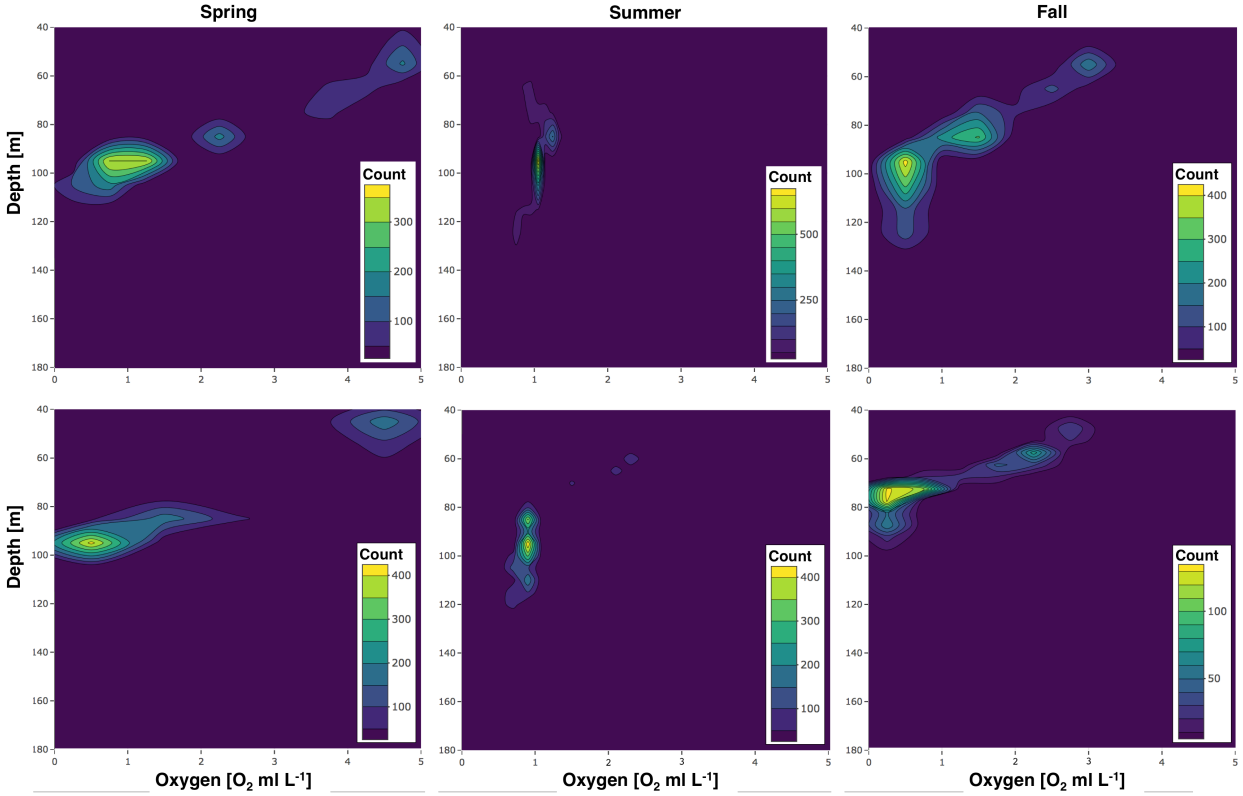

Figure 3.3. Two-dimensional histogram contour plots of megafaunal abundance with depth and oxygen in each season surveyed in 2013 (top row) and 2016 (bottom row) show the inter- and intra-annual shifts in abundance distribution. Weak deep-water oxygen renewal in 2016 led to species experiencing progressively lower dissolved oxygen levels throughout the year, culminating in the fall 2016 transect where prolonged and shoaling hypoxia caused abundance declines, and forced the megafaunal abundance peak to occur in a comparatively shallow and severely hypoxic (O_2 < 0.5 ml L^{-1}) zone.

Of the 91 unique species pairs assessed in the null models, 27 showed non-random associations in 2013 and 20 in 2016, both well above the 4.55 pairs expected at a 5% false detection rate (Table 3.4). The greater number of associations in 2013 was driven in large part by decapod crustaceans (n = 8 pairs). The absence of these species

from the Fall 2016 transect may have limited the ability of the randomization algorithm to detect associations despite potentially significant associations in spring and summer 2016. Aggregated pairs made up 59 % of the significant associations in 2013 and 40 % in 2016; decapod pairs also drove this pattern.

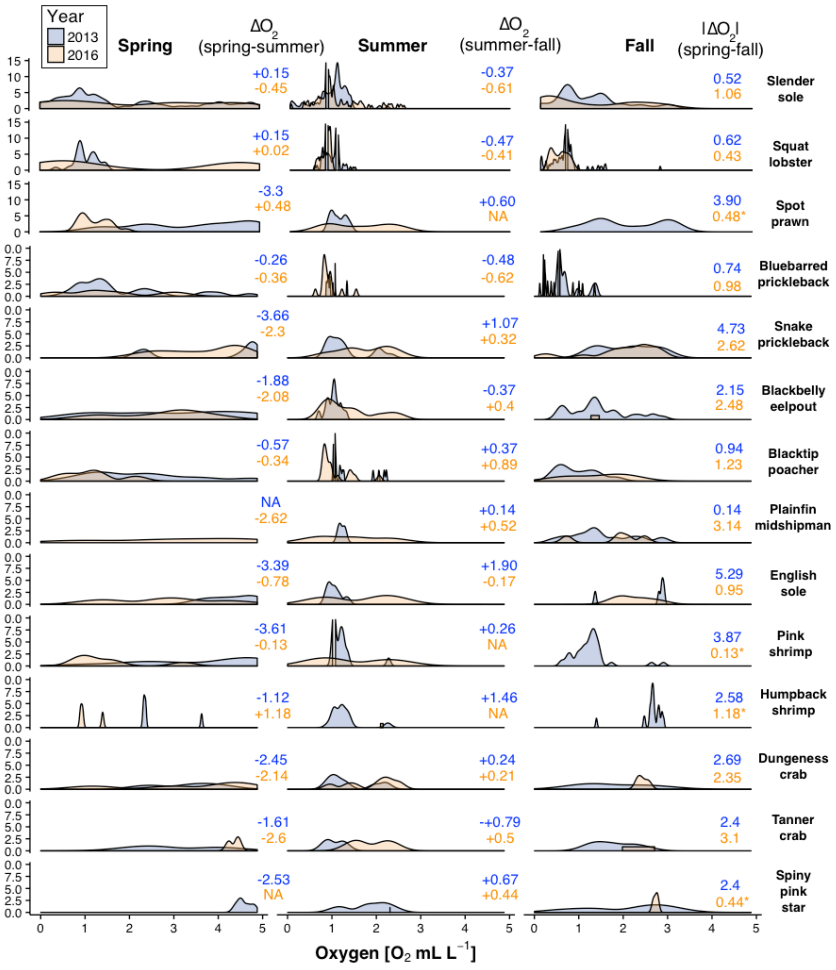

Figure 3.4. Kernel density plots of oxygen distributions in 2013 vs. 2016 across sampling seasons for 14 mobile species. Square-root transformed abundances are represented by waterfall height. Disappearance of multiple crustacean species, abundance declines, and distribution shifts to lower oxygen levels occurred in Fall 2016. Changes in median oxygen occurrence between seasons are listed between panels, and the total change throughout the year is listed at right with an asterisk for species that were not present in all seasons.

Species	$O_{2\text{-mean}}$ Spring	$O_{2\text{-mean}}$ Summer	$O_{2\text{-mean}}$ Fall	$O_{2\text{-min}}$ Spring	$O_{2\text{-min}}$ Summer	$O_{2\text{-min}}$ Fall	Density Spring	Density Summer	Density Fall
Slender sole	1.38 ± 0.07, 2.01 ± 0.17	1.02 ± 0.01, 0.87 ± 0.2	0.89 ± 0.03, 0.79 ± 0.11	0.03, 0.07	0.03, 0.02	0.00, 0.03	9.56 ± 0.43, 4.13 ± 0.45	9.48 ± 0.13, 7.25 ± 0.43	10.35 ± 0.40, 2.73 ± 0
Bluebarred prickleback	1.47 ± 0.14, 1.48 ± 0.88	1.04 ± 0.01, 0.88 ± 0.03	0.65 ± 0.03, 0.31 ± 0.08	0.54, 0.34	0.88, 0.63	0.52, 0.12	0.73 ± 0.11, 0.07 ± 0.17	0.60 ± 0.13, 0.44 ± 0.10	1.30 ± 0.40, 0.39 ± 0.31
Snake prickleback	4.17 ± 0.47, 3.82 ± 0.18	1.17 ± 0.07, 1.80 ± 0.15	2.08 ± 0.11, 2.23 ± 0.15	2.15, 2.20	0.87, 0.83	1.29, 0.21	0.11 ± 0.10, 0.85 ± 0.28	0.45 ± 0.05, 0.26 ± 0.08	0.82 ± 0.16, 0.46 ± 0.10
Blackbelly eelpout	2.95 ± 0.27, 2.88 ± 0.28	1.04 ± 0.02, 1.20 ± 0.08	1.31 ± 0.09, 1.37 ± 0.19	0.68, 0.93	0.69, 0.79	0.58, 1.27	0.56 ± 0.05, 0.39 ± 0.10	0.48 ± 0.03, 0.75 ± 0.09	0.76 ± 0.10, 0.02 ± 0.37
Blacktip poacher	2.05 ± 0.28, 1.08 ± 0.21	1.15 ± 0.07, 0.93 ± 0.05	0.87 ± 0.09, 1.51 ± 0.37	0.90, 0.35	1.03, 0.80	0.52, 0.68	0.26 ± 0.07, 0.25 ± 0.43	0.28 ± 0.05, 0.43 ± 0.13	0.43 ± 0.07, 0.08 ± 0.16
Plainfin midshipman	na, 2.96 ± 1.13	1.22 ± 0.04, 1.34 ± 0.42	1.43 ± 0.18, 1.83 ± 0.59	na, 0.97	1.14, 0.61	0.43, 0.73	na, 0.08 ± 0.11	0.04 ± 0.05, 0.05 ± 0.05	0.27 ± 0.06, 0.04 ± 0.12
English sole	4.36 ± 0.22, 2.75 ± 0.61	1.01 ± 0.04, 1.70 ± 0.29	2.70 ± 0.38, 2.20 ± 0.24	3.61, 1.28	0.87, 0.81	1.37, 1.90	0.08 ± 0.06, 0.13 ± 0.09	0.17 ± 0.04, 0.14 ± 0.08	0.05 ± 0.07, 0.06 ± 0.18
Squat lobster	1.01 ± 0.02, 2.01 ± 0.19	0.98 ± 0.01, 0.82 ± 0.004	0.56 ± 0.01, 0.41 ± 0.02	0.40, 0.25	0.54, 0.56	0.01, 0.21	10.27 ± 5.10, 9.36 ± 7.17	7.57 ± 0.25, 11.81 ± 1.01	14.25 ± 1.12, 8.33 ± 9.60
Spot prawn	3.64 ± 0.10, 1.15 ± 0.03	1.05 ± 0.02, 1.55 ± 0.13	1.92 ± 0.07, na	1.12, 0.79	0.87, 0.82	0.66, na	3.73 ± 0.23, 4.48 ± 7.75	1.36 ± 0.12, 0.69 ± 0.15	4.56 ± 0.39, na
Pink shrimp	4.01 ± 0.41, 1.28 ± 0.33	1.14 ± 0.01, 1.41 ± 0.34	1.25 ± 0.02, na	1.22, 0.88	1.01, 0.81	0.60, na	0.49 ± 0.57, 0.20 ± 0.31	5.60 ± 0.52, 0.13 ± 0.07	4.75 ± 1.78, na
Humpback shrimp	2.46 ± 0.23, 1.02 ± 0.19	1.20 ± 0.05, 2.12 ± 0.06	2.67 ± 0.04, na	2.31, 0.90	0.92, 2.09	1.40, na	0.14 ± 1.02, 0.06 ± 0.45	0.33 ± 0.09, 0.02 ± 0.17	1.12 ± 1.24, na
Dungeness crab	3.37 ± 0.67, 3.72 ± 0.94	1.26 ± 0.21, 2.03 ± 0.26	1.73 ± 0.57, 2.42 ± 0.10	2.44, 1.16	0.90, 0.96	1.26, 2.35	0.03 ± 0.10, 0.08 ± 0.11	0.08 ± 0.04, 0.08 ± 0.05	0.03 ± 0.11, 0.03 ± 0.09
Tanner crab	2.94 ± 1.04, 4.38 ± 0.13	1.05 ± 0.14, 1.89 ± 0.16	1.74 ± 0.21, 2.35 ± 0.73	2.32, 4.24	0.87, 1.50	1.30, 1.98	0.02 ± 0.09, 0.04 ± 0.24	0.03 ± 0.05, 0.12 ± 0.11	0.10 ± 0.10, 0.02 ± 0.13
Spiny pink star	4.56 ± 0.11, na	1.90 ± 0.23, 2.31	2.29 ± 0.48, 2.74 ± 0.04	4.41, na	1.11, 2.31	0.70, 2.68	0.03 ± 0.08, na	0.06 ± 0.08, 0.01 ± 0.16	0.07 ± 0.09, 0.03 ± 0.15

Table 3.3. Mean (± 2*SE) and minimum oxygen occurrence for sessile organisms in each sampling season, with sample years separated by commas (e,g, 2013, 2016). Densities 20 m^{-2} (± 2*SE) of sessile taxa show a drop in seawhip abundance in fall 2016. Sessile organisms experienced relatively low oxygen in fall 2016 when compared to the earlier year when deep-water oxygen was renewed in late summer.

Species	**$O_{2\text{-mean}}$ Spring**	**$O_{2\text{-mean}}$ Summer**	**$O_{2\text{-mean}}$ Fall**	**$O_{2\text{-min}}$ Spring**	**$O_{2\text{-min}}$ Summer**	**$O_{2\text{-min}}$ Fall**	**Density Spring**	**Density Summer**	**Density Fall**
Tiny ball sponge	1.91±0.08, 1.08±0.04	1.15±0.01, 0.86±0.01	0.93±0.03, 0.11±0.01	0.86, 0.14	1.03, 0.81	0.52, 0.02	–	–	–
White finger sponge	1.32±0.00, 0.74±0.18	1.20±0.01, 0.97±0.15	1.12±0.02, 0.12±0.02	1.31, 0.18	1.04, 0.88	0.03, 0.02	–	–	–
Giant anemone	3.16±0.48, 2.84±0.78	1.38±0.16, 1.51±0.17	1.41±0.24, 0.78±0.74	2.32, 0.90	0.88, 0.82	0.65, 0.10	0.10 ± 0.07, 0.18 ± 0.11	0.14 ± 0.04, 0.35 ± 0.12	0.21 ± 0.13, 0.09 ± 0.16
Seawhip	4.13±0.05, 3.83±0.05	1.26±0.04, 2.00±0.02	2.52±0.04, 2.03±0.08	1.79, 2.48	0.87, 0.96	1.22, 0.21	13.99 ± 1.18, 5.78 ± 1.27	11.98 ± 1.03, 10.20 ± 1.73	26.26 ± 3.59, 2.61 ± 0.46

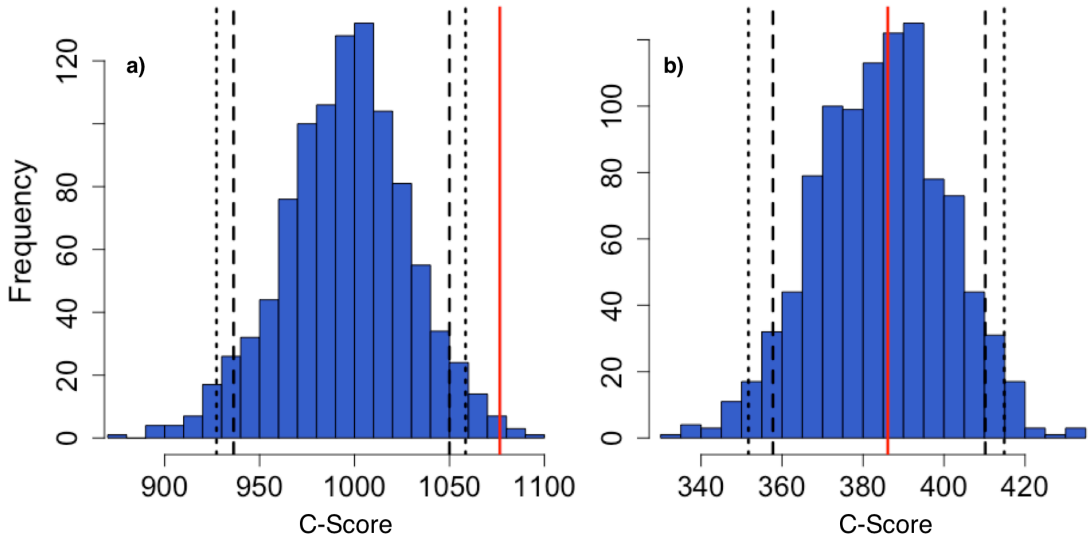

Figure 3.5. Distributions of community checkerboard scores (c-scores) in a) 2013 and b) 2016. Blue bars represent frequencies of c-scores from 500 null model iterations. Red lines represent observed c-scores, while long and short dashed lines represent the 95% one-tailed and two-tailed confidence intervals for significant departures from null model expectations. The 2013 observed score indicates a significantly aggregated community ($p < 0.001$), suggesting increased community homogenization in the later year.

Critical transition points along oxygen gradient

The most parsimonious multivariate regression tree (MRT) explained 38% of the variance in community structure; five splits in community structure with environmental variables, four of which were due to dissolved oxygen, were shown. Season, year, and depth did not contribute to any of the splits, while there was one split with temperature in oxygen greater than 1.8 ml L^{-1}; high spot prawn and slender sole abundances in normoxic waters of two relatively cool 2013 transects contributed to this split (Figure 3.7). The branch below 0.2 ml L^{-1} oxygen described the greatest number of quadrats (n=339) and

was largely the lower dissolved oxygen limit of all megafaunal habitation. Oxygen-related splits also occurred at 0.9, 1.1 and 1.8 ml L^{-1}.

FI scores in each 0.25 ml L^{-1} oxygen window agree with the breakpoints detected by MRT and detect major changes in community order from 1-2 ml L^{-1} (Figure 3.8a). 2013 FI scores in dissolved oxygen from 1.25-2.00 ml L^{-1} did not differ significantly from those generated randomly (Figure 3.8b), while all other FI scores indicate a more ordered community than communities generated from randomly selected quadrats. Species accumulation curves in each 0.25 ml L^{-1} oxygen window show a species diversity minimum in the 0-0.25 ml L^{-1} oxygen window and, in contrast to the trend in FI, increased incrementally from 0-1 ml L^{-1} (Figure 3.8c).

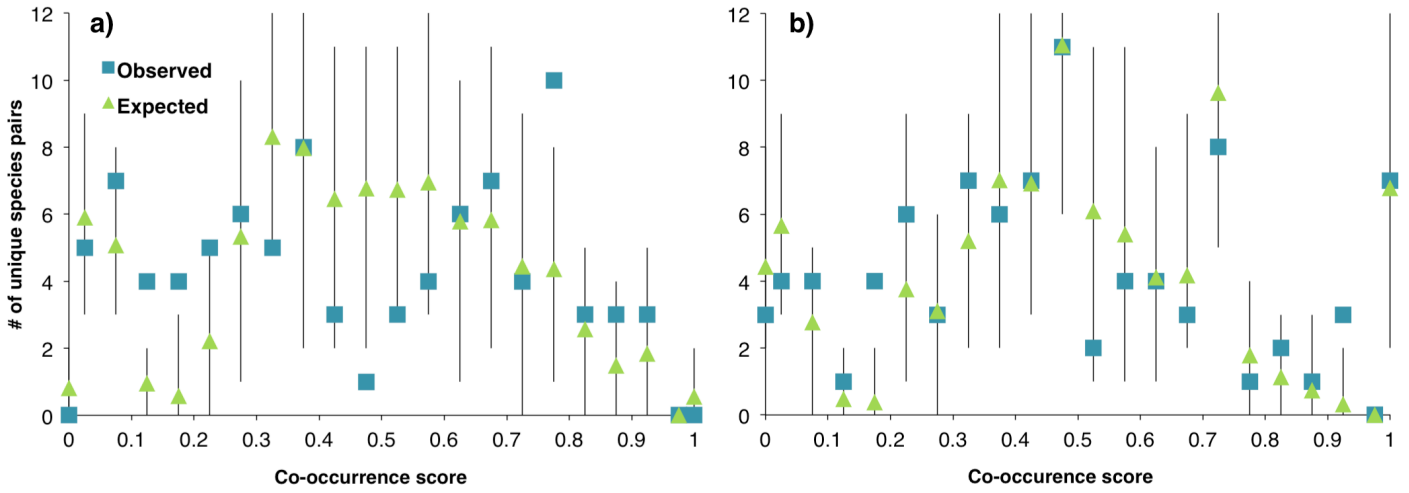

Figure 3.6. Observed vs. expected frequencies of species pair co-occurrence scores from Pairs null models in 2013 vs. 2016 transects. Error bars represent 95% confidence intervals for expected number of species pairs at each co-occurrence score range. Increases in completely overlapping (c-score=0) and segregated (c-score=1) species pairs occurred in 2016, suggesting shifts in community structure from 2013.

Change in long-term oxygen

Mean dissolved oxygen steadily decreased at the 95 m VENUS node. The maximum mean hourly oxygen failed to reach 3 ml L^{-1} in 2014 for the first time since the time-series began in 2006 and did so again in 2015-2016 (Figure 3.9a). A linear regression showed that the slope of the yearly oxygen decrease steepened from -0.05 in 2014 (Chu & Tunnicliffe 2015a) to -0.07. The one-year running mean of oxygen also steadily declined from 2010-2017 with a brief increase in 2013-2014 and fell below the severe hypoxia threshold in 2015 (Figure 3.9b); the yearly mean also fell below this threshold for the first time in 2015 (Figure 3.9d). One-year running variance also fell to the lowest recorded levels in 2015-2016 as oxygen hovered near zero and set a lower limit on the variability (Figure 3.9c).

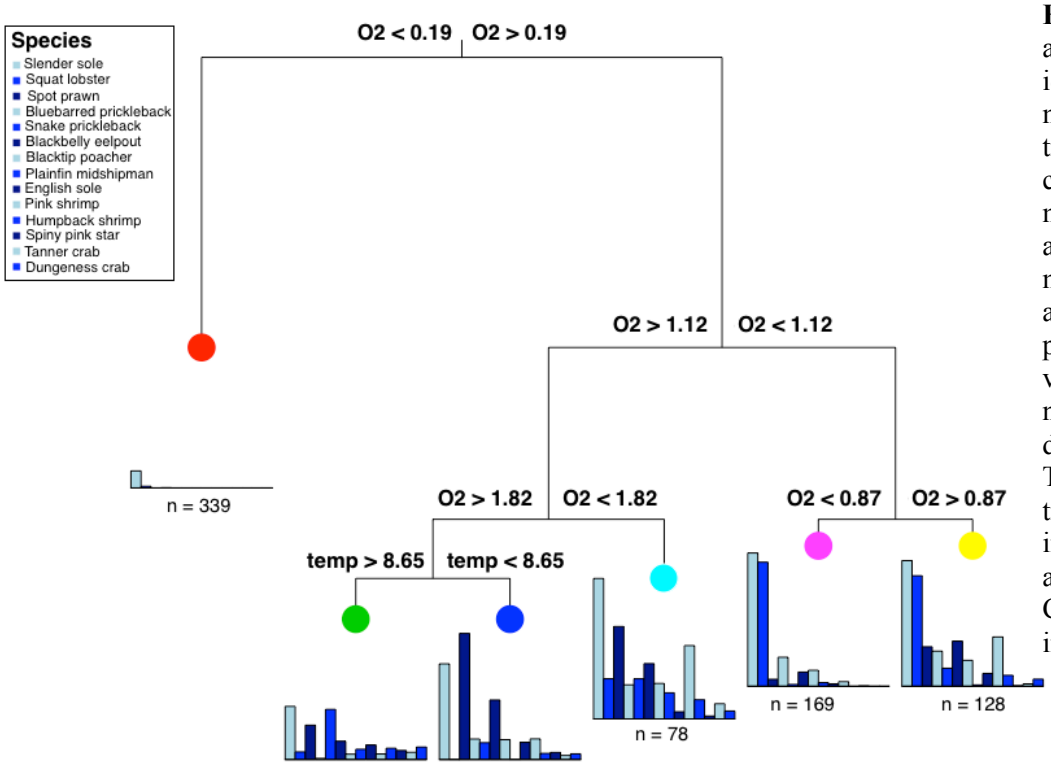

Figure 3.7. Breaks in assemblage structure identified using multivariate regression tree analysis, using combined data (n=902 20 m^{-2} quadrats) from 2013 and 2016. Mobile megabenthic species abundances (bar plots), primary explanatory variable values and the number of quadrats are displayed for each leaf. The most parsimonious tree (5 splits) did not include year or season and explained ~ 38 % (1 – CV Error) of the variance in community structure.

	Slender sole	Squat lobster	Spot prawn	Bluebarred prickleback	Snake prickleback	Blackbelly eelpout	Blacktip poacher	Plainfin midshipman	English sole	Pink shrimp	Humpback shrimp	Dungeness crab	Tanner crab	Spiny pink star
Slender sole	x	na, na	na, na	na, na	**6.7, 2.4**	na, na	na, na	na, na	**2.6, na**	na, na	na, na	**na, 2.8**	**na, 5.8**	**4.6**
Squat lobster	x	x	**15.6, na**	-2.3, na	**14.1, 8.5**	**3.6, 3.1**	na, na	**2.9, na**	**7.2, 3.2**	na, na	**2.1, na**	**3.3, 5.1**	**3.6, 4.1**	**5.1**
Spot prawn	x	x	x	na, na	-5.1, na	**-3.7, -2.9**	na, na	**-3.5, na**	-4.2, na	**na, -3.67**	**-3.1, -2.3**	na, na	-2.7, na	na,
Bluebarred prickleback	x	x	x	x	**5.1, 2.7**	na, na	**-4.8, -3.7**	na, na	na, na	na, na	na, na	**na, 3.4**	**na, 2.1**	**2.8**
Snake prickleback	x	x	x	x	x	na, na	**3.5, na**	na, na	na, na	na, na	na, na	-2.7, na	-2.9, na	-2.5
Blackbelly eelpout	x	x	x	x	x	x	na, na	na, na	na, na	na, na	na, na	na, na	na, na	na,
Blacktip poacher	x	x	x	x	x	x	x	na, na	**2.3, na**	-3.6, na	na, na	na, na	na, na	na,
Plainfin midshipman	x	x	x	x	x	x	x	x	na, na	-3.5, na	na, na	na, na	-2.6, na	na,
English sole	x	x	x	x	x	x	x	x	x	na, na	na, na	na, -2.3	na, na	na,
Pink shrimp	x	x	x	x	x	x	x	x	x	x	**-3.5, -3.3**	na, na	na, na	na,
Humpback shrimp	x	x	x	x	x	x	x	x	x	x	x	na, -2.2	na, na	na,
Dungeness crab	x	x	x	x	x	x	x	x	x	x	x	x	na, -2.1	na,
Tanner crab	x	x	x	x	x	x	x	x	x	x	x	x	x	na,
Spiny pink star	x	x	x	x	x	x	x	x	x	x	x	x	x	x

Table 3.4. Corrected Z-scores from PAIRS null model analysis show species pairs significantly more segregated (positive) or aggregated (negative) than null model expectations. Results from 2013 and 2016 are separated by commas and associated pairs with significantly different ($p < 0.01$) oxygen distributions, as determined by bootstrap comparisons using data from both years combined, are in bold.

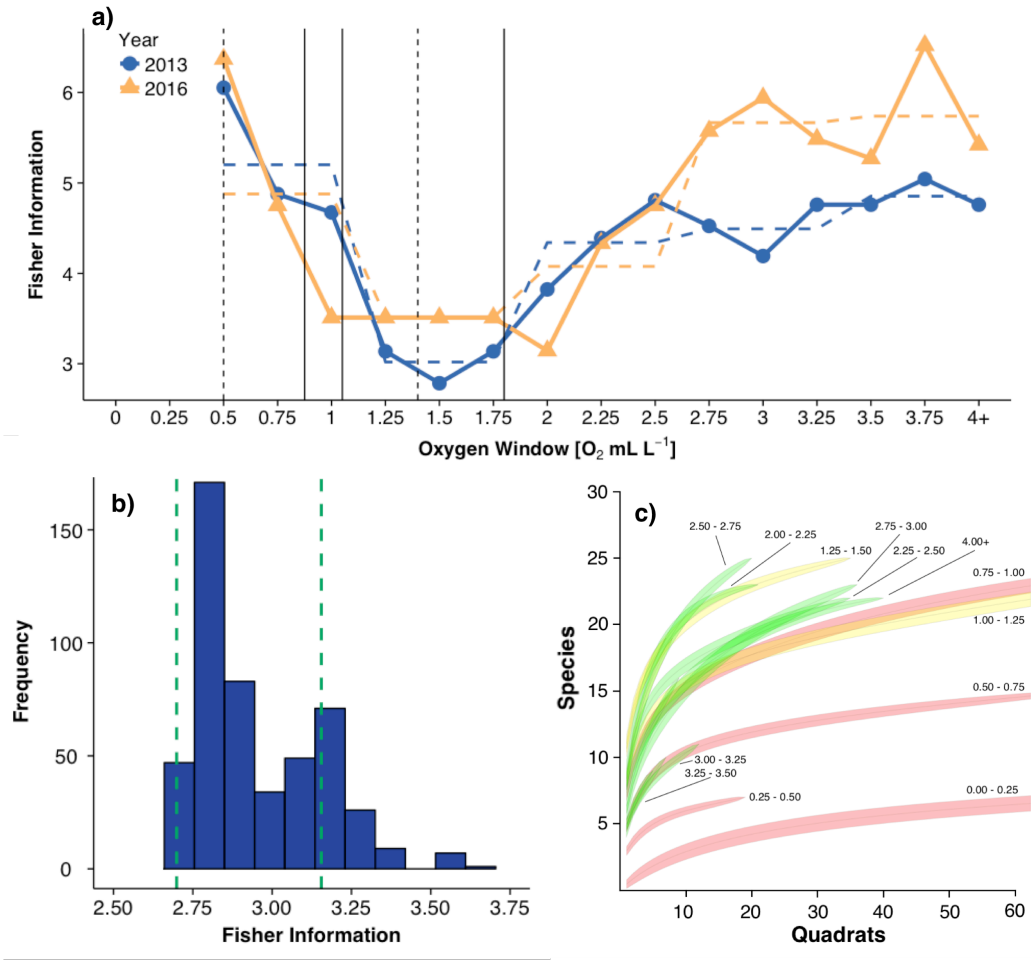

Figure 3.8. a) Fisher Information (FI) and 3-point mean FI (dashed lines) in each 0.25 ml L^{-1} dissolved oxygen window in 2013 versus 2016. Literature-derived hypoxia and severe hypoxia thresholds are displayed with dashed vertical lines, while solid lines show community thresholds determined by multivariate regression tree. Both regression tree and Fisher Information indicate spatial transitions between ~1-2 ml L^{-1} dissolved oxygen; moving from low oxygen to high, Fisher Information shows changes before the breakpoints determined by multivariate regression tree, suggesting utility as an 'early warning system' for community changes along ecological gradients.

b) Frequency distribution of 500 FI scores generated from species densities in 50 randomly selected quadrats. Vertical dashed lines mark 95% confidence intervals for non-random FI; 2013 FI scores in 1.25-2.00 ml L^{-1} oxygen are not significantly different than those generated by randomly selecting quadrats.

c) Expected species accumulation curves generated for each 0.25 ml L^{-1} dissolved oxygen window using combined data from all surveyed species in both years show low diversity in hypoxic (< 1 ml L^{-1}; red curves) versus 'intermediate' (1-2 ml L^{-1}; yellow curves) and normoxic (>2 ml L^{-1}; green curves) zones.

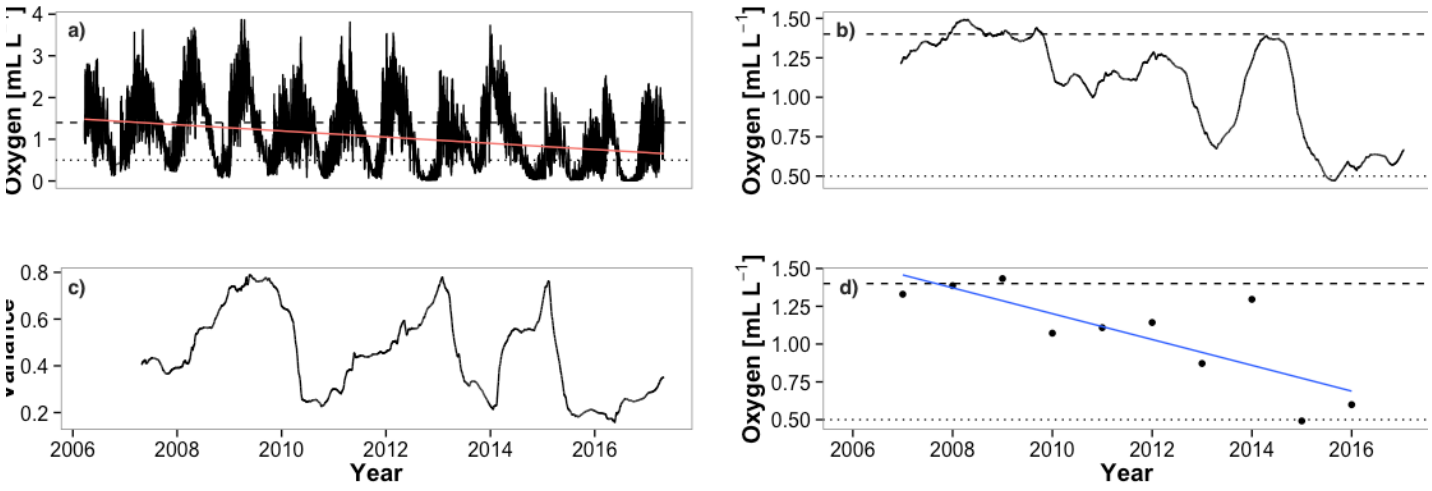

Figure 3.9. VENUS Oxygen records from April 2006-April 2017 records show long-term deoxygenation and a decrease in the amplitude of the seasonal pattern after 2014. Dashed and dotted lines represent sublethal (1.4 ml L-1) and lethal (0.5 ml L-1) thresholds. Significant linear relationships ($p < 0.01$) are shown with solid lines.

a) 1-hour interval dissolved oxygen record.
b) One-year running mean of dissolved oxygen
c) One-year running variance of dissolved oxygen
d) Yearly dissolved oxygen means for calendar years of 2007-2016.

DISCUSSION

Variable bottom oxygen and community structure between years

2016 bottom oxygen concentrations did not follow the course of recovery following summer depletion seen in 2013 (Figure 3.1; Table 3.1). A weak deep-water renewal in 2015 coupled with the warm-water mass that entered into Saanich Inlet around the same time and sank to 100 – 200 m depth in 2016 (Ross 2017) may have enhanced hypoxic conditions in the spring and summer 2016 transects. Fall 2016 bottom oxygen concentrations reflected another muted deep-water renewal, as the spatial extent of hypoxia was similar to that seen in the summer. Although a diminished renewal occurred in 2010 (Chu & Tunnicliffe 2015a), only one partial transect was completed in December

of that year. Thus, this study represents the first insights into how renewal failure influences bottom oxygen concentrations and community structure from pre-bloom spring conditions through prolonged hypoxia occurring from summer to fall.

In addition, the Northeast Pacific is a global hotspot for long-term deoxygenation (Ito et al. 2017), which likely contributed to record minima in bottom oxygen and mean yearly oxygen at the VENUS node. Oxygen variability was also at its ten-year low entering 2016 (Figure 3.9c), and decreases in environmental variability can signal impending ecological shifts (Dakos et al. 2012). Variability may be particularly important in low-oxygen, as variable oxygen provides species with brief respites from aerobic stress that allow them to persist at low mean oxygen levels (Chu & Tunnicliffe 2015a).

Community structure reflected the changes in bottom oxygen concentrations, with major differences in species composition and abundances between years. Expanded hypoxic conditions in 2016 led to a larger proportion of organisms experiencing hypoxia in all seasons than in 2013, which may have contributed to the strong abundance declines seen in the latter portion of 2016; while no difference in overall animal density between years occurred in the spring or summer transects, most species – including the four most abundant species (i.e. seawhip, slender sole, squat lobster and spot prawn) – occurred in higher densities in fall 2013 than in 2016, where protracted hypoxia occurred on much of the slope (Table 3.2; Table 3.3). Spot prawn declined from spring to summer 2016 and were absent for the first time in the 11-year time-series in the fall transect, along with several other less abundant decapods (Chu & Tunnicliffe 2015a). Spot prawns typically occupy oxygen ranges well above their aerobic metabolism threshold, suggesting active evasion of hypoxic conditions (Chu & Gale 2017). Field distributions of spot prawns

have shown sensitivity to low-oxygen in previous years (Jamieson & Pikitch 1988), and their abundance declined as hypoxia expanded in summer 2013 (Chu & Tunnicliffe 2015a). The slow progression of hypoxia over the course of the year may have also impaired behaviours related to the avoidance of hypoxia in crustaceans that use short temporal changes in dissolved oxygen coupled with cues from current direction to orient themselves toward higher oxygen (Bell 2003). Seawhip declines may have hastened the disappearance of spot prawn and other decapods typically seen amongst seawhip stands (Chu & Tunnicliffe 2015a). The increase of nudibranchs concurrent with these declines may have been caused by the expansion of a food source in the seawhips felled from oxygen stress. Alternatively, decreased competition with spot prawn may have fostered the nudibranch proliferation. While a lack of biological information on the burrowing sea cucumber precludes us from knowing the reasons for their occurrence in the severely hypoxic portions of the fall 2016 transect, their sudden appearance is a notable change from previous transects.

We also note decreases in the both the strength of interaction, as represented by species-pair Z-scores, and abundance of several strongly interacting species that may lead to future losses in ecosystem functioning and/or diversity (Danovaro et al. 2008; Sorte et al. 2016). In particular, slender sole are important re-suspenders of organic material (Yahel et al. 2008), and their decline in Fall 2016 (Table 3.2) may impact benthic-pelagic coupling in the inlet. This result is surprising given that slender sole stand to benefit from deoxygenation, as they have one of the lowest measured critical oxygen thresholds measured in fish (Chu & Gale 2017), allowing them to forage in severe hypoxia where competition is reduced. Furthermore, slender sole have increased in the Northeast Pacific

ichthyoplankton as deoxygenation has proceeded since 1980 (Guan 2015; Johnson-Colegrove 2015). The decline in seawhip density observed in Fall 2016 (Table 3.3) is also notable due to the biotic habitat they provide, which fosters diversity (Brodeur 2001). In a summer 2017, spot prawn were present but were still notably sparse, potentially due to the muted recovery of slow-growing seawhip habitat; nudibranchs were still present in high abundances relative to previous years, and the holothurian seen in 2016 was absent (Gasbarro unpub. data). Taken together, these observations suggest hysteresis in the recovery of some component species, and that Fall 2016 anomalies were a 'flicker' into an alternative stable state; these are both noted features of ecological systems nearing critical transitions (Scheffer et al. 2012).

One of the principal effects of ocean deoxygenation is the compression of benthic habitats into shallower waters (Stramma et al. 2008). The changes in both bottom oxygen and community structure from 2013 to 2016 both suggest stronger habitat compression in the latter year, and provide some insights into the affected species. The length of transect overlain by hypoxic water increased, and by normoxic water decreased, in 2016. However, the greatest proportional change between years occurred in the 'transitional' zone from 1.1 – 1.8 ml L^{-1} O_2; this zone covered 9.6 - 14.7 % as much transect length as in 2013 (Table 1). This steepening of the oxygen gradient allows species to emigrate upslope over relatively short distances to avoid unfavorable low-oxygen conditions. Separation between species in the normoxic and hypoxic zones is subsequently enhanced, with the net effect of community homogenization. Thus, when both component species of a given pair occupy similar oxygen ranges (i.e. normoxia or hypoxia), they generally were more aggregated in 2016. Those that inhabit opposite zones were more partitioned.

This may explain why more pairs displayed complete overlap or separation another in 2016 (Figure 3.6), and why some significantly associated pairs from 2013 were either weakly or non-associated in 2016 (Table 3.4). Squat lobsters and spot prawn, for example, showed the strongest segregation of the 91 tested species pairs in 2013, but were not significantly associated in 2016, providing evidence that they were forced together in the latter year by the broad expanse of severe hypoxia over the shelf.

Assemblage transitions along the oxygen gradient

Multivariate regression tree (MRT) and Fisher Information (FI) analyses of assemblage structure identified a coenocline from low to high oxygen with transitional zones consistent between years despite the changes in bottom oxygen distribution and species composition noted above. The FI breakpoints at which our mobile assemblage changed also did not match patterns in the species accumulation curves, suggesting that FI is robust to changes in species identity and richness (Figure 3.7; Fath & Cabezas 2004). The lower breakpoint in assemblage structure detected by MRT (0.2 ml L^{-1}; Figure 3.6) and the low diversity in the 0.00-0.25 ml L^{-1} O_2 window (Figure 7c) both agree with diversity declines found on continental margins in this range of oxygen (Sperling et al. 2016) and largely represent the lower oxygen limits of mobile megafaunal presence at approximately 0.2 ml L^{-1}. The high-oxygen node at 1.8 ml L^{-1} found by MRT and the loss of order shown by FI below about 2 ml L^{-1} both occur at oxygen levels that likely are not limiting aerobic metabolism for a majority of the component species (Chu & Tunnicliffe 2015a). This high-oxygen transition may be caused by convergence between low and high-oxygen assemblages in this zone facilitating increased species turnover and/or species interactions. Alternatively, behavioral effects can be induced in

this range of oxygen (Gray et al. 2002), but may not have been captured by our snapshot samples. Fish generally avoid oxygen levels well above their critical oxygen tensions (Breitburg 2002). This occurs even when movement towards higher oxygen increases the possibility of predation, suggesting a choice between low-oxygen and predation risk (Breitburg 1992). Secondary variables that covary with oxygen but were outside the scope of this study, e.g. pCO_2 (Paulmier et al. 2011), may have also played a role in setting this upper transition point.

No major changes in Fisher Information occurred near sublethal (1.4 ml L^{-1}) and lethal (0.5 ml L^{-1}) hypoxia thresholds common in the literature. However, the East Pacific hypoxia threshold described by Chu & Gale (2017) of 0.88 mL L^{-1} more closely matches our FI transition and the MRT node at 0.87 mL L^{-1}, suggesting that thresholds based in physiological traits may be more accurate for predicting community changes, and that global thresholds should be employed with caution given the evolutionary and environmental discrepancies between ocean basins (Vaquer-Sunyer & Duarte 2008; Deutsch et al. 2015). The MRT and transition at ~ 1.1 ml L^{-1} oxygen may relate to the oxygen levels that induce shoaling in some of most abundant megafaunal species (e.g. slender sole, spot prawn, pink shrimp) on the transect (Chu & Tunnicliffe 2015a). Spatial resorting of species due to deoxygenation occurs in large part because species live near the oxygen thresholds needed to maintain their aerobic respiration (Seibel 2011); thus, deoxygenation decreases the metabolic viability of many benthic habitats, and alters species abundances and distributions (Deutsch et al. 2015). Indices of community order (and disorder) may be able to detect these metabolically induced spatial shifts along environmental gradients. This approach may be especially useful in environments, such

as the deep sea, where hyperbaric constraints require technologically challenging *in situ* physiological techniques and metabolic trait data are sparse or non-existent for many taxa (Hughes et al. 2011). Additionally, the fidelity of our observed FI scores to MRT and regional hypoxia thresholds indicates that it may serve as a tool to detect community transitions along various ecological gradients.

Conclusions

Our results show notable differences in both bottom oxygen and benthic community structure from 2013 to 2016, with protracted summer hypoxia causing abundance declines, compositional shifts and community homogenization. We also present an adaptation of the Fisher Information index that is a useful complement to biological data in determining ecological transitions in multivariate systems. Despite the changes in bottom oxygen and community structure noted above, we found relatively static breakpoints in assemblage structure along the dissolved oxygen gradient in both years, suggesting that community-level transitions occur at fixed oxygen levels in this region. Additionally, the changes observed in 2016 may provide the first glimpse into the future benthic community structure of Saanich Inlet should extended low-oxygen events such as those seen in 2015-2016 become more frequent. Complete recovery is possible, however, and the successional process has been documented following a similar extended hypoxic event in a Swedish fjord (Rosenberg et al. 2002). Our results also display the utility of long-term ecological time-series, and highlight the fact that long-term sampling is crucial in determining the natural variability and capacity for change in complex systems where distinctive events can occur even over ten years of surveys. In seafloor ecosystems, where rapid change may outpace the ability of many slow-growing

organisms to respond (Moffit et al. 2015), consistent long-term sampling may be even more essential. As global change proceeds, it will become increasingly important to locate the thresholds and understand the consequences of such events in order to determine the resiliency of benthic ecosystems.

Literature Cited

Ahmad N, Derrible S, Eason T, Cabezas H (2016) Using Fisher information to track stability in multivariate systems. Open Science 3:160582

Anderson JJ, Devol AH (1973) Deep water renewal in Saanich Inlet, an intermittently anoxic basin. Estuarine and Coastal Marine Science 1:1–10

Bell GW, Eggleston DB, Wolcott TG (2003) Behavioral responses of free-ranging blue crabs to episodic hypoxia.: I. Movement. Marine Ecology Progress Series 259:215–225

Benjamini Y, Yekutieli D (2001) The control of the false discovery rate in multiple testing under dependency. Ann Statist 29:1165–1188

Breitburg DL (1992) Episodic hypoxia in Chesapeake Bay: interacting effects of recruitment, behavior, and physical disturbance. Ecological Monographs 62:525–546

Breitburg D (2002) Effects of hypoxia, and the balance between hypoxia and enrichment, on coastal fishes and fisheries. Estuaries and Coasts 25:767–781

Breitburg DL, Loher T, Pacey CA, Gerstein A (1997) Varying effects of low dissolved oxygen on trophic interactions in an estuarine food web. Ecological Monographs 67:489–507

Brodeur RD (2001) Habitat-specific distribution of Pacific ocean perch (Sebastes alutus) in Pribilof Canyon, Bering Sea. Continental Shelf Research 21:207–224

Chandler PC, King SA, and Perry RI (eds) (2017) State of the physical, biological and selected fishery resources of Pacific Canadian marine ecosystems in 2016. Can. Tech. Rep. Fish. Aquat. Sci.

Chu JWF, Gale KSP (2017) Ecophysiological limits to aerobic metabolism in hypoxia determine epibenthic distributions and energy sequestration in the northeast Pacific ocean. Limnology and Oceanography

Chu JWF, Tunnicliffe V (2015a) Oxygen limitations on marine animal distributions and the collapse of epibenthic community structure during shoaling hypoxia. Global Change Biology 21:2989–3004

Chu JWF, Tunnicliffe V (2015b) Data from: Oxygen limitations on marine animal distributions and the collapse of epibenthic community structure during shoaling hypoxia. Global Change Biology 21:2989–3004. Dryad Digital Repository.

Dakos V, Carpenter SR, Brock WA, Ellison AM, Guttal V, Ives AR, Kéfi S, Livina V, Seekell DA, Nes EH van, Scheffer M (2012) Methods for Detecting Early Warnings of Critical Transitions in Time Series Illustrated Using Simulated Ecological Data. PLOS ONE 7:e41010

Danovaro R, Gambi C, Dell'Anno A, Corinaldesi C, Fraschetti S, Vanreusel A, Vincx M, Gooday AJ (2008) Exponential decline of deep-sea ecosystem functioning linked to benthic biodiversity loss. Current Biology 18:1–8

De'ath G (2002) Multivariate regression trees: a new technique for modeling species–environment relationships. Ecology 83:1105–1117

Deutsch C, Ferrel A, Seibel B, Pörtner H-O, Huey RB (2015) Climate change tightens a metabolic constraint on marine habitats. Science 348:1132–1135

Dewey R, Sastri A, Mihaly S (2015) The 2014 perspective from Oceans Network Canada. In: Chandler PC, King SA, and Perry RI (eds) State of the physical,

biological and selected fishery resources of Pacific Canadian marine ecosystems in 2014. Can. Tech. Rep. Fish. Aquat. Sci.

Diaz RJ, Rosenberg R (2008) Spreading dead zones and consequences for marine ecosystems. Science 321:926–929

Eason T, Cabezas H (2012) Evaluating the sustainability of a regional system using Fisher information in the San Luis Basin, Colorado. J Environ Manage 94:41–49

Fath BD, Cabezas H, Pawlowski CW (2003) Regime changes in ecological systems: an information theory approach. J Theor Biol 222:517–530

Fath BD, Cabezas H (2004) Exergy and Fisher Information as ecological indices. Ecol Model 174:25–35

Gotelli NJ (2000) Null model analysis of species co-occurrence patterns. Ecology 81:2606–2621

Gotelli NJ, Hart EM, Ellison AM (2015) Co-occurrence Analysis. EcosimR. Available at www.ecosimr.org

Gray JS, Wu RS, Or YY (2002) Effects of hypoxia and organic enrichment on the coastal marine environment. Marine Ecology Progress Series 238:249–279

Grego M, Riedel B, Stachowitsch M, De Troch M (2014) Meiofauna winners and losers of coastal hypoxia: case study harpacticoid copepods. Biogeosciences; Katlenburg-Lindau 11:281

Grundle DS, Timothy DA, Varela DE (2009) Variations of phytoplankton productivity and biomass over an annual cycle in Saanich Inlet, a British Columbia fjord. Continental Shelf Research 29:2257–2269

Guan L (2015) Spatial and temporal dynamics of larval fish assemblages in the Strait of Georgia. Ph.D. Thesis. Univ.of Victoria.

Herlinveaux R (1962) Oceanography of Saanich Inlet in Vancouver Island, British-Columbia. Journal of the Fisheries Research Board of Canada 19:1–37

Hughes SJM, Ruhl HA, Hawkins LE, Hauton C, Boorman B, Billett DSM (2011) Deep-sea echinoderm oxygen consumption rates and an interclass comparison of metabolic rates in Asteroidea, Crinoidea, Echinoidea, Holothuroidea and Ophiuroidea. J Exp Biol 214:2512–2521

Ito T, Minobe S, Long MC, Deutsch C Upper ocean O2 trends: 1958–2015. Geophys Res Lett:2017GL073613

Jamieson GS, Pikitch EK (1988) Vertical distribution and mass mortality of prawns, Pandalus platyceros, in Saanich Inlet, British Columbia. Fish Bull 86: 601−608

Johnson-Colegrove A, Ciannelli L, Brodeur RD (2015) Ichthyoplankton distribution and abundance in relation to nearshore dissolved oxygen levels and other environmental variables within the Northern California Current System. Fisheries oceanography 24:495–507

Karunanithi A, Cabezas H, Frieden BR, Pawlowski C (2008) Detection and assessment of ecosystem regime shifts from Fisher Information. Ecology and Society 13

Keeling RF, Körtzinger A, Gruber N (2010) Ocean deoxygenation in a warming world. Annual Review of Marine Science 2:199–229

Levings C, Foreman R, Tunnicliffe V (1983) Review of the benthos of the Strait of Georgia and Contiguous Fjords. Can J Fish Aquat Sci 40:1120–1141

Manning CC, Hamme RC, Bourbonnais A (2010) Impact of deep-water renewal events on fixed nitrogen loss from seasonally-anoxic Saanich Inlet. Marine Chemistry 122:1–10

Matabos M, Tunnicliffe V, Juniper SK, Dean C (2012) A Year in Hypoxia: Epibenthic Community Responses to Severe Oxygen Deficit at a Subsea Observatory in a Coastal Inlet. PLoS One 7:e45626

Moffitt SE, Hill TM, Roopnarine PD, Kennett JP (2015) Response of seafloor ecosystems to abrupt global climate change. PNAS 112:4684–4689

Paulmier A, Ruiz-Pino D, Garçon V (2011) CO_2 maximum in the oxygen minimum zone (OMZ). Biogeosciences 8:239–252

Rosa R, Seibel BA (2008) Synergistic effects of climate-related variables suggest future physiological impairment in a top oceanic predator. PNAS 105:20776–20780

Rosenberg R, Agrenius S, Hellman B, Nilsson HC, Norling K (2002) Recovery of marine benthic habitats and fauna in a Swedish fjord following improved oxygen conditions. Marine Ecology Progress Series 234:43–53

Ross T (2017) La Niña, the blob and another warmest year. In: Chandler PC, King SA, and Perry RI (eds) State of the physical, biological and selected fishery resources of Pacific Canadian marine ecosystems in 2016. Can. Tech. Rep. Fish. Aquat. Sci.

Ryan JA, Ulrich JM (2017). xts: eXtensible Time Series. R package version 0.10-0. https://CRAN.R-project.org/package=xts

Sastri A, Dewey R, Pawlowicz R (2016) Deep water and sea-surface properties in the Strait of Georgia during 2015: ferries and cabled instruments. In: Chandler PC, King SA, and Perry RI (eds) State of the physical, biological and selected fishery

resources of Pacific Canadian marine ecosystems in 2015. Can. Tech. Rep. Fish. Aquat. Sci.

Scheffer M, Carpenter SR, Lenton TM, Bascompte J, Brock W, Dakos V, Koppel J van de, Leemput IA van de, Levin SA, Nes EH van, Pascual M, Vandermeer J (2012) Anticipating critical transitions. Science 338:344–348

Somero GN, Beers JM, Chan F, Hill TM, Klinger T, Litvin SY (2016) What Changes in the carbonate system, oxygen, and temperature portend for the Northeastern Pacific ocean: a physiological perspective. BioScience 66:14–26

Schluter D (1984) A variance test for detecting species associations, with some example applications. Ecology 65:998–1005

Sperling EA, Frieder CA, Levin LA (2016) Biodiversity response to natural gradients of multiple stressors on continental margins. Proc R Soc B 283:20160637

Stone L, Roberts A (1990) The checkerboard score and species distributions. Oecologia 85:74–79

Stramma L, Johnson GC, Sprintall J, Mohrholz V (2008) Expanding oxygen-minimum zones in the tropical oceans. Science 320:655–658

Stramma L, Schmidtko S, Levin LA, Johnson GC (2010) Ocean oxygen minima expansions and their biological impacts. Deep Sea Research Part I: Oceanographic Research Papers 57:587–595

Stramma L, Prince ED, Schmidtko S, Luo J, Hoolihan JP, Visbeck M, Wallace DWR, Brandt P, Körtzinger A (2012) Expansion of oxygen minimum zones may reduce available habitat for tropical pelagic fishes. Nature Clim Change 2:33–37

Ulrich W (2008) Pairs – a FORTRAN program for studying pair-wise species associations in ecological matrices. Available at: www.uni.torun.pl/~ulrichw

Vaquer-Sunyer R, Duarte CM (2008) Thresholds of hypoxia for marine biodiversity. Proc Natl Acad Sci U S A 105:15452–15457

Wang D, Gouhier TC, Menge BA, Ganguly AR (2015) Intensification and spatial homogenization of coastal upwelling under climate change. Nature 518:390–394

Yahel G, Yahel R, Katz T, Lazar B, Herut B, Tunnicliffe V (2008) Fish activity:: a major mechanism for sediment resuspension and organic matter remineralization in coastal marine sediments. Marine Ecology Progress Series 372:195–209

Zaikova E, Walsh DA, Stilwell CP, Mohn WW, Tortell PD, Hallam SJ (2010) Microbial community dynamics in a seasonally anoxic fjord: Saanich Inlet, British Columbia. Environmental microbiology 12:172–191

Zeileis A, Grothendieck G (2005). zoo: S3 Infrastructure for Regular and Irregular Time Series. Journal of Statistical Software, 14(6), 1-27. doi:10.18637/jss.v014.i06

Chapter 4 : General Conclusion

Major Outcomes

I present the results of nine remotely operated vehicle ascents up the previously unstudied confining walls of Douglas Channel, BC in Chapter 2. I describe the composition and abundance of animals both with depth and along the fjord axis and relate these findings to the mass flux structure of the fjord derived from nearby moored current-meter records. Animal abundance increased in the upper 150 m – where a consistent oceanic inflow occurs (Wan et al. 2017) – and was significantly correlated with the winter mass flux of the fjord, suggesting a tight coupling between faunal density and an inflow that facilitates particle delivery to the suspension-feeding assemblages. This finding of animal abundance augmented by high flow is consistent with findings on shallow subtidal rock walls (Leichter & Witman 1997) and other abrupt topographies in the deep sea (i.e. > 200 m) where particle delivery is enhanced (Genin et al. 1992; Rowden et al. 2010; Huvenne et al. 2011). The increase in animal cover in the upper 150 m was driven by greater abundances of hexactinellids, demosponges, zoanthids and articulate brachiopods, and suggests a food-limitation below these depths. I also assessed the taxonomic and functional richness of the wall fauna using species-trait-abundance matrices, and found that the deep portions (> 400 m) of our site near the fjord mouth contained the most diverse assemblages. Overall, these results illustrate that fjord walls are an extensive and ecologically relevant ecosystem supporting an abundant and diverse fauna important in the overall scheme of Northeast Pacific biodiversity.

In Chapter 3. I describe the 2016 seasonal patterns in the abundance and composition of epibenthic megafauna along a soft-bottom transect line in Saanich Inlet,

BC. This deep-shallow transect line runs from anoxia to normoxia, and contains a suite of mobile species that move in response to the seasonal pattern of oxygen depletion and repletion related to the flushing of the fjord basin (Chu & Tunnicliffe 2015). A weak deep-water renewal in 2015-2016, in conjunction with a warm-water surface anomaly (Chandler et al. 2017), interrupted this oxygen cycle; comparisons with 2013 transects show that changes in both benthic oxygen and community structure occurred as a result of these oceanographic conditions. Anoxic (~ 0 ml L^{-1} dissolved oxygen), severely hypoxic (<0.5 ml L^{-1}), and hypoxic (<0.88 ml L^{-1}) waters shoaled across all seasons from 2013 to 2016, with changes from low to high oxygen occurring over relatively short bottom distances in the latter year. Additionally, the major peaks in megafaunal abundance occurred at lower oxygen levels in all seasons in 2016. The change was most notable in Fall 2016, where the peak occurred in severe hypoxia and over 20 m shallower than in 2013. The density of multiple mobile and sessile epibenthos declined in Fall 2016 as well. A nudibranch and a holothurian species, the former rare and the latter absent from all previous transects, were abundant in Fall 2016, suggesting that some species may benefit from changing dissolved oxygen conditions as their competitors are excluded.

The shoaling oxygen affected the mobile epibenthos by compressing the available habitat, as null models showed a suite of 14 species was more aggregated in 2016 than 2013. Analysis of species-pair relationships also showed community homogenization, with more species completely overlapped or segregated than in 2013. Using the same 14-species suite of mobile megafauna as the null model analyses, I also describe community transitions along the oxygen gradient, and show that these transitions occurred at similar

locations in 2013 and 2016. In addition, the observed breakpoints in assemblage structure matched more closely with oxygen thresholds based in Northeast Pacific ecophysiology than with common global thresholds, suggesting that regional thresholds may be better suited to predict the ecological consequences of deoxygenation (Chu & Gale 2017). I also show, using data from a seafloor observatory node in Saanich Inlet, that the long-term decrease in dissolved oxygen accelerated from 2014-2016 as a result of the successive weak deep-water renewal events. Yearly mean oxygen and oxygen variability reached record lows in 2016, and may be complicit in the observed changes in community structure.

Big Picture

The ecological implications of my two thesis chapters must be understood in the context of a Northeast Pacific ocean where changes in the major abiotic variables shaping marine ecosystems (i.e. temperature, dissolved oxygen, and carbonate chemistry) outpace those in the global ocean; vertical and biogeographic shifts in species distributions are already occurring, and the interactive effects of these stressors are still poorly resolved (Somero et al. 2016). In addition, the communities of both Douglas Channel and Saanich Inlet are tied to regional and large-scale physical dynamics that regulate the annual flushing, and therefore, the water characteristics of their respective fjords.

The results from our surveys in Douglas Channel illustrate that vertical walls are important ecosystems in the Northeast Pacific that (i) contain diverse, high-biomass assemblages that likely influence the organic cycling through fjord basins (ii) house a variety of ecologically sensitive deep-water coral and glass sponge assemblages, and (iii) have the potential to serve as biodiversity reservoirs in a changing ocean by providing

refugia from various natural and anthropogenic stressors occurring on adjacent slopes. The deep (> 50 m depth) wall biota of Douglas Channel are relatively insulated from temperature, dissolved oxygen, and, given the coupling between dissolved oxygen and pCO_2 in the Northeast Pacific (Reum et al. 2014), acidification stress. However, the link between animal abundance and the water mass flux character of the fjord suggests a sensitivity of these assemblages to changes in physical forcing. In particular, a decrease in wind-driven circulation such as that in the equatorial Pacific (McPhaden & Zhang 2002) could decrease both the estuarine outflow and the compensatory intermediate inflow that was associated with the most dense assemblages in the fjord. In contrast, Northeast Pacific coastal upwelling strength and duration slightly increased from 1988-2010 (Jacox et al. 2010; Wang et al. 2015), and continued increases may augment biomass in the deep portions of fjords like Douglas Channel where annual upwelling onto the shelf drives a nutrient-rich deep-water renewal (Johannessen et al. 2015).

The changes in epibenthic community structure in Saanich Inlet observed over the course of 2016 imply stark changes in seafloor ecosystems vulnerable to deoxygenation. While the observed abundance declines and community homogenization are expected results of deoxygenation (Stramma et al. 2012; Sato & Levin 2017), the response following renewal in late 2016 is unknown. However, a summer 2017 transect showed that many species that declined in 2016 still occurred in low numbers relative to 2013 (Gasbarro unpub. data). In contrast, animal distributions largely re-established themselves in a few months following deoxygenation in summer 2013 (Chu & Tunnicliffe 2015). This recovery slow-down is an indicator of decreased resilience and of systems approaching critical transitions (van Nes & Scheffer 2007). Future benthic communities

may oscillate between periods of mortality and repopulation, as in a seasonally anoxic Danish fjord (Jørgenson 1980). Alternatively, the changes in community structure observed in Fall 2016 may become more permanent if deoxygenation continues. These changes in animal abundance and distributions will likely continue to affect the benthos in unforeseen ways as new trophic interactions are introduced (Breitburg et al. 2009). As the spatiotemporal extent of naturally occurring hypoxia in the ocean increases due to climate change (Rabalais et al. 2010), studies determining how seasonal hypoxic events of varying intensity and scale affect community structure will become increasingly important.

Future Directions

The vertical wall assemblages in Douglas Channel were largely composed of long-lived suspension-feeders. While the ROV survey design allowed for a baseline snapshot of these assemblages that established major patterns in diversity and abundance, the degree of influence by longer-term factors t(e.g. climate change, direct anthropogenic impacts) can only be speculated; if Douglas Channel becomes a major conduit for shipping, impact assessments can follow this baseline. The relationship of animal abundance with the mass flux structure of the fjord remains a question for further study. Settlement plates deployed at various depths and locations in the fjord, in conjunction with seston composition and density measurements from water samples, would allow tests of possible mechanisms behind the observed abundance distributions. Measurements of respiration and filtration rates could help elucidate the relationship between diversity, abundance, and ecosystem functioning on the walls. A better characterization of the extent of unsedimented bedrock surfaces throughout the fjord would improve

extrapolations of the importance of the wall fauna in overall ecosystem functioning. Further surveys of the deep wall biota of Northeast Pacific fjords and inlets could refine the emerging North-South distinction in fjord fauna and allow for a mechanistic understanding of this phenomenon.

As the Saanich Inlet epibenthos recovers from the extended 2016 hypoxic event, continued monitoring could identify successional stages in recovery and reveal the community resilience to such events. The potential importance of secondary variables, particularly pCO_2, could help to explain more variance in the community response. Low-pH, aragonite-undersaturated waters in the connecting Strait of Georgia highlight the potential importance of carbonate chemistry in this system (Moore-Maley et al. 2016). With sufficient data, it may be possible to refine the relationship between dissolved oxygen, temperature, and pCO_2 on the fjord bottom into a single global change metric. My analyses of assemblage transitions could be run along the range of this metric rather than solely oxygen, and may help explain the high-oxygen breakpoint in assemblage structure. In addition, a multi-stressor framework may provide more accurate predictions of ecological thresholds applicable to other Northeast Pacific systems.

Data Deposition

The data from Chapter 2 is to be stored in the University of Victoria's Dataverse repository. All original data from Chapter 3 will be stored in a repository managed by the Canadian Healthy Oceans Network.

Literature Cited

Breitburg DL, Loher T, Pacey CA, Gerstein A (1997) Varying effects of low dissolved oxygen on trophic interactions in an estuarine food web. Ecological Monographs 67:489–507

Chandler PC, King SA, and Perry RI (eds) (2017) State of the physical, biological and selected fishery resources of Pacific Canadian marine ecosystems in 2016. Can. Tech. Rep. Fish. Aquat. Sci.

Chu JWF, Tunnicliffe V (2015) Oxygen limitations on marine animal distributions and the collapse of epibenthic community structure during shoaling hypoxia. Global Change Biology 21:2989–3004

Chu JWF, Gale KSP (2016) Ecophysiological limits to aerobic metabolism in hypoxia determine epibenthic distributions and energy sequestration in the northeast Pacific ocean: Ecophysiological constraints in hypoxia. Limnology and Oceanography

Genin A, Paull C, Dillon W (1992) Anomalous Abundances of Deep-Sea Fauna on a Rocky Bottom Exposed to Strong Currents. Deep-Sea Research Part a-Oceanographic Research Papers 39:293-

Huvenne VAI, Tyler PA, Masson DG, Fisher EH, Hauton C, Hühnerbach V, Bas TPL, Wolff GA (2011) A picture on the wall: innovative mapping reveals cold-water coral refuge in submarine canyon. PLOS ONE 6:e28755

Jacox MG, Moore AM, Edwards CA, Fiechter J (2014) Spatially resolved upwelling in the California Current System and its connections to climate variability. Geophys Res Lett 41:3189–3196

Johannessen SC, Wright CA, Spear DJ (2015) Seasonality and physical control of water properties and sinking and suspended particles in Douglas Channel, British Columbia. Canadian Technical Report of Hydrography and Ocean Sciences. 308

Jørgensen BB (1980) Seasonal oxygen depletion in the bottom waters of a Danish fjord and its effect on the benthic community. Oikos 34:68–76

Leichter JJ, Witman JD (1997) Water flow over subtidal rock walls: Relation to distributions and growth rates of sessile suspension feeders in the Gulf of Maine - Water flow and growth rates. J Exp Mar Biol Ecol 209:293–307

McPhaden MJ, Zhang D (2002) Slowdown of the meridional overturning circulation in the upper Pacific Ocean. Nature 415:603–608

Moore-Maley BL, Allen SE, Ianson D (2016) Locally driven interannual variability of near-surface pH and ΩA in the Strait of Georgia. J Geophys Res Oceans 121:1600–1625

Nes EH van, Scheffer M (2007) Slow recovery from perturbations as a generic indicator of a nearby catastrophic shift. The American Naturalist 169:738–747

Rabalais NN, Díaz RJ, Levin LA, Turner RE, Gilbert D, Zhang J (2010) Dynamics and distribution of natural and human-caused hypoxia. Biogeosciences 7:585–619

Reum JCP, Alin SR, Feely RA, Newton J, Warner M, McElhany P (2014) Seasonal Carbonate chemistry covariation with temperature, oxygen, and salinity in a fjord

estuary: implications for the design of ocean acidification experiments. PLOS ONE 9:e89619

Rowden AA, Schlacher TA, Williams A, Clark MR, Stewart R, Althaus F, Bowden DA, Consalvey M, Robinson W, Dowdney J (2010) A test of the seamount oasis hypothesis: seamounts support higher epibenthic megafaunal biomass than adjacent slopes. Marine Ecology 31:95–106

Sato KN, Levin LA, Schiff K (2017) Habitat compression and expansion of sea urchins in response to changing climate conditions on the California continental shelf and slope (1994–2013). Deep Sea Research Part II: Topical Studies in Oceanography 137:377–389

Somero GN, Beers JM, Chan F, Hill TM, Klinger T, Litvin SY (2016) What changes in the carbonate system, oxygen, and temperature portend for the northeastern Pacific Ocean: A Physiological Perspective. BioScience 66:14–26

Stramma L, Prince ED, Schmidtko S, Luo J, Hoolihan JP, Visbeck M, Wallace DWR, Brandt P, Körtzinger A (2012) Expansion of oxygen minimum zones may reduce available habitat for tropical pelagic fishes. Nature Clim Change 2:33–37

Wan D, Hannah CG, Foreman MGG, Dosso S (2017) Subtidal circulation in a deep-silled fjord: Douglas Channel, British Columbia. J Geophys Res Oceans.

Wang D, Gouhier TC, Menge BA, Ganguly AR (2015) Intensification and spatial homogenization of coastal upwelling under climate change. Nature 518:390–394

Appendix A: Supplementary Material for Chapter 2

Table A.1. Transect metadata for all sites in Douglas Channel. Each individual record is a non-overlapping habitat or biological observation taken on a per-second protocol in VideoMiner.

	Maitland Island	**Mckay Reach**	**Squally Reach**
Dive date	Sep. 28-29 2015	Sep. 29, 2015	Oct. 1, 2015
ROPOS Dive No.	R1880	R1883	R1884, R1885
Number of transects	3	3	3
Surveyed depth range (m)	43-323	48-428	166-682
No. of habitat and biological records	18770	27336	32631
% of transect records with dominant substratum type:			
Bedrock	56.7	75.6	29.4
Sediment	40.6	20.1	70.6
Biogenic (shell hash, dead glass sponge)	2.7	4.3	0
% of transect records with relief type:			
Flat or rolling	2.4	0.5	1.2
Shallow (<45º from horizontal)	29.5	10.4	12.3
Medium (between 45º and 90º)	22.9	47.4	42.1
Steep (~90º or close; includes overhangs)	22.7	30.7	18.3
Steps (Alternates between steep & shallow)	22.4	11.0	26.1

Table A.2. List of 53 observed species in Douglas Channel imagery and their broad taxonomic designation; designated groups include serpulids (SP), asteroids (AS), echinoids (EC), decapods (DE), non-hexactinellid sponges (OS), actinarians (AC), gastropods (GA), cup corals (CC), bubblegum corals (BC), ophiuroids (OP), crinoids (CR), articulate brachiopods (AB), lyssacine glass sponges (LHx), dictyonine glass sponges (DHx), inarticulate brachiopods (IB), zoanthids (ZO), and rockfish (RF). Asterisks denote tentative identifications of encrusting species that were not included in the total species tally.

Phylum	Order	Species	Designation
Porifera	Clathrinida	*Clathrina* cf. *coriacea**	OS
Porifera	Clathrinida	Porifera1*	OS
Porifera	Leucosolenida	*Leucandra heathi**	OS
Porifera	Axinellida	*Auletta krautteri*	OS
Porifera	Halichondrida	*Hymeniacidon spp.*	OS
Porifera	Poecilosclerida	*Cladorhiza spp.*	OS
Porifera	Poecilosclerida	*Mycale bellabellensis*	OS
Porifera	Poecilosclerida	*Myxilla lacunosa**	OS
Porifera	Tetractinellida	*Stelletta clarella**	OS
Porifera	Tetractinellida	*Poecillastra tenuilaminaris*	OS
Porifera	Verongiida	*Hexadella spp.**	OS
Porifera	Hexactinosida	*Aphrocallistes vastus/ Heterochone calyx*	DHx
Porifera	Hexactinosida	*Farrea occa*	DHx
Porifera	Lyssacinosida	*Rhabdocalyptus dawsoni/ Staurocalyptus dowlingi*	LHx
Porifera	Homosclerophorida	*Plakina atka*	OS
Cnidaria	Actinaria	*Cribrinopsis fernaldi*	AC
Cnidaria	Actinaria	*Stomphia didemon*	AC
Cnidaria	Actinaria	*Liponema brevicornis*	AC
Cnidaria	Alcyonacea	*Paragorgia arborea*	BC
Cnidaria	Alcyonacea	*Swiftia beringi*	
Cnidaria	Alcyonacea	*Primnoa pacifica*	
Cnidaria	Antipatharia	*Antipathes spp.*	
Cnidaria	Ceriantharia	*Pachycerianthus fimbriatus*	
Cnidaria	Scleractinia	*Caryophyllia alaskensis*	
Cnidaria	Scleractinia	*Caryophyllia arnoldi*	
Cnidaria	Trachymedusae	*Ptychogastria polaris*	
Cnidaria	Zoanthidae	*Epizoanthus scotinus*	
Annelida	Sabellida	*Protula pacifica*	SP
Annelida	Sabellida	*Serpula vermicularis*	SP
Nemertea	unknown	*Nemertean1*	

Brachiopoda	Craniida	*Novocrania californica*	IAB
Brachiopoda	Terebratulida	*Laqueus vancouveriensis*	IB
Arthropoda	Decapoda	*Munida quadrispina*	DE
Arthropoda	Decapoda	*Pandalus spp.*	DE
Mollusca	Vetigastropoda	*Calliostoma platinum*	GA
Mollusca	Caenogastropoda	*Fusitron oregonensis*	GA
Echinodermata	Forcipulatida	*Stylasterias forreri*	AS
Echinodermata	Forcipulatida	*Pycnopodia spp.**	AS
Echinodermata	Paxillosida	*Leptychaster anomalus*	AS
Echinodermata	Paxillosida	*Leptychaster arcticus*	AS
Echinodermata	Paxillosida	*Ctenodiscus crispatus*	AS
Echinodermata	Paxillosida	*Gephyreaster swifti*	AS
Echinodermata	Spinulosida	*Henricia sanguinolenta*	AS
Echinodermata	Valvatida	*Ceramaster patagonicus*	AS
Echinodermata	Valvatida	*Hippasteria spinosa*	AS
Echinodermata	Valvatida	*Lophaster furcilliger*	AS
Echinodermata	Valatida	*Pteraster tesselatus*	AS
Echinodermata	Comatulida	*Florometra serratissima*	CR
Echinodermata	Echinoida	*Strongylocentrotus pallidus*	EC
Echinodermata	Echinoida	*Strongylocentrotus franciscanus*	EC
Echinodermata	Aspidochirotida	*Parastichopus leukothele*	
Echinodermata	Aspidochirotida	*Parastichopus californicus*	
Echinodermata	Dendrochirotida	*Eupentacta pseudoquinquesemita*	
Echinodermata	Ophiurida	*Ophiopholis aculeata*	OP
Chordata	Stolidobranchia	*Cnemidocarpa finmarkiensis*	
Chordata	Aplousobranchia	*Diplosoma listerianum*	
Chordata	Chimaeriformes	*Hydrolagus colliei*	
Chordata	Peuronectiformes	*Hippoglossus stenolepis*	
Chordata	Scorpaeniformes	*Sebastes babcocki*	

Figure A.1. Boxplots of sUTC (left panel) and sΔ+ (right panel) per depth band above and below 200 m 'breakpoint' seen in animal abundances. Asterisks indicate significant differences between the groups as determined by Welch's ANOVA ($p < 0.05$).

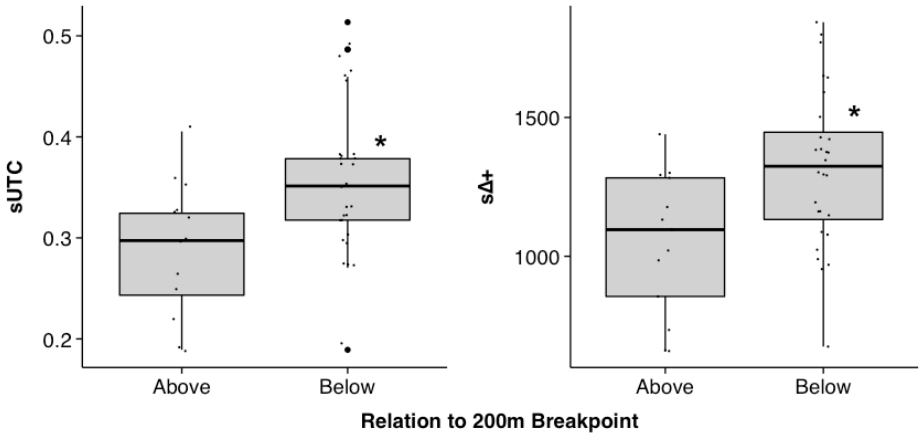

Figure A.2. Taxonomic distinctness (Δ+) by depth band with sites denoted by symbol. Dashed line represents expected value of Δ+ under the assumption of random assembly from the regional species pool. Depth band labels display the base of each band. Three of four depth bands with Δ+ values under the expected value occur at depths shallower than 100 m.

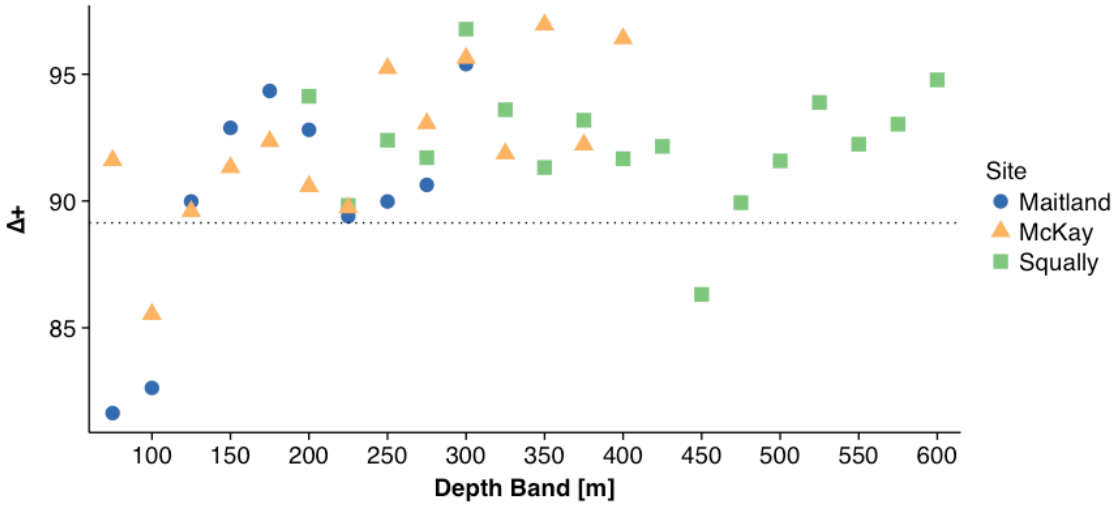

Figure A.3. Species clusters based on functional traits. Tree height refers to the number of trait dissimilarities.

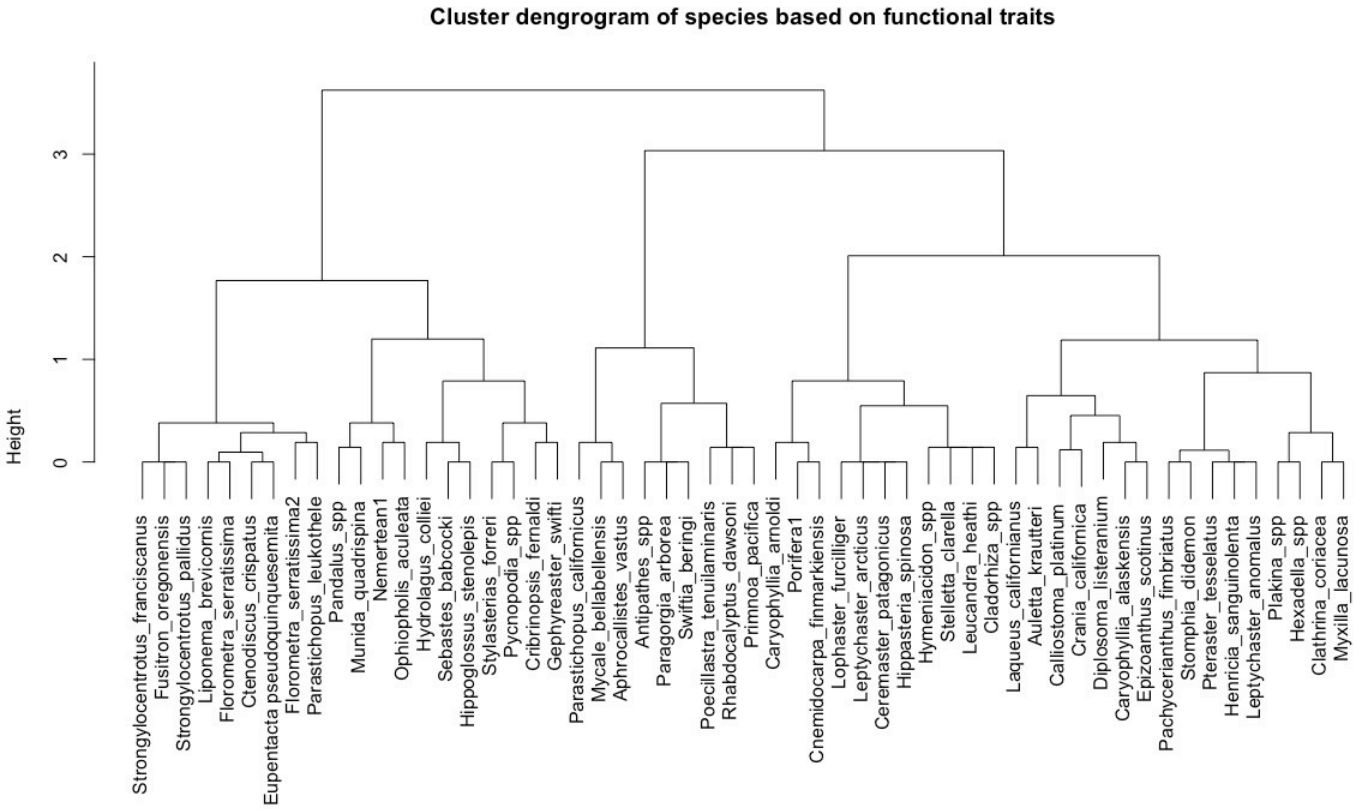

Appendix B: Supplementary Material for Chapter 3

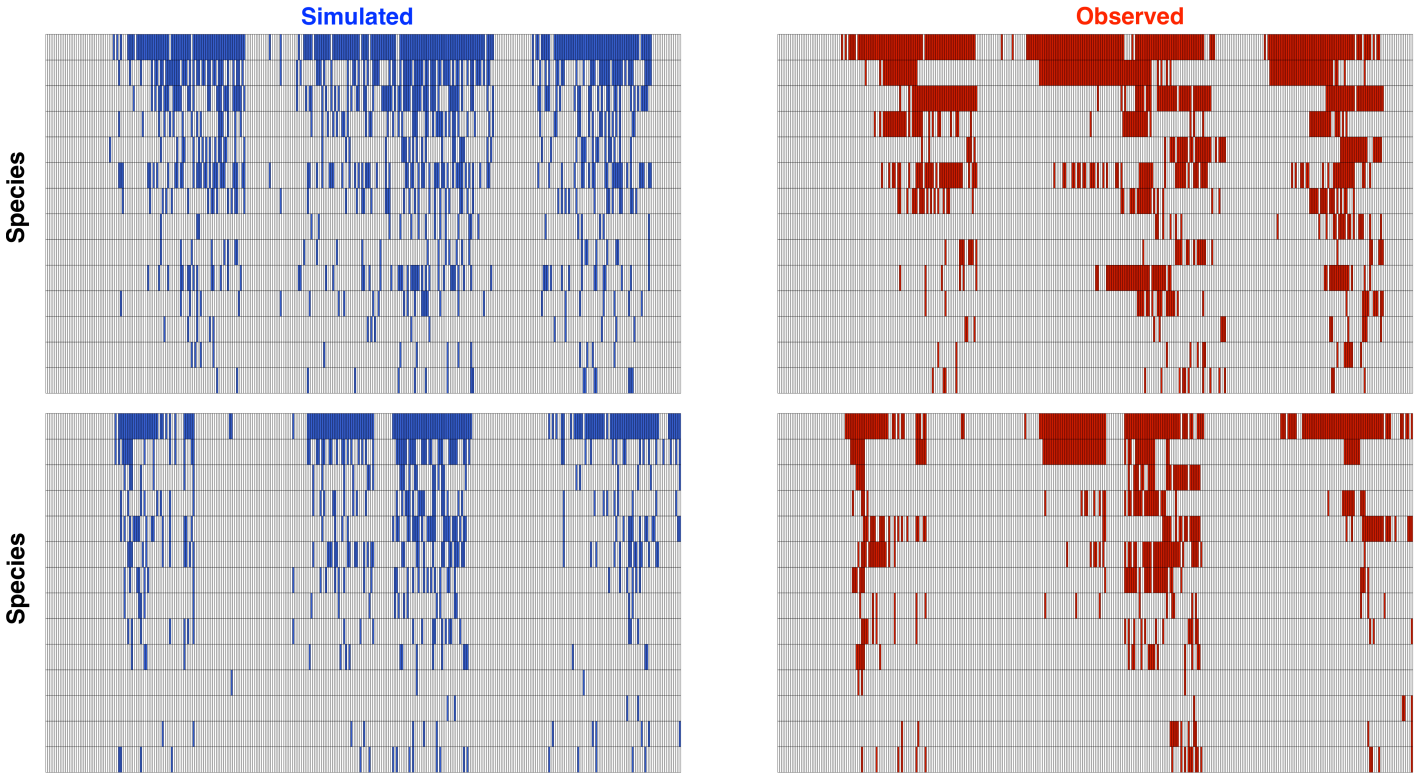

Figure B.1. Co-occurrence matrices showing species presence in one null model iteration (blue) vs. observed presence (red) in a) 2013 and b) 2016. Each row represents one of 14 species included in the null model, with each column representing one 20 m^2 quadrat.

https://drive.google.com/open?id=0B5oVHBF7bslBV2tFbmpyOFV3czA

Figure B.2. Video clips at corresponding depths/seasons in 2013 (right half of frame) versus 2016 (right half of frame). Flatfish were present in the deep portions (~ 145 m) of the Summer 2013 transect but were absent in the later year. Fall comparisons at ~60 m depth show squat lobsters rather than spot prawns, decreased seawhip density, and the presence of striped nudibranchs in 2016.